The Potential Toxic Effects of Chronic Doxorubicin Treatment on the Rat Pancreas and the Role of Ghrelin in this Context

by

Kirsten Lee Scott

Thesis presented in fulfilment of the requirements

for the degree of

Master of Science (Physiological Sciences)

in the Faculty of Science

at Stellenbosch University

Supervisor: Dr Balindiwe Sishi

March 2018

Declaration

By submitting this thesis electronically, I declare that the entirety of the work contained therein is my own, original work, that I am the sole author thereof (save to the extent explicitly otherwise stated), that reproduction and publication thereof by Stellenbosch University will not infringe any third-party rights and that I have not previously in its entirety or in part submitted it for obtaining any qualification.

March 2018

Abstract

Introduction: Doxorubicin (DOX), is a chemotherapeutic drug that has potent anti-neoplastic actions. It is for this reason that it remains one of the most widely used chemotherapeutic agents that has led to an increase in the survival rates of cancer patients. However, DOX's efficacy in treating a variety of cancers is a double-edged sword due to its cumulative, dose-dependent toxicity, particularly in cardiomyocytes. Since DOX's anti-neoplastic activities are separate to the mechanisms underlying its toxicity, there is a need to investigate adjuvant therapies that do not interfere with DOX's ability to kill cancerous cells, but have the potential to protect against its toxicity. Ghrelin, a brain-peptide commonly known for its appetite inducing and growth hormone (GH) releasing actions, has previously been shown to reduce oxidative stress, apoptosis, inflammation and fibrosis, all of which contribute to DOX-induced toxicity, in different contexts. However, over the years, literature has predominantly focused on DOX's effects on the heart, while very few studies are available regarding DOX's effects on the pancreas. Therefore, this study investigated the effects of DOX on the pancreas and whether ghrelin can provide protection against these effects in a model of chronic DOX-induced cardiotoxicity.

Materials and Methods: Male Sprague-Dawley were randomly divided into four treatment groups. The vehicle group received 200 µl of physiological saline, the ghrelin group received 100 µg/kg three times a week, the DOX group received 2.5 mg/kg once a week, and the combination group (DOX+ghrelin) received both treatment regimens. All treatments were conducted *via* intraperitoneal injection over a period of eight weeks. A week after the last injection, animals were euthanised, blood was collected, and organs were harvested. After the pancreata were weighed, they were non-specifically divided into two sections, where one half was presevered in 4% formaldehyde solution for histological analysis, and the other half was snap frozen in liquid nitrogen for biochemical analysis. Serum inflammatory markers as well as pancreatic hormones insulin and glucagon were measured using a multiplex assay. General morphological changes, collagen deposition, and the number of α- and β-cells were assessed by employing H&E, Masson's Trichrome, and immunohistochemical stains, respectively. In addition to lipid peroxidation, oxidative stress was assessed by the ORAC, SOD and glutathione assays. Finally, Western blotting was utilised to determine the expression of the apoptotic marker, cleaved caspase-3.

Results: Following eight weeks of treatment, DOX significantly reduced appetite (152.95 ± 10.23 g, $p<0.05$) and weight gain (186.88 ± 10.35 g, $p<0.0001$) when compared to the saline treated animals. Ghrelin, in the presence of DOX did not significantly differ when compared to the DOX treated group. DOX caused significant collagen deposition which is an indication of fibrosis in the pancreas of these animals (4.80 ± 0.78%, $p<0.0001$), whereas DOX+ghrelin significantly reduced collagenous areas (2.22 ± 0.39%, $p<0.001$) when compared to the DOX group. Our oxidative stress analyses revealed that both the DOX (0.51 ± 0.028 µmol TE/g, $p<0.01$) and DOX+ghrelin (0.47 ± 0.01 µmol TE/g, $p<0.05$) groups considerably increased their anti-oxidant capacity when compared to the vehicle (0.37 ± 0.05 µmol TE/g). Moreover, SOD activity was significantly downregulated in both the DOX (1.49 ± 0.18 U/mg, $p<0.01$) and DOX+ghrelin (1.54 ± 0.12 U/mg) groups when compared to the vehicle. Cleaved caspase 3 was also elevated during DOX treatment but reduced in the combination group. No other noteworthy changes were observed in any of the other parameters measured.

Discussion and Conclusion: The results of this study indicate that DOX is a cytotoxic agent that induces a loss of appetite and detrimental effects such as oxidative stress, fibrosis and cell death in pancreatic tissue. The use of ghrelin as an adjuvant treatment in this context was beneficial as weight gain was promoted, while fibrosis and cell death were reduced. Although the exact mechanisms underlying ghrelin's orexigenic effects are still unknown, it is believed that ghrelin acts through the hypothalamic-pituitary axis to promote appetite. Ghrelin's anti-fibrotic effects are induced through the downregulation of pro-inflammatory and pro-fibrotic cytokines, while apoptosis is prevented *via* the inhibition of cytochrome c leakage from the mitochondria. Since ghrelin had no effect in improving the activity of SOD, its anti-oxidant effects could not be proved in this tissue. In conclusion, while these results shed some light into understanding the mechanisms by which ghrelin counteracts DOX's effects, further research is necessary to assess ghrelin's potential as an adjuvant treatment regimen for DOX-induced pancreatic injury.

Uittrteksel

Inleiding: Doksorubisien (DOX), is ‘n chemoterapeutiese middel wat sterk anti-neoplastiese werking toon. Weens hierdie rede is dit steeds een van die mees algemeen chemoterapeutiese middels wat oorlewing in kanker pasiënte verhoog. Daarbenewens, is die gebruik van DOX weens die effektiwiteit teen verskeie kankers paradoksaal weens die kumulatiewe, dosis-afhanglike toksisiteit veral in kardiomiosiete. Omrede DOX se anti-neoplastiese aktiwiteite apart staan van die onderliggende toksisiteitsmeganismes, is daar ‘n behoefte om adjuvante terapie te ondersoek wat nie met DOX se vermoë inwerk om kankerselle te vernietig nie, maar om teen die toksisiteit te beskerm. Grelien, ‘n breinpeptied wat algemeen bekend is vir sy aptytinduserende, en groeihormoon (GH) vrystellingseienskappe, is voorheen bewys om oksidatiewe stres, apoptose, inflammasie en fibrose, wat bydraes lewer tot DOX geïnduseerde tokisisteit, in verskeie kontekse, te verlaag. Geskiedkundig, fokus die literatuur meestal op DOX se effek op die hart, terwyl daar min studies die effek op die pankreas rapporteer. As gevolg hiervan, het hierdie studie die effekte van DOX op die pankreas, en of grelien beskerming kan bied teen hierdie newe-effekte in ‘n chroniese DOX geïnduseerde kardiotoksisiteitmodel.

Materiale en Metodes: Manlike Sprague-Dawley rotte is ewekansig verdeel in vier behandelingsgroepe. Die draergroep het ‘n fisiologiese soutoplossing ontvang, die grelien groep, 100 µg/kg drie keer per week, die DOX groep, 2.5 mg/kg een keer per week, en die kombinasie groep (DOX+grelien) het beide behandelings ontvang. Alle behandelings is *via* intraperitoneale toediening oor ‘n agt-weke periode gedoen. Een week na die laaste toediening, is die diere deur middel van eutanasie doodgemaak, waarna bloedmonsters versamel, en die organe verwyder is. Nadat die pankrease geweeg is, is hulle in twee dele gedissekteer, waar die een helfte met ‘n 4% formaldehiedoplossing vir histologiese analiese voorbereid is, en die ander helfte met vloeibare stikstof bevries is vir biochemiese analieses. Serum inflammatoriese merkers, sowel as pankreatiese hormone en glukagon, is deur middel van ‘n multiplekstoetsing gedoen. Algemene morfologiese veranderinge, kollageenneerlegging, en aantal α- en β-selle is deur middel van H&E, Masson’s Trichrome, en immunohistochemiese kleuring onderskeidelik ondersoek. Addisioneel tot lipiedperoksidasie, is oksidatiewe stres deur die ORAC, SOD en glutatioontoetse

ondersoek. Laastens, is Westerse kladtegniek gebruik om die uitdrukking van die apoptotiese merker, gesplyte kaspase-3 te ondersoek.

Resultate: Na afloop van die agt-weke behandeling, het DOX betekenisvol aptyt verlaag (152.95 ± 10.23 g, $p<0.05$) asook gewigstoename (186.88 ± 10.35 g, $p<0.0001$) vergeleke met die soutoplossing groep. Grelien, in die teenwoordigheid van DOX, het nie aptyt en gewigstoename betekenisvol gestimuleer teenoor die DOX groep nie. DOX het ‘n beteknisvolle neerlegging van kollageen in die pankreasse van hierdie diere veroorsaak wat aantoon dat fibrose teenwoordig is (4.80 ± 0.78%, $p<0.0001$), terwyl DOX+grelien hierdie kollageenareas verlaag het (2.22 ± 0.39%, $p<0.001$) vergeleke met die DOX groep. Die oksidatiewe stresanalises toon aan dat beide DOX (0.51 ± 0.028 µmol TE/g, $p<0.01$) en DOX+grelien (0.47 ± 0.01 µmol TE/g, $p<0.05$) groepe hulle anti-oksidantkapasiteit verhoog vergeleke met die draer groep (0.37 ± 0.05 µmol TE/g). Die SOD aktiwiteit is betekenisvol afgereguleer in beide die DOX (1.49 ± 0.18 U/mg, $p<0.01$) en DOX+grelien (1.54 ± 0.12 U/mg) groepe vergeleke met die draer groepe. Gesplyte kaspase-3 is ook verhoog tydens DOX behandeling, maar verlaag in die kombinasie groep. Geen ander merkbare veranderinge is aangetoon in enige van die ander parameters nie.

Bespreking en Gevolgtrekking: Die resultate van hierdie studie toon dat DOX ‘n sitotoksiese middel is en verlies aan aptyt met skadelike effekte soos oksidatiewe stres, fibrose en seldood in pankreatiese weefsel, induseer. Die gebruik van grelien as ‘n adjuvante behandelingsmiddel in hierdie konteks was voordelig omrede gewigstoename bevorder was, terwyl fibrose en seldood verlaag is. Hoewel die presiese meganismes van grelien se oreksigeniese effekte onbekend is, is dit moontlik dat grelien deur die hipotalamiese-pituitêre aksis werk en sodoende aptyt bevorder. Grelien se anti-fibrotiese effekte word deur die afregulering van pro-inflammatoriese en pro-fibrotiese sitokiene bewerk, terwyl apoptose verhoed word *via* die inhibering van sitochroom c lekkasie vanuit die mitochondria. Omrede grelien geen effek op die verbetering van SAD aktiwiteit getoon het in die studie nie, kan die anti-oksidant effek nie in hierdie weefsel bewys word nie. Gevolglik kan ons wel lig werp op die meganismes waarby grelien, DOX se newe-effekte kan teëwerk, maar verdere navorsing is nodig om die potensiaal van grelien as ‘n adjuvante terapie vir DOX-geïnduseerde pankreatiese skade voor te stel.

Acknowledgements

To my supervisor, Dr Bali Sishi. Thank you for all you have done for me and for giving me this amazing opportunity. You believed in me from the beginning and pushed me to conquer the mountain even when at times it seemed impossible to keep climbing. Your constructive criticism propelled me to always strive for better, and has helped me develop and refine my scientific ability.

To Dr Toni Goldswain, I am truly grateful. Thank you for everything. Your mentorship and guidance has left its mark, and has helped shape the person I am today. I will always be so thankful to you.

Thank you to my family for their unconditional love and support. In particular, I would like to thank my parents and my sister for your endless encouragement and for believing in me throughout this rollercoaster of a journey. Thank you to my parents for the financial support – I will forever be grateful for all the hardwork and sacrifices you have made over the years to enable me to study further.

Thank you to Cara and Jess for helping to create a place in Stellenbosch which I called home, and for all the laughs, giggles and venting sessions at the end of long days.

Reggie Williams, Simoné Nel and Rochelle van Wyk at the Anatomy & Histology Division of the Biomedical Department at the Faculty of Medicine & Health at Tygerberg, thank you for your assistance with the histological work and analysis, and for teaching me how to better appreciate histology in research.

Dr Novel Chegou and Candice Snyders at the Molecular Biology & Human Genetics Division at the Faculty of Medicine & Health Sciences at Tygerberg, thank you for your help and enduring patience with the multiplex assay. Working in your labs with you was an amazing experience and the work you are doing is incredible.

Fanie Rautenbach at the Oxidative Stress Research Centre at CPUT, thank you for your guidance and patience with the oxidative stress analysis, and for teaching me how to perform the different assays.

Thank you to Dr Theo Nell for translating my abstract into Afrikaans, and to Ashwin Issacs and Dr Lydia Lacerda for your help and for maintaining a functional lab for us

to work in. Thank you to Dr Danzil Joseph for all the laughs and guidance in the lab, and to Jason, Rhys and Muneeb for the coffee dates that kept me laughing.

Thank you to CORG, DSG and everyone at the Department of Physiological Sciences for the support and for giving me the opportunity to complete my MSc.

Life will give you whatever experience is most helpful for the evolution of your consciousness. How do you know this is the experience you need? Because this is the experience you are having at this moment.

- *Eckhart Tolle*

TABLE OF CONTENTS

List of Figures

List of Tables

List of Abbreviations

6-HD	6-hydroxydopamine
α-cells	Alpha-cells
α-SMA	Alpha-smooth muscle actin
β-cells	Beta-cells
δ-cells	Delta-cells
ε-cells	Epsilon-cells
AAPH	2,2'-azobis(2-methylproprionamidine) dihydrochloride
AEC	3-amino-9-ethylcarbazole
ANOVA	Analysis of variance
AP	Alkaline phosphatase
Apaf-1	Apoptosis protease protein-1
ATP	Adenosine triphosphate
AUC	Area under the curve
Bak	Bcl-2 homologous antagonist/killer
Bax	Bcl-2 associated X protein
Bcl-2	B-cell lymphoma 2
Bcl-3	B-cell lymphoma 3-encoded
BHT	Butylated hydroxytroluene
C7	Carbon number 7
C4	Carbon number 4
Ca^{2+}	Calcium
cAMP	Cyclic adenosine monophosphate

CCK	Cholecystokinin
CDs	Conjugated dienes
CRP	C-reactive protein
Cu/ZnSOD	Copper Zinc SOD
Cyt c	Cytochrome c
DAB	3,3’-diaminobenzidine tetrahydrochloride hydrate
DETAPAC	Diethylenetriaminepentaacetic acid
DNA	Deoxyribonucleic acid
DNR	Daunorubicin
DOX	Doxorubicin
DTNB	5 5'-dithiobis-(2-nitrobenzoic acid)
DXZ	Dexrazoxane
ECG	Electrocardiogram
ECM	Extracellular matrix
EDTA	Ethylenediaminetetraacetic acid
EPI	Epirubicin
ER	sarco(endo)plasmic reticulum
FADD	Fas-Associated death receptor domain
FasL	Fas ligand
Fe	Iron
Fe^{3+}	Ferric ion
Fe^{2+}	Ferrous ion
$Fe^{IV}=O$	Perferryl iron

GAPDH	Glyceraldehyde 3-phosphate dehydrogenase
GH	Growth hormone
GHS-R-1α	Growth hormone secretagogue receptor type 1-alpha
GLUT-2	Glucose transporter 2
GLUT-4	Glucose transporter 4
GPx	Glutathione peroxidase
GR	Glutathione reductase
GSH	Reduced glutathione
GSSG	Oxidised glutathione
H^+	Proton
H&E	Haematoxylin & Eosin
H_2O	Water
$HOO^\bullet$	Hydroperoxyls
H_2O_2	Hydrogen peroxide
HRP-linked	Horseradish peroxidase-linked
IDA	Idarubicin
LF PVDF	Low fluorescence polyvinylidene fluoride
IgG	Immunoglobulin G
IκB	Inhibitory-kappa-B
IκBα	IκB-alpha
IL-1β	Interleukin 1-beta
IL-6	Interleukin 6
IR	Insulin receptor

IRS	Insulin receptor substrate
IREs	Iron-responsive elements
IRPs	Iron-regulatory proteins
LSD	Least Squared Difference
M2VP	1-methyl-2-vinylpyridinium
MDA	Malondialdehyde
MMPs	Matrix metalloproteinases
MnSOD	Manganese SOD
monoHER	7-mono-O-(β-hydroxyethyl)-rutoside
mPTP	Mitochondrial permeability transition pore
NPY4 receptor	Neuropeptide Y4 receptor
Na^+/Ca^{2+}	Sodium-calcium
Na_3VO_4	Sodium orthovanadate
NADH	Reduced nicotinamide adenine dinucleotide
NADPH	NAD (phosphate)
$NAD(P)^+$	Oxidised NAD(P)H
NaF	Sodium fluoride
NFκB	Nuclear factor kappa-light-chain-enhancer of activated B cells
NP-40	Nonidet P 40
O_2	Oxygen
$O_2^{\bullet -}$	Superoxide radicals
$OH^{\bullet}$	Hydroxyl radicals

OPA	Ortho-Phosphoric acid
ORAC	Oxygen Radical Absorbance Capacity
PARP-1	Poly (adenosine diphosphate-ribose) polymerase-1
PCA	Perchloric acid
PDGF	Platelet-derived growth factor
PI3K	Phosphatidylinositol-4,5-bisphosphate 3-kinase
PMSF	Phenylmethylsulfonyl fluoride
PP-cells	Pancreatic polypeptide-cells
PTFE	Polytetrafluoroethylene
RIPA	Radio-immunoprecipitation
ROS	Reactive oxygen species
SEM	Standard Error of Mean
Serine-3	Serine position 3
SOD	Superoxide dismutase
TBARS	Thiobarbituric acid reactive substances
TBS-T	Tris Buffered Saline-Tween Solution
TGF-β1	Transforming growth factor-beta1
TNB	5-thio-2-nitrobenzoic acid
TNF-α	Tumour necrosis factor-alpha
UV	Ultra-violet

Unit of Measurements

%	Percentage
°C	Degrees
µg	Microgram
µl	Microlitre
µm	Micrometre
µmol	Micromole
µM	Micromolar
AU	Arbitrary units
cm	Centimetre
g	Relative centrifugal force
g	Gram
kDa	Kilodalton
kg	Kilogram
l	Litre
M	Molar
mg	Milligram
ml	Millilitre
m^2	Metres-squared
nm	Nanometre
mM	Millimolar
pg	Picogram
rpm	Revolutions per minute

V	Voltage

CHAPTER 1: Literature Review

1.1 Embryology and structure of the pancreas

During early human development, both the dorsal and ventral buds originate from the endodermal lining of the primitive foregut tube and contribute to the formation of the pancreas (El-Gohary & Gittes, 2012). As the duodenum rotates to become C-shaped, the ventral bud follows to eventually lie below and fuse with the dorsal bud. The ventral bud forms the uncinate process of the pancreas as well as the inferior portion of the head, while the dorsal bud forms the remaining part of the head, as well as the tail and body of the pancreas (Sadler & Langman, 2006). Both the endocrine and exocrine tissue of the pancreas develop simultaneously from the two buds, in which the pancreatic precursor cells appear to have plasticity and can differentiate into either endocrine cells or exocrine cells during development (Tsuchitani et al., 2016). The human pancreas is a compact organ that is located in the upper region of the abdomen. It is located posterior to the stomach, and lies between the duodenum and the spleen (Figure 1.1) (Moore et al., 2008).

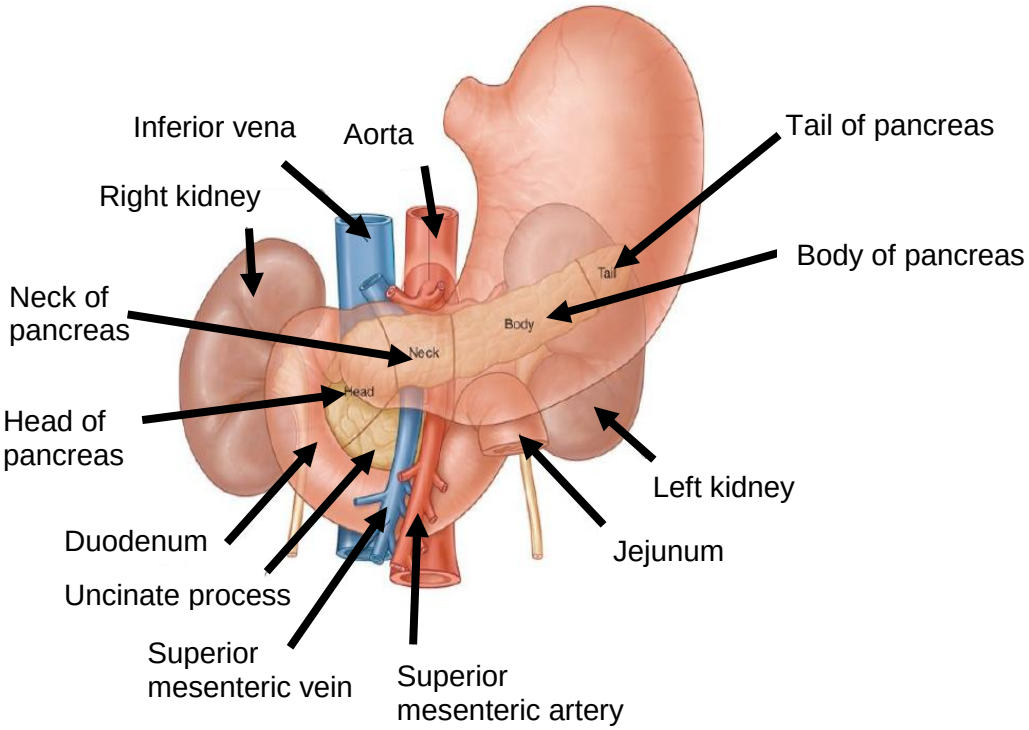

Figure 1.1: The location of the human pancreas relative to other organs in the body. The pancreas is situated posterior to the stomach and lies between the duodenum and the spleen. Sections include the tail, body, neck, head and uncinate process. Adapted from Drake *et al.* (2010).

Interestingly, the rat pancreas is classified as an intermediate of the human pancreas where the splenic part is relatively compact, and the duodenal part is found to be dispersed within the mesentery. Although much controversy exists regarding the identification of the different parts of the rat pancreas, the regions of the rat pancreas can be identified based on the anatomy of the human pancreas. The duodenal section (derived from the ventral bud) and para-biliary section (derived from the dorsal bud) are situated near the duodenum and form the head of the pancreas. The gastric and splenic sections (both derived from the dorsal bud) are situated between the head of the stomach and spleen and form the body of the pancreas, and thus the terminal end of the splenic section is situated near the hilum of the spleen and forms the tail of the pancreas (Figure 1.2) (Elayat *et al.,* 1995; Tsuchitani *et al.,* 2016)

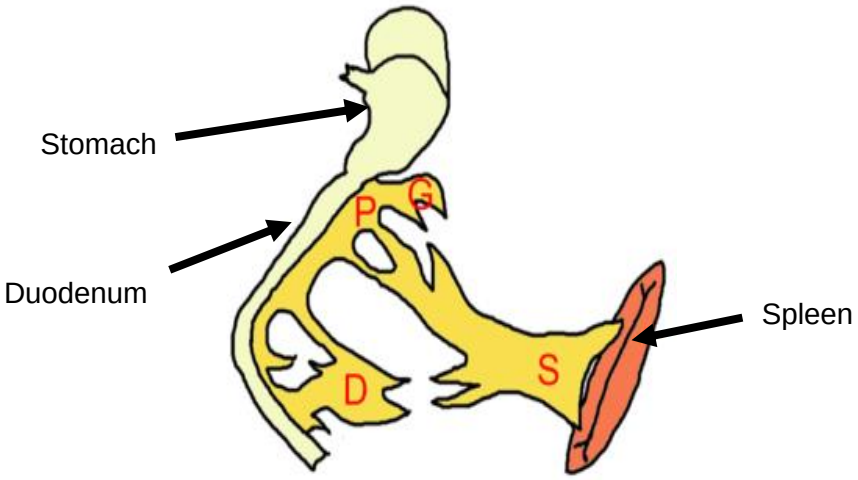

Figure 1.2: An illustration of the rat pancreas in its position relative to the spleen and the gut. The pancreas is situated between the spleen, the stomach and the duodenum. Abbreviations: S (Splenic section); D (Duodenal section); P (Parabiliary section); G (Gastric section). Adapted from Tsuchitani *et al*. (2016).

The exocrine tissue consists of lobular acini and ducts that are enclosed in a capsule and held together by connective tissue (Wieczorek *et al.,* 1998). The acinar and duct cells in the exocrine tissue secrete pancreatic digestive juices into the duodenum of the stomach (Moore *et al.*, 2008). In contrast, the endocrine tissue consists of the islets of Langerhans that are not enclosed in a capsule but are embedded in collagen fibres (Wieczorek *et al*., 1998). The islets of Langerhans consist of four different cell types: insulin-secreting beta (β)-cells, glucagon-secreting alpha (α)-cells, somatostatin-

secreting delta (δ)-cells, and pancreatic polypeptide (PP)-secreting cells. These cells secrete the pancreatic hormones into the bloodstream. The arrangement of these cells within the pancreas is, however, species specific and is believed to have a significant influence on pancreatic function (Elayat *et al.*, 1995; Hauge-Evans *et al.*, 2009).

1.2 Composition and distribution of cells in both the human and rat endocrine pancreas

In the human pancreas the islets consist of ±54% β-cells, ±35%, α-cells, ±10% δ-cells, and less than 1% of PP-cells (Wieczorek *et al.*, 1998; Brissova *et al.*, 2005; Steiner *et al.*, 2010). Erlandersen *et al.* (1976) demonstrated that human islets contain a central β-cell core surrounded by α-, δ-, and PP-cells, while Brissova *et al.* (2005) and Cabrera *et al.* (2006) indicated that the four cell types are in fact randomly arranged and dispersed within the islets. In addition, it has previously been shown that smaller islets have a β-cell core surrounded by α-, δ- and PP-cells, while larger islets have α-, δ- and PP-cells in the core surrounded by β-cells (Bosco *et al.*, 2010; Farhat *et al.*, 2013). Based on the above mentioned studies, it is clear that there is still some controversy around the location of these cells within the islets. Regarding the islet composition between different regions of the pancreas, reports are conflicting. Some studies indicate that the head and uncinate process are richer in PP-cells, while the tail portion is richer in β- and α-cells (Gersell *et al*., 1979; Elayat *et al.*, 1995). However, Wieczorek *et al*. (1998) reported no differences between islet density of δ- and PP-cells throughout the pancreas, and Cabrera *et al.* (2016) more recently reported no changes in islet composition between regions, except that α-cells are more abundant in the neck. When comparing the human and rodent pancreas, the human pancreas is described as having less β-cells and more α-cells than the rodent pancreas (Kim *et al.*, 2009; Steiner *et al.*, 2010).

Rodent islets are composed of 60-85% β-cells, 15-25% α-cells, 6-10% δ-cells and less than 1% of PP-cells (Brissova *et al.*, 2005; Steiner *et al.*, 2010). In contrast to human islets, rat islets are extensively and consistently described in the literature as having a central β-cell core surrounded by a mantle consisting of α-, δ- and PP-cells (Zafar & Mughal, 2002; Brissova *et al.*, 2005; Cabrera *et al.*, 2006; Kim *et al.*, 2009). The majority of the mantle is made up of α-cells, while δ-cells are located in the periphery

either between the α-cells, or between the β- and α-cells. The PP cells are found either isolated or in small clusters in the periphery of islets (Erlandersen *et al.*, 1976; Wieczorek *et al.*,1998). With regards to the composition of rodent islets between different regions of the pancreas, α- and PP-cells are indicated to be more abundant in the head section, while β- and δ-cells are more abundant in the tail section (Elayat *et al.*, 1995; Zafar & Mughal, 2002).

1.3 The functional role of the pancreas

The differences between species in terms of islet structure may be a result of the variation in the mechanisms involved in the development of the pancreas. However, both metabolic and physiological conditions are suspected to have a greater influence in defining the structure of the islets. *In vivo* experimental models have shown that conditions such as pregnancy and obesity can alter the structure of islets and increase β-cell mass (Steiner *et al.*, 2010). As previously mentioned, exocrine cells produce pancreatic digestive juices consisting of pancreatic enzymes produced and stored in secretory vesicles (known as zymogens) in the acinar cells, and an aqueous alkaline solution secreted by duct cells lining the pancreatic ducts. Following gastric digestion, duodenal acidification and entry of fatty acids or bile trigger the release of secretin hormone from the duodenal mucosa, while vagal stimulation and entry of fatty acids or amino acids trigger the mucosa to release the cholecystokinin (CCK) hormone. Secretin stimulates duct cell secretion and CCK stimulates exocytosis of pancreatic enzymes in acinar cells. These digestive juices travel through the pancreatic ducts and enter the duodenum via the major duodenal papilla (main pancreatic duct opening) or minor duodenal papilla (accessory duct opening) (Moore *et al.*, 2008; Steer, 2012; Puri *et al.*, 2015). The proteolytic enzymes (trypsinogen, chymotrypsinogen and procarboxypeptidase) are responsible for the breakdown of protein into amino acids and are secreted in their inactive forms. Enterokinase within the duodenum converts trypsinogen into active trypsin, which is then responsible for converting chymotrypsinogen and procarboxypeptidase into active chymotrypsin and carboxypeptidase, respectively. Amylase is responsible for the breakdown of carbohydrates or starch into glucose, and pancreatic lipase breakdown triglycerides (fats) into fatty acids and monoglycerides. In addition, bile produced by the gallbladder enters the duodenum through the major duodenal papilla where it emulsifies large fat molecules into smaller droplets, which are easier for lipase to digest (Sherwood, 2001;

Kaurich, 2008, Moore *et al.,* 2008). Figure 1.3 below illustrates a coronal section through the human pancreas.

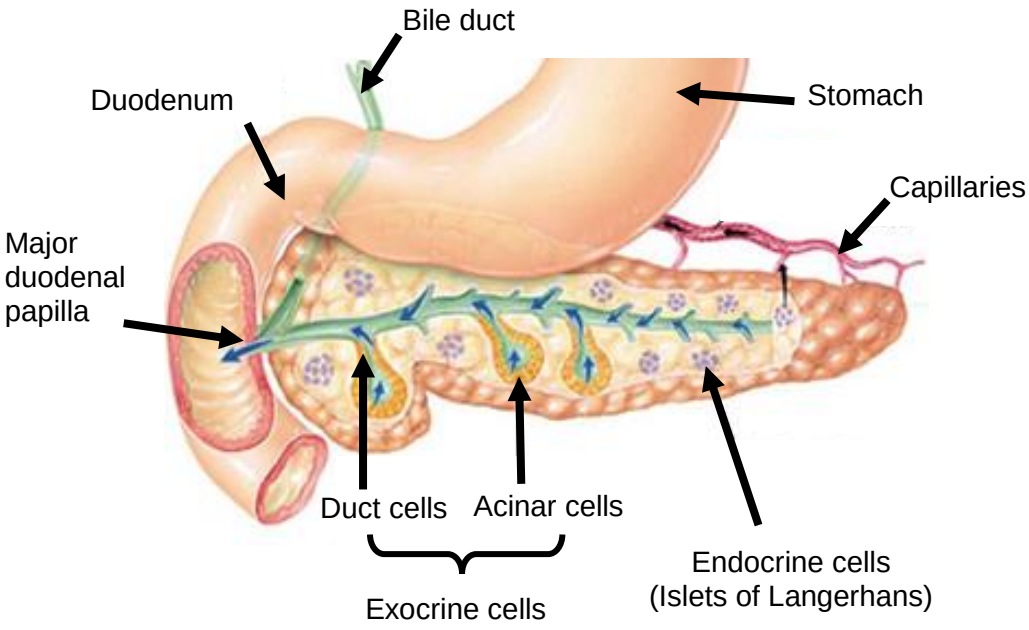

Figure 1.3: Exocrine and endocrine cells of the human pancreas. The exocrine pancreas secretes digestive juices into the duodenum which are composed of an aqueous alkaline solution secreted by the ductal cells and digestive enzymes secreted by the acinar cells. The endocrine pancreas (islets of Langerhans) secretes pancreatic hormones into the blood. Adapted from Sherwood (2001).

The islets of the pancreas produce and secrete the pancreatic hormones insulin, glucagon, somatostatin and PP. It is well known that insulin and glucagon regulate the body's blood glucose levels. While insulin secretion is primarily stimulated by glucose, it can also be stimulated by amino acids, other hormones and certain drugs (Robertson & Harmon, 2007; Puri *et al.*, 2015). Glucose enters β-cells via glucose transporter 2 (GLUT-2) and is metabolised into adenosine triphosphate (ATP), which consequently depolarises β-cells, causing calcium (Ca^{2+}) to enter the cell and promote exocytosis of insulin. Insulin increases the uptake of glucose, fatty acids and amino acids from the blood into the liver, skeletal muscles and adipocytes (Sherwood, 2001; Steer, 2012). When circulating levels of blood glucose reach abnormally low levels, insulin secretion ceases in order to prevent hypoglycaemia, which then triggers the secretion of glucagon (Robertson & Harmon, 2007; Hauge-Evans *et al.*, 2009). Glucagon is secreted in the post-absorptive state and mainly targets the liver, where it causes

increased glycogenolysis (glycogen breakdown) and gluconeogenesis (glucose production) via the cyclic adenosine monophosphate (cAMP) second messenger pathway, ultimately resulting in increased blood glucose levels. In addition, glucagon also leads to increased blood fatty acid levels by accelerating lipolysis (breakdown of adipocytes) (Sherwood, 2001; Jiang and Zhang, 2003; Rafacho *et al.*, 2014). The dysregulation of insulin and glucagon secretion is associated with both Type I and II diabetes. Type I diabetes is an autoimmune disease causing β-cell destruction and is associated with a low plasma insulin to glucagon ratio, promoting hyperglycaemia. Type II diabetes is associated with increased plasma concentrations of both insulin and glucagon, where over stimulation of insulin secretion as well as toxic glucose levels can cause damage to β-cells and patients may require insulin therapy (Steer, 2012).

Somatostatin is mainly produced and secreted by the gastrointestinal system, with the neuroendocrine cells of the central nervous system contributing a small portion (Hauge-Evans *et al.*, 2009). This hormone has a variety of functions within the body and can be secreted into the blood, synaptic clefts, and intercellular spaces (Arimura & Fishback, 1981). For the most part, somatostatin inhibits endocrine systems by suppressing growth hormone (GH) release from the anterior pituitary in the hypothalamus (Hauge-Evans *et al.*, 2009). In addition, somatostatin secreted by gut δ-cells inhibits the digestion of nutrients in the stomach, causing a decrease in nutrient absorption (Sherwood, 2001). Although δ-cells make up only a small portion of the islets, somatostatin produced by these cells influences glucose homeostasis. In contrast to the effects of insulin and glucagon within the body, somatostatin within the pancreas does not act on other organs. Rather, it inhibits both insulin and glucagon secretion through its paracrine effects, whereby both β-cells and α-cell express somatostatin receptors (Arimura & Fishback, 1981; Robertson & Harmon, 2007; Hauge-Evans *et al.*, 2009; Rafacho *et al.*, 2014). Since other organs produce the majority of somatostatin, pancreatic diseases are generally not associated with dysregulation of somatostatin (Steer, 2012)

PP is not only secreted by PP-cells of the islets, it is also released into circulation by the small and large intestines. PP has a wide variety of effects on the gastrointestinal tract, such as gastric motility, gallbladder contraction and stimulating secretion by

pancreatic islet cells (Wook et al., 2014). Low PP plasma levels are reported in obese patients, whereas high levels are reported in patients suffering from anorexia nervosa (Lassmann et al., 1980; Uhe et al., 1992). This is because PP suppresses both food intake and gastric emptying while increasing energy expenditure, thereby creating a negative energy balance (Sherwood, 2001; Kojima et al., 2007). This is achieved by PP inhibiting vagal nerve activity, as well as suppressing expression of both the feeding-stimulatory neuropeptides within the hypothalamus (involved in regulating food intake and body weight) and the gastric peptide ghrelin (involved in stimulating the appetite) (Asakawa et al., 2003). PP has the highest affinity for the neuropeptide Y4 (NPY4) receptor. This receptor is expressed in many organs, including the gastrointestinal tract, pancreas and hypothalamus, which further highlights its importance in regulating food intake. Recently, Wook et al. (2014) showed that apart from all somatostatin-containing cells in the nervous system, the NPY4 receptor is only expressed by the somatostatin-secreting δ-cells in the pancreas. This study illustrated that human islets treated with PP increased insulin secretion. Since NPY4 receptors are only expressed on δ-cell and somatostatin is a known inhibitor of insulin secretion, it is thought that PP acts by inhibiting δ-cell secretion, ultimately alleviating the inhibition of insulin secretion. These functions highlight the vital role of the pancreas in maintaining glucose homeostasis, producing and secreting critical digestive juices, and regulating the gastrointestinal tract during digestion. However, similar to other organs, the pancreas can be damaged by different stressors, including drugs such as Doxorubicin (DOX), a potent chemotherapeutic agent.

1.4 Doxorubicin

DOX forms part of a class of anti-cancer drugs known as anthracyclines (Misiti *et al.*, 2003), and together with Daunorubicin (DNR), was among the first anthracyclines to be discovered. In 1958, the anthracycline antibiotic DNR was isolated from a red pigment-producing bacterium *Streptomyces peucetius* in the south-eastern part of Italy and was found to display anti-tumour effects. It was only in 1969, near the Adriatic Sea, that DOX was isolated from a mutant of the original *Streptomyces* species, which explains DOX's alternative name (Adriamycin). DOX is currently commercially available and is produced by the *Streptomyces peucetius* subspecies *caesius* (Weiss, 1992; Lomovskaya *et al.*, 1999; Misiti *et al.*, 2003).

While DNR is highly effective in treating both acute lymphoblastic leukaemia and acute myeloblastic leukaemia, DOX, in addition to being highly potent against haematological malignancies, has been shown to be effective in treating a wide range of tumours, including breast cancer, sarcomas, lymphomas, as well as childhood malignancies (Minotti *et al.*, 2004; Štěrba *et al.*, 2011). DOX has been shown to be greatly effective against cancerous cells with a high proliferation rate (Yi *et al.*, 2006), and as such there are only a very few cancers that DOX is ineffective in treating (Weiss, 1992). Therefore, DOX remains the most widely used chemotherapeutic drug. Although effective, DOX has significant off-target toxicity, particularly in cardiomyocytes (Gewirtz, 1999).

1.4.1 Classification of Doxorubicin-induced cardiotoxicity

Cardiotoxicity is a well-known side effect of anthracycline treatment and refers to the damage induced on the heart by toxic substances, causing impaired cardiovascular function (Moulin *et al.*, 2015). DOX and DNR are among the most potent cardiotoxic agents, which have been shown to lead to the development and progression of heart failure in cancer survivors, and more so in patients with pre-existing heart disease, the elderly and children (Ghigo *et al.*, 2016).

Cardiotoxicity can be classified into three main categories, namely acute, chronic and delayed-onset cardiotoxicity. Acute toxicity occurs during or within a few minutes following DOX administration. Signs and symptoms of this form include cardiac arrhythmias, sinus tachycardia and electrocardiogram (ECG) alterations, which can last over 24 hours. These symptoms are minor and clinically manageable (Singal *et al.*, 1997; De Beer *et al.*, 2001; Barrett-Lee *et al.*, 2009; Octavia *et al.*, 2012). Chronic cardiotoxicity may occur within weeks, months or years after a patient's last dose of DOX, in which symptoms include dilated cardiomyopathy and decreased left ventricular ejection fraction that may eventually lead to chronic heart failure (Von Hoff *et al.*, 1979; Singal *et al.*, 1997; De Beer *et al.*, 2001; Octavia *et al.*, 2012). Delayed-onset cardiotoxicity may occur years to decades after DOX treatment. Although the clinical symptoms are not well defined in the literature, it is known that dilated or restrictive cardiomyopathy, as well as myocardial arrhythmias are clinical symptoms of delayed-onset cardiotoxicity (Bernaba *et al.*, 2010). This form of cardiotoxicity clinically manifests in patients over many years and is triggered by cardiovascular

stress, such as viral infections and pregnancy (Ali *et al.*, 1994; Sereno *et al.*, 2008). Additionally, delayed-onset cardiotoxicity has been described to occur mostly in childhood cancer survivors (Leandro *et al.*, 1994; Lipshultz *et al.*, 2008). Therefore, although DOX is an effective chemotherapeutic agent and has led to the increased survival rate of childhood cancer patients, there is an increased risk of these patients developing chronic cardiotoxicity (Harake *et al.*, 2012; Ezquer *et al.*, 2015).

Both chronic and delayed cardiotoxicity are dose dependent and result in detrimental changes that are often irreversible (Gewirtz, 1999; Misiti *et al.*, 2003; Oliveira *et al.*, 2013). When administered intravenously to cancer patients, the distribution half-life of DOX in the plasma is between 3 - 5 minutes, highlighting DOX's rapid uptake into cells, while its terminal half-life is between 24 – 36 hours, suggesting that DOX takes a longer time to be eliminated from tissues (Zheng *et al.*, 2006). The incidence of DOX-induced cardiotoxicity rapidly increases above the cumulative dose of 550 mg/m^2, thus, the recommended lifetime cumulative dose of DOX for cancer patients ranges between 450 – 500 mg/m^2 (Von Hoff *et al.*, 1979; Yeh *et al.*, 2009; Warpe *et al.*, 2015). Although reducing the cumulative dose of DOX has been shown to reduce acute cardiotoxicity, there has been no significant decrease in late-onset cardiac complications reported, thus, there is no established dose of DOX deemed reasonably safe (De Angelis *et al.*, 2016). As such, the leading cause of death amongst cancer survivors is now cardiovascular disease (Ghigo *et al.,* 2016).

While major efforts have been made to produce anthracycline analogs that are less toxic to the heart, only a few have been approved for clinical use (Figure 1.4). The chemical structures of DOX and DNR are almost identical. Both contain an aglyconic moiety (known as doxorubicinone), consisting of tetracyclic rings that contain quinone-hydroquinone moieties, and a sugar moiety (known as daunosamine), which is attached by a glycosidic bond at carbon number 7 (C7). The difference between these analogs is that the side chain of DOX ends with a primary alcohol, while DNR ends with a methyl group (Minotti et al., 2004; Sies & Packer, 2004). Although minor, these structural differences play a major role in the efficacy of these two drugs against cancerous cells. Epirubicin (EPI) is a semi-synthetic derivative of DOX, where the hydroxyl group at carbon number 4 (C4) in the sugar moiety undergoes a positional change. Idarubicin (IDA) is derived from DNR, in which the 4-methoxy group is removed at C4 in the doxorubicinone moiety. Although EPI and IDA have been

clinically approved and have been used as alternative chemotherapeutic agents to DNR and DOX in the clinical setting, they are less potent in killing cancerous cells than DNR and DOX and are also cardiotoxic (Minotti *et al.*, 2004; Šimůnek *et al.*, 2009).

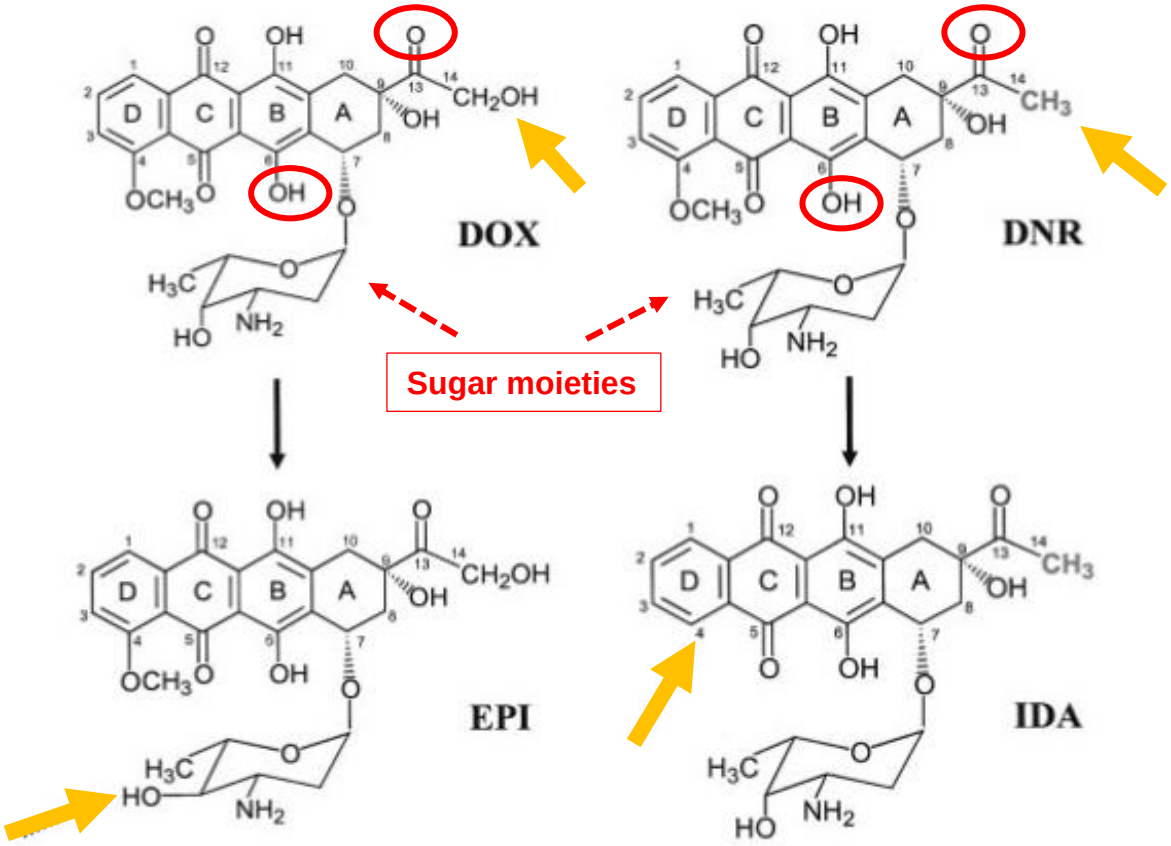

Figure 1.4: The chemical structures of DOX and is derivatives. The chemical structures of the four anthracycline analogs used in the clinical setting. Anthracyclines are composed of an aglyconic moiety, consisting of tetracyclic rings (indicated as A-D) that contain quinone-hydroquinone moieties (indicated by red circles). The sugar moiety is attached by a glycosidic bond to the aglyconic moiety at C7. The difference in these analogs are in the side chains (indicated by orange arrows). Abbreviations: DOX (Doxorubicin), DNR (Daunorubicin), EPI (Epirubicin), IDA (Idarubicin), C7 (carbon number 7). Adapted from Minotti *et al*. (2004).

1.5 Doxorubicin's mechanism of action

The mechanisms by which DOX kills cancer cells are different to the mechanisms involved in cardiotoxicity (Myers, 1998), therefore this review will only focus on the cardiotoxic effects of DOX. It should be noted that the exact underlying mechanisms involved are yet to be fully elucidated.

1.5.1 Doxorubicin-induced oxidative stress

The most common and frequently reported mechanism of DOX-induced cardiotoxicity is the generation of free radicals including reactive oxygen species (ROS), which causes oxidative stress and oxidative damage. Oxidative stress is a physiological condition that results when the balance between free radicals and anti-oxidants in the cell is disturbed, and the generation of free radicals exceeds the ability of anti-oxidants, leading to oxidative damage (Asensi *et al.,* 1999; Mizutani *et al.*, 2003, Rahman, 2007). DOX can generate free radicals in two ways, either via enzymes in the mitochondrial respiratory chain, or via enzyme-independent pathways involving transition metals such as iron (Fe). Since DOX contains both quinone and hydroquinone moieties within its structure (Figure 1.4), it can be both oxidised and reduced to generate free radicals (Figure 1.5). More specifically, the quinone residue of DOX is reduced by oxidoreductases in the mitochondria, namely mitochondrial reduced nicotinamide adenine dinucleotide (NADH) dehydrogenase (Davies & Doroshow, 1986), NAD(phosphate) (NADPH)-dependant carbonyl reductase (Olson *et al.*, 1988), complex I of the mitochondrial respiratory chain (Goormaghtigh *et al.*, 1987), and membrane-bound cytochrome P450 reductase (Kostrzewa-Nowak *et al.*, 2005). This process occurs via a one-electron transfer in the presence of NAD(P)H to form the semiquinone radical. In the presence of oxygen (O_2), the semiquinone radical donates its unpaired electron to form superoxide radicals ($O_2^{\bullet -}$), which are dismutated by superoxide dismutase (SOD) to form hydrogen peroxide (H_2O_2). The semiquinone radical can also react with H_2O_2 to form hydroxyl radicals ($OH^{\bullet}$) that can damage deoxyribonucleic acid (DNA), proteins and lipids. Alternatively, the semiquinone radical is able to accept electrons back, regenerating the DOX parent structure. This series of reactions is termed “redox cycling” and emphasises the fact that a small concentration of DOX is able to generate large amounts of free radicals (Goodman & Hochstein, 1977; Kalyanaraman *et al.*, 2002; Minotti *et al.*, 2004).

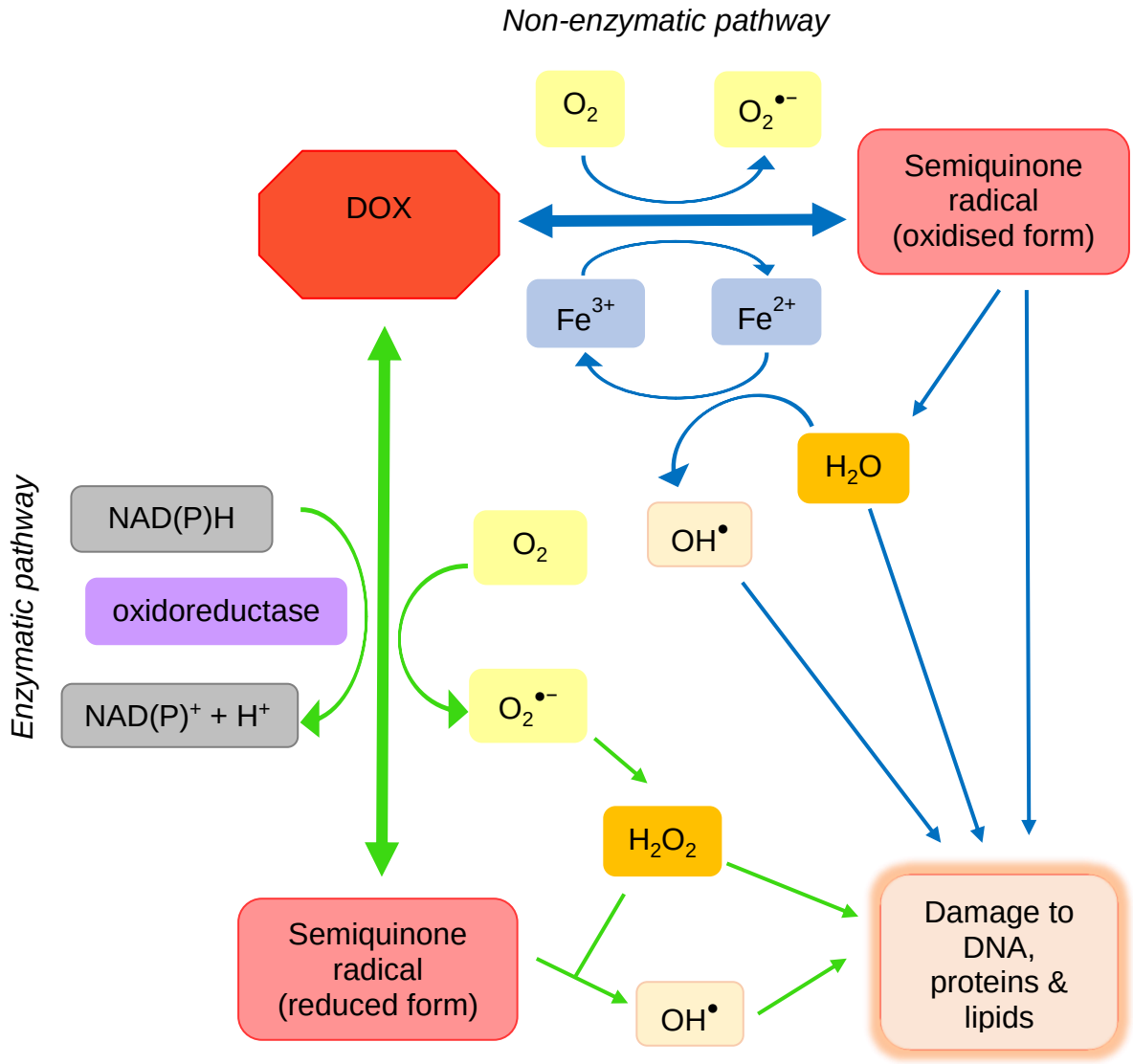

Figure 1.5: The proposed mechanisms involved in DOX-induced oxidative stress. DOX can generate free radicals in two ways, either via enzymes in the mitochondrial respiratory chain (indicated in green arrows), or via enzyme-independent pathways involving transition metals such as iron (Fe) (indicated in blue arrows). These free radicals cause damage to DNA, proteins and lipids within cells. Abbreviations: DOX (Doxorubicin), NAD(P)H (reduced nicotinamide adenine dinucleotide (phosphate)), $NAD(P)^+$ (oxidised NAD(P)H), H^+ (proton), O_2 (oxygen), $O_2^{\bullet-}$ (superoxide radicals), H_2O_2 (hydrogen peroxide), $OH^\bullet$ (hydroxyl radicals), Fe^{3+} (ferric ion), Fe^{2+} (ferrous iron).

The second way that DOX can generate free radicals is via non-enzymatic pathways involving Fe. $O_2^{\bullet-}$ generation by DOX is able to release Fe from Fe-containing centres of molecules, causing an increase in intracellular free Fe levels. DOX is able to chelate Fe and form complexes, which in turn react with O_2 to form ROS, contributing to oxidative stress (Beckman & Ames, 1998; Ghigo *et al.*, 2016). The Fe-catalysed

Haber-Weiss reaction is a two-step process, in which the first step of the reaction involves the reduction of ferric ion (Fe^{3+}) to ferrous ion (Fe^{2+}). The second step of the reaction, known as the Fenton reaction, involves the reaction of this newly formed Fe^{3+} and H_2O_2 to form the highly toxic $OH^{\bullet}$ (Bredehorst *et al.,* 1987) (Figure 1.5). In addition, H_2O_2 can combine with free Fe to form perferryl iron (Fe^{IV}=O), in which both $OH^{\bullet}$ and Fe^{IV}=O are potent oxidants that cause irreversible cell damage by inactivating key proteins and enzymes located within the sarco(endo)plasmic reticulum (ER) and mitochondrial respiratory chain (Keizer *et al.*, 1990; Kalyanaraman *et al.*, 2002; Šimůnek *et al.*, 2009).

Additionally, free intracellular Fe levels are tightly regulated by the storage molecule, ferritin, and the receptor, transferrin, both of which play a role in controlling the interaction between iron-regulatory proteins (IRPs) and specific iron-responsive elements (IREs) located within genes (Šimůnek *et al.*, 2009; Montaigne *et al.*, 2012). The formation of DOX-Fe complexes reduces the amount of free Fe that is available to bind to IRPs. Therefore, IRPs sense a decrease in intracellular free Fe and respond by binding to IREs. Ferritin expression is downregulated and transferrin receptors are upregulated, resulting in increased free Fe levels. However, this consequently means that more Fe is available to bind to DOX, contributing to free radical generation and subsequent cellular damage (Kalyanaraman *et al.*, 2002; Montaigne *et al.*, 2012, Ghigo *et al.,* 2016).

1.5.2 Doxorubicin-induced cell death

Apoptosis is a form of programmed cell death (cellular suicide) that is a crucial physiological process responsible for removing damaged, redundant and mutated cells from tissues. Dysregulation of apoptosis in cells can lead to pathophysiological disorders (Jones & Gorges, 1997; Ellerby & Bredesen, 2000). Apoptotic signals include oxidative stress and cytotoxic agents such as DOX, where studies have demonstrated DOX-induced cell death as a result of oxidative stress in endothelial cells and cardiomyocytes (Sawyer *et al.*, 1999; Kotamraju *et al.*, 2000). This can occur as a result of DOX's ability to activate both the extrinsic and intrinsic apoptotic pathways (Figure 1.6). DOX can initiate apoptosis both indirectly and directly through ROS generation and by inducing mitochondrial leakage of cytochrome c, respectively (Lee et al., 2002; Nitobe et al., 2003; Tsang et al., 2003; Kim et al., 2006; Zhang et al.,

2012). The extrinsic apoptotic pathway, or death receptor pathway, involves the activation of pro-apoptotic ligands and cell surface receptors (Crompton, 2000). The binding of death ligands to cell receptors from the tumour necrosis factor (TNF)-receptor family results in the proteolytic activation of caspases, the executioners of apoptosis and inter-nucleosomal DNA fragmentation (Nagata, 1997). One of the most important regulators of the extrinsic apoptotic pathway in many organisms is the Fas/Fas ligand system, in which Fas is a member of the TNF-receptor family that is expressed in a variety of tissues. The binding of Fas ligand to the Fas receptor results in the formation of a homotrimetric complex that recruits the Fas-associated death receptor domain (FADD), ultimately leading to the activation of caspases downstream (Yonehara, 1989; Suda *et al.*, 1993; Nagata, 1997; Tolosa *et al.*, 2005). Studies investigating DOX-induced toxicity have reported overexpression of Fas ligand and high levels of TNF-α in cardiomyocytes suggesting induction of the extrinsic apoptotic pathway (Krown *et al.*, 1996; Nakamura *et al.*, 2000; Gustafsson & Gottlieb, 2003).

The intrinsic apoptotic pathway is characterised by the release of cytochrome c from the mitochondria, which enters the cytosol and activates caspases (Crompton, 2000). This release is triggered by mitochondrial depolarisation which can occur either via B-cell lymphoma 2 associated X protein (Bax) and Bax/Bcl-2 homologous antagonist/killer (Bak) activation, or opening of the mitochondrial permeability pore (mPTP). Bax and Bad are pro-apoptotic proteins located in the cytosol. Following stress signals, these proteins undergo conformational changes and form a pore in the outer mitochondrial membrane, subsequently depolarising the mitochondria. Both ROS and increased intra-mitochondrial Ca^{2+} can stimulate opening of the mPTP. Cytochrome c in the cytosol forms an apoptosome complex with apoptosis protease protein-1 (Apaf-1) and caspase-9, leading to the proteolytic activation of caspase-3 (Tsujimoto, 1998; Minotti *et al.*, 2004; Saelens *et al.*, 2004; Kim *et al.*, 2006; Parrish *et al.*, 2013). Caspase-mediated apoptosis is accomplished through the cleavage of several cell survival proteins, where activated caspase-3 cleaves poly (adenosine diphosphate-ribose) polymerase-1 (PARP-1), a nuclear enzyme involved in DNA repair and transcriptional regulation (Kaufmann *et al.*, 1993; Tewari *et al.*, 1995; Fischer *et al.*, 2003; Poirier *et al.*, 2002; Chaitanya *et al.*, 2010). Additionally, activation of tumour suppressor protein p53 has also been implicated to induce apoptosis. p53 is responsible for the upregulation of genes involved in DNA repair and cell cycle

arrest, and in conditions where oxidative stress levels are high, p53 augments Bax (pro-apoptotic) and attenuates Bcl-2 (anti-apoptotic), thereby inducing apoptosis (Minotti *et al.*, 2004; Yee & Vousden, 2005; Kim *et al.*, 2006; Liu *et al.*, 2008).

It is believed that DOX's ability to activate the intrinsic apoptotic pathway occurs as a result of DOX binding to, and depolarising, the mitochondria. It is well known that DOX has a high affinity for cardiolipin, a phospholipid involved in the maintainance of the electro-chemical gradient of the electron transport chain during ATP synthesis (Goormaghtigh *et al.*, 1990; Harake *et al.*, 2012). This phospholipid is closely associated with the inner mitochondrial membrane and is required for optimal activity of oxidative phosphorylation complexes. In addition, ROS can cause oxidation of cardiolipin, triggering the release of cytochrome c into the cytosol either through the mPTP or Bax/Bak pore (Kim *et al.*, 2006; Pereira *et al.*, 2011; Zhang *et al.*, 2012; Paradies *et al.*, 2014). Interestingly, although free radicals, particularly H_2O_2, contribute to the opening of mPTP, studies show H_2O_2 formation precedes both the loss of mitochondrial membrane integrity and caspase-3 activation during DOX-mediated apoptosis (Kroemer *et al.*, 1997; Hampton *et al.*, 1998; Chandra *et al.*, 2000; Mizutani *et al.*, 2005).

It was initially believed that DOX only indirectly induced apoptosis through ROS generation (Wang *et al.*, 2002; Nitobe *et al.*, 2003), however, it has since been demonstrated that DOX can in fact initiate apoptosis directly by stimulating the opening of Ca^{2+} channels (Zorzato *et al.*, 1985) and inhibiting the sodium-calcium (Na^+/Ca^{2+}) exchanger (Caroni *et al.*, 1981) on the ER, resulting in disruption of Ca^{2+} homeostasis (Kim *et al.*, 2006; Octavia *et al.*, 2012; Zhang *et al.*, 2012). This results in an increase in cytosolic Ca^{2+} concentration, which in itself promotes ROS formation through Ca^{2+}-sensitive ROS-generating enzymes (Zhang *et al.*, 2009). Since the ER is closely associated with mitochondria, the intra-mitochondrial Ca^{2+} levels rise, stimulating mPTP opening (Olson *et al.*, 1974; Brookes *et al.*, 2008; Williams *et al.*, 2013).

However, the type of cell death that results from DOX treatment depends on both the dosage and duration of treatment (Tacar *et al.,* 2013). Since cardiolipin is involved with the electron transport chain and ATP production, DOX can interfere with these processes. With depletion of ATP and mPTP opening, the structural and functional integrity of the cell cannot be maintained, resulting in mitochondrial swelling,

irreversible cellular damage and ultimately, necrotic cell death (Montaigne *et al.*, 2012). Necrotic cell death is an uncontrolled process, characterised by disruption of the cell membrane, reduced ATP, and cell swelling (Gustafsson & Gottlieb, 2003). Considering all of the above, it is clear that DOX is a toxic agent that causes major damage to the cell and its organelles and thus similar events are likely to occur in the pancreas, however, there is a lack of studies investigating this.

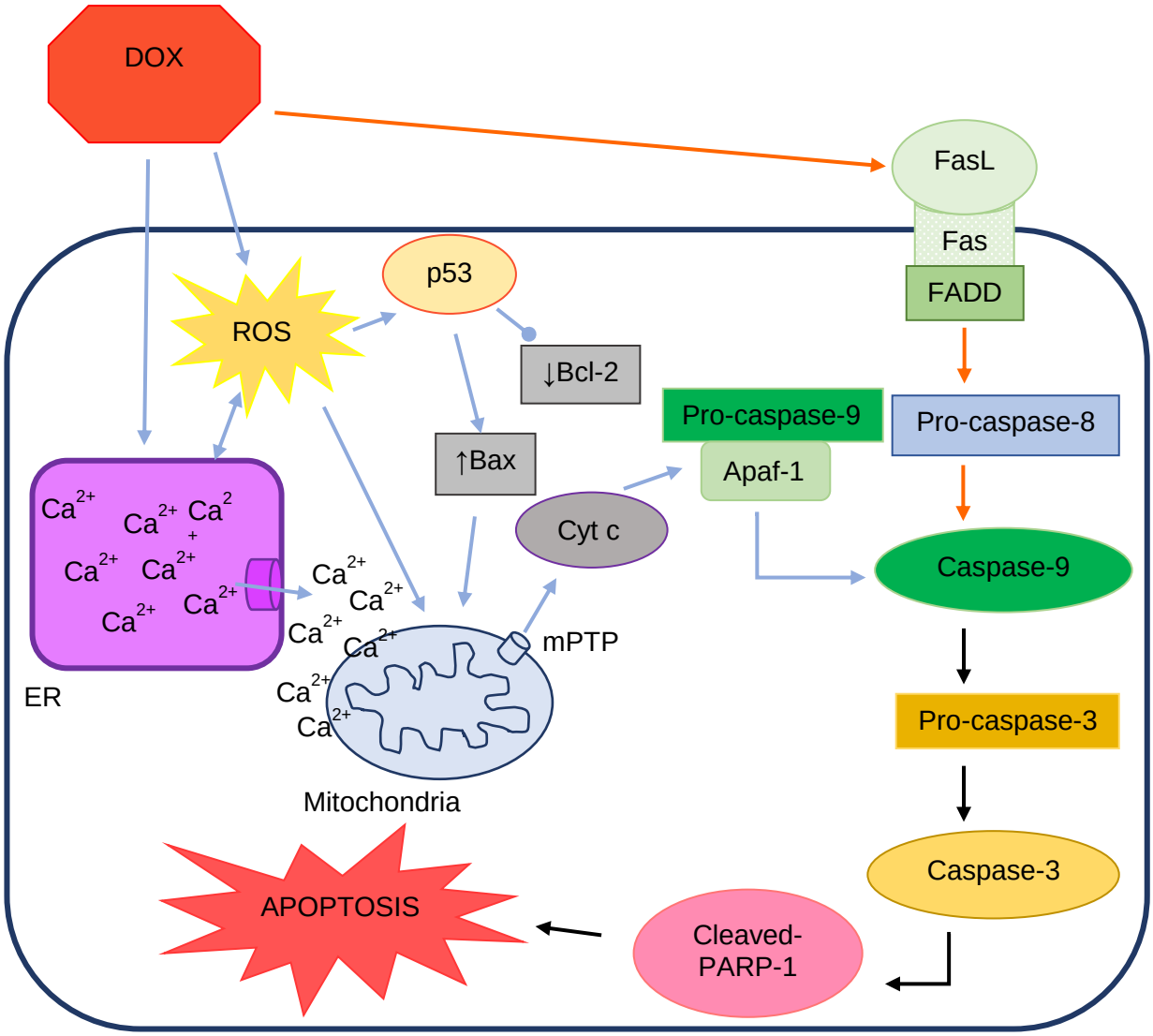

Figure 1.6: Doxorubicin-induced apoptosis through both the intrinsic and extrinsic apoptotic pathways. DOX initiates the extrinsic apoptotic pathway (indicated with black arrows) via the death receptor pathway (such as Fas/FasL system). Binding of FasL to its receptor ultimately leads to the activation of the caspases downstream. DOX can initiate the intrinsic apoptotic pathway (indicated with light blue arrows) through ROS generation, which affects Ca^{2+} homeostasis within the ER and activates the tumour suppressor protein p53, leading to opening of the mPTP, Cyt c leakage, and activation of caspases. Abbreviations: DOX (Doxorubicin), ROS (reactive oxygen species), Bax (Bcl-2 Associated X protein), Bcl-2 (B-cell lymphoma family protein 2), FasL (Fas ligand), Fas (Fas receptor), FADD (Fas associated protein with death domain), ER (sarco(endo)plasmicreticulum), mPTP (mitochondrial permeability transition pore), Cyt c (cytochrome c), Apaf-1 (apoptosis protease protein-1), Cleaved-PARP-1 (cleaved-poly (adenosine diphosphate-ribose) polymerase-1), round arrow head (inhibits), → (leads to),↑ (increases), ↓ (decreases).

1.6 Pancreatic cell death and inflammation

The type of cell death that occurs during pancreatic cell injury can influence the extent of inflammation. Pancreatitis is an inflammatory disorder of the pancreas resulting from acinar cell damage and can be classified as acute or chronic. Acute pancreatitis is associated with leakage of pancreatic digestive enzymes from acinar cells, while chronic pancreatitis is associated with atrophy of acinar cells and fibrotic replacement of organ architecture (Jones & Gorges, 1997). The severity of inflammation is directly proportional to the extent of necrosis and inversely proportional to the extent of apoptosis in the acinar cells (Kaiser *et al.*, 1995) (Figure 1.7). The magnitude of necrosis is dependent on neutrophil recruitment to the pancreas following injury, where neutrophils can shift acinar cell death from apoptosis to necrosis (Sandoval *et al.*, 1996). This limits neutrophil recruitment to the site of injury, and thereby prevents the shift from apoptosis to necrosis which could potentially ameliorate the severity of pancreatitis (Jones & Gorges, 1997).

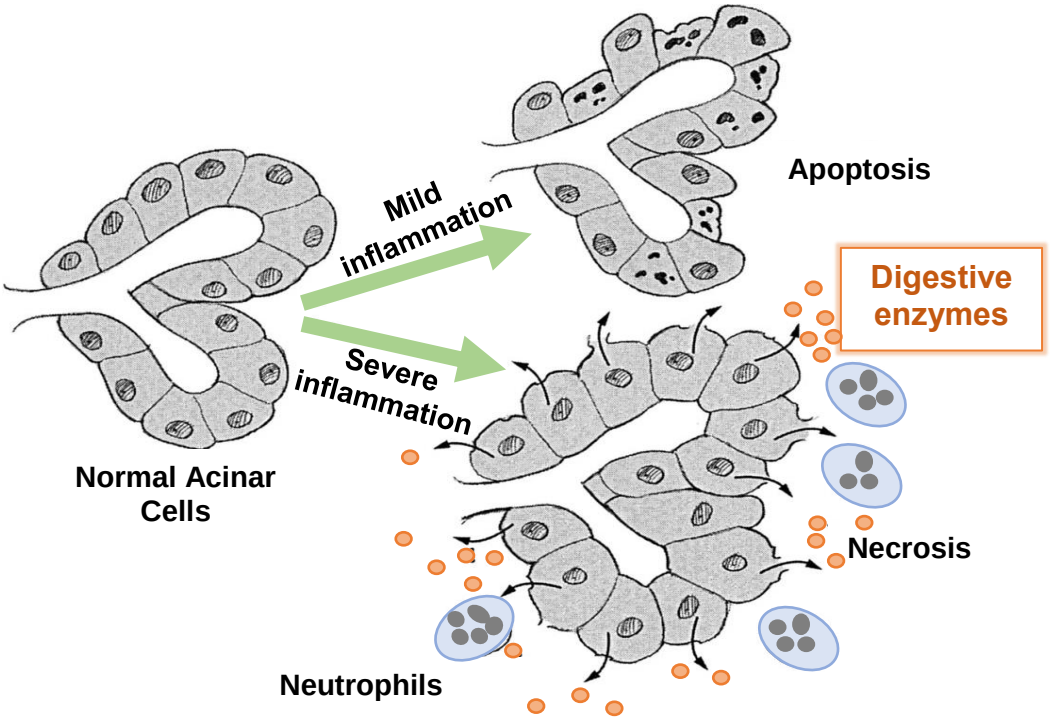

Figure 1.7: Apoptotic or necrotic cell death of acinar cells in the pancreas. During pancreatic injury, apoptotic cell death is associated with reduced tissue damage and mild inflammation, while necrotic cell death is associated with neutrophil infiltration and severe inflammation. Adopted from Jones & Gorges (1997).

1.6.1 Causes and mechanisms involved in pancreatitis

Acute pancreatitis has been associated with pancreatic duct obstruction (by gallstones, or Ca^{2+} granules and muco-glycoproteins), alcohol abuse, idoipathic factors (in which the cause is unknown and could be related to anatomical abnormalities or metabolic disturbances) and other factors (including certain drugs). However, the pathophysiology underlying drug-induced pancreatitis is yet to be established (Salvador *et al.*, 2014; Granger & Remick, 2005; Matull *et al.*, 2006; Bachmann *et al.*, 2011; Lankisch *et al.,* 2015).

Irrespective of the mechanism, obstruction or damage to pancreatic ducts can hinder exocytosis of digestive enzymes contained in zygomens within acinar cells. These zygomen vesicles consequently merge with cellular lysosomes and form autophagic-like vacuoles that contain both digestive and lysosomal enzymes. The lysosomal enzyme, cathepsin B, is able to activate trypsin, subsequently leading to the activation of other digestive enzymes. These vacuoles are released into the intersitial spaces and cause auto-digestion of pancreatic tissue, leading to consequent pancreatic injury and stimulation of the inflammatory response (Jones & Gorges, 1997; Kaurich, 2008). Furthermore, Ca^{2+} acts as a signalling molecule in acinar cells that has a critical role in controlling secretion of digestive enzymes. Prolonged elevation of intracellular Ca^{2+} (triggered by various stimuli, including oxidative stress) can lead the development of pancreatitis, where inappropriate activation and overproduction of digestive enzymes can result in pancreatic damage, which triggers an inflammatory response (Tonsi *et al.*, 2009; Li *et al.*, 2014; Lankisch *et al.*, 2015).

It has been shown that the inflammatory response can be stimulated independently of trypin activation. New insights indicate that trypsin activation is only associated with the development of acute pancreatitis, whereas chronic pancreatitis develops independently of this activation. The causal factors of chronic panceatitis are believed to be similar to those of acute pancreatitis as it usually evolves from acute pancreatitis. The exact underlying mechanisms are however unknown. Although alcohol abuse is described as a major cause of chronic pancreatitis, only a small percentage of alcoholics develop this condition, therefore suggesting that other factors are involved (Yamamoto *et al.,* 2006; Lankisch *et al.*, 2015). In most patients, local inflammation of the pancreas can be rectified before becoming severe. Unfortunately, in a small

percentage of patients in which the local inflammatory response is not controlled, systemic inflammation develops, ultimately leading to multiple organ damage (Granger & Remick, 2005; Matull *et al.*, 2006; Tonsi *et al.*, 2009). Prolonged and continuous inflammation within the pancreas contributes to the development of chronic pancreatitis and irreversible morphological alterations result, in which fibrosis is a major characteristic. Damage to β- and α-cells can also lead to pancreatic disorders, including diabetes (Bachmann *et al.* 2011; Steer, 2012; French & Charnely, 2016).

Sustained activation of the nuclear factor kappa-light-chain-enhancer of activated B cells (NF-κB) pathway has been reported to be implicated in the development of chronic pancreatitis (Raghuwansh *et al.,* 2013). NF-κB is an important transcription factor that mediates the orchestration of inflammatory molecules by controlling their gene expression (Baeurle & Baichwal, 1995; Wulczyn *et al.*, 1996; Ghosh *et al.*, 1998). NF-κB remains inactive in the cytoplasm of resting cells. Incoming signals such as oxidative stress and inflammatory cytokines at the cell surface trigger the hyperphosphorylation of inhibitory-kappa-B (IκB) proteins, including IκB-alpha (IκBα) and B-cell lymphoma 3-encoded (Bcl-3) proteins, allowing the release of NF-κB, where it translocates into the nucleus and stimulates gene transcription (Altavilla *et al.*, 2003). Studies have demonstrated the role of NF-κB in cerulein-induced pancreatitis, where downregulation of NF-κB significantly protected the pancreas against damage by reducing various inflammatory cytokines (Gukovsky *et al.*, 1998; Steinle *et al.*, 1999). Pancreatitis can also be attributed to oxidative stress, where oxidative stress does not only damage the pancreas directly, but also activates NF-κB and stimulates the inflammatory cascade (Schreck *et al., 1*991). Powerful anti-oxidants such as vitamin E are known to reduce oxidative stress and consequently lead to NF-κB inhibition (Hattori *et al.*, 1995; Altavilla *et al.*, 2001).

In the context of DOX, acute pancreatitis is a potential side effect induced by this chemotherapeutic agent (Saleh & Ali, 2015). However, there are major flaws in the cases reporting a link between DOX treatment and the development of pancreatitis. Firstly, investigators in these cases did not eliminate the more common causes of acute pancreatitis, including gallstones and alcohol abuse. Secondly, in some cases DOX was administered in combination with other medications (Badalov *et al.*, 2007). Despite this, DOX is listed as one of the drugs that is implicated in causing pancreatitis

and further investigations are needed to elucidate the effects of DOX on the development of pancreatitis (Trivedi & Pitchumoni, 2005; Kaurich, 2008).

1.6.2 Diagnosing pancreatitis

The most commonly used biomarker for the diagnosis of acute pancreatitis is serum amylase, however its sensitivity can be influenced by chronic alcoholism and hypertriglyceridemia. Serum interleukin 6 (IL-6) and C-reactive protein (CRP) are two other inflammatory associated cytokines used to predict acute pancreatitis in patients. Serum IL-6 levels can be detected between 12 and 24 hours after a patient is admitted to hospital, and peak before CRP levels (Matull *et al.*, 2006). Although IL-6 is sensitive enough to be used to detect early acute pancreatitis, its concentration in the serum rapidly declines, and thus limits its use in the clinical setting (Pezzilli *et al.*, 1999; Matull *et al.*, 2006). Plasma TNF-α levels can also be detected early during acute pancreatitis. To support the role of the TNF-α/NF-kB signalling pathway during pancreatitis, NF-κB knockout mice demonstrated reduced TNF-α levels, leukocyte accumulation, and consequently reduced tissue damage. However, TNF-α has a short half-life in the serum which should be taken into account when measuring its serum levels (Altavilla *et al.*, 2003).

1.7 Fibrosis within the pancreas

As previously described, chronic pancreatitis is characterised by continuous and progressive fibrosis in the pancreas, though the exact mechanism underlying fibrosis remains unknown (Kozak *et al.*, 2016). Repairing injured tissues is a complex process that results in the deposition of extracellular matrix (ECM) proteins by fibroblasts, and although deposition of these proteins is usually temporary, repeated tissue injury seen in chronic pathologies can lead to fibrosis and, ultimately, organ dysfunction (Meneghin & Hogaboam, 2007; Wynnand & Ramalingam, 2012). There are usually four overlapping stages of tissue repair, namely haemostasis, inflammation, proliferation and remodelling, in which many cells play a role in each phase (Guo & DiPietro, 2010). During haemostasis and inflammation, platelets secrete cytokines, including platelet-derived growth factor (PDGF) and transforming growth factor-beta1 (TGF-β1). These cytokines recruit white blood cells (macrophages, neutrophils and natural-killer cells) to the injured site which remove debris and dead cells, while simultaneously releasing more cytokines that simulate fibroblast activation and

proliferation, leading to ECM protein production (Koh & DiPietro, 2011). Macrophages release TGF-β1, TNF-α and interleukin 1-beta (IL-1β) cytokines which promote differentiation and proliferation of fibroblasts into active fibroblasts, and supresses the production of key degradative enzymes of ECM proteins, such as matrix metalloproteinases (MMPs), ultimately leading to the replacement of damaged cells by fibrotic tissue (Petrov *et al.,* 2002; Hall *et al.*, 2003; Wynnand & Ramalingam, 2012; Midgley *et al.*, 2013).

Tissue injury and inflammation increase ROS generation, and TNF-α can promote the accumulation of leukocytes within the pancreatic tissue, causing further inflammation and organ injury (Altavilla *et al.*, 2003; Shroff, Mamalis and Jagdeo, 2014). As inflammation and oxidative stress cannot be easily separated, increased ROS production has also been implicated to have a role in pancreatic parenchyma destruction, leading to fibrosis (Angelino *et al.*, 2015; French & Charnely, 2016). Under stress conditions, over-activity of hepatic detoxification enzymes generate ROS in bile, which can undergo reflux up the pancreatic duct, and damage the pancreatic tissue. In addition, repeated cycles of inflammation and necrosis can result in necrosis-induced fibrosis (French & Charnely, 2016).

Stellate cells in the liver play a critical role in fibrogenesis and are the main producers of collagen as well as other ECM proteins. Similar cells have been identified in the pancreas, termed pancreatic stellate cells (Haber *et al.*, 1999). In a healthy pancreas, these cells are described as having characteristic intracellular lipid droplets, and are located in the peri-acinar spaces with long cytoplasmic extensions that encircle the base of pancreatic acini. Quiescent, pancreatic stellate cells stain positively for desmin, an intermediate cytoskeletal filament protein, and active pancreatic stellate cells stain positively for alpha-smooth muscle actin (α-SMA), a cytoskeletal protein (Haber *et al.*, 1999; Kishi *et al.*, 2003). While the mechanisms involved in pancreatic fibrosis remain to be elucidated, both human and experimental studies demonstrate that persistent activation of pancreatic stellate cells is involved in chronic pancreatitis development, where these cells are the major source of collagen (Kozak *et al.*, 2016). Moreover, the degree of lymphocyte infiltration correlates with the severity of pain experienced by patients (French & Charnely, 2016). Activated pancreatic stellate cells are responsive to pro-fibrotic cytokines PDGF and TGF-β1, where in response to PDGF, pancreatic stellate cells increase proliferation, and in response to TGFβ1,

these cells increase collagen synthesis, contributing to fibrosis (Kishi *et al.*, 2003; Haber *et al.*, 1999). In an *in vivo* model of pancreatic duct ligation-induced fibrosis α-SMA and collagen Type I expression was weak on day 7 with very little fibrosis visible. On the tenth day, α-SMA expression was elevated and fibrosis was shown to be significantly increased, illustrating the relationship between pancreatic stellate cell activation and fibrosis induction. Since α-SMA and collagen Type I were modestly expressed prior to fibrosis, this implies that pancreatic stellate cell activation precedes fibrogenesis. With regards to the fate of quiescent pancreatic stellate cells after ligation, desmin-positive pancreatic stellate cells still existed and somewhat increased in the interlobular areas even on the tenth day following ligation when pancreatic stellate cells had already been activated and fibrosis was evident (Kishi *et al.*, 2003).

1.8 Toxicity of Doxorubicin is not limited to the heart

As mentioned previously, DOX is an effective and potent anti-cancer drug, however, it is associated with severe side effects. While literature has mainly focused on the damaging effects induced by DOX on the heart, very few studies have investigated DOX's effect on pancreatic function. Rodent studies have indicated a strong correlation between DOX and elevated blood glucose and triglyceride levels, as well as dysregulation of adipocyte and muscle metabolism (Arunachalam *et al.*, 2013; Biondo *et al.*, 2016; De Lima Junior *et al.*, 2016). While chemotherapeutic drugs have been suggested to lead to the development of diabetes in patients, the direct link between DOX and diabetes in the clinical setting is yet to be determined (Feng *et al.*, 2013). Glucose-stimulated insulin secretion is a hallmark of β-cell function and *in vitro* studies previously showed that DOX inhibited glucose-stimulated insulin secretion in rat β-cells (DeLeers & Goormaghtigh, 1985; Dispenzieri & Loprinzi, 1997; Geetha *et al.*, 1999), although the mechanisms involved remain to be elucidated. In addition, DOX was shown to induce apoptosis in isolated β-cells by increasing pro-apoptotic Bax and decreasing anti-apoptotic Bcl-2, resulting in increased cytochrome c release and caspase-3 activation (Zhang *et al.*, 2007). Recently Heart *et al.* (2016) demonstrated that DOX was highly toxic to isolated murine islets and β-cells, even at doses less than that which is administered to patients. This study further elucidated that DOX damaged DNA, causing upregulation of p53 and ultimately activation of caspase-3. Although the use of caspase inhibitor, Z-VAD-FMK, protected the β-cells temporarily at a range of DOX doses, it was unable to prevent the loss of cell viability.

DOX may cause similar damage to streptozotocin, a well-known toxin of β-cells, where damage to these cell membranes causes insulin release and subsequent cell death. Based on the above, it is clear that more research is required to elucidate the exact mechanisms involved in DOX toxicity within the pancreas in order to not only assess the risk of patients undergoing treatment, but also to find and develop protective agents against potential DOX-induced pancreatic damage.

1.9 Protective agents used against Doxorubicin-induced damage

As DOX toxicity is associated with elevated oxidative stress, many studies have concentrated on reducing oxidative stress in an effort to reduce the consequent damage. The first anti-oxidant that was reported to reduce DOX-induced oxidative stress was alpha-tocopherol (Vitamin E). While vitamin E reduced oxidative stress, it was unable to prevent mitochondrial dysfunction caused by chronic DOX treatment (Berthiaume *et al.*, 2005). Vitamin E administered in combination with DOX prevented damage to visceral organs, including the heart, liver, testes and kidneys (Shivakumar *et al.*, 2012). Synthetic aminothiol (N-(2-mercaptopropionyl glycine) has been shown to exhibit anti-oxidative properties that may prevent acute cardiotoxicity in rats (El-Missiry *et al.*, 2001), and amlodipine, a Ca^{2+} channel antagonist with potent anti-oxidant activity, was shown to inhibit DOX-induced apoptosis in cardiomyocytes (Yamanaka *et al.*, 2003). Despite these powerful anti-oxidants, very little evidence exists to support the notion that anti-oxidants and other anti-oxidant like synthetic drugs are able to fully prevent DOX's off-target toxicity.

Since DOX can react with free Fe to generate free radicals, the ability of Fe-chelators to remove excess free Fe has been investigated. Currently Dexrazoxane (DXZ) is the only Fe-chelator used in clinical studies as it has been shown to reduce DOX-induced toxicity (Imondi *et al.*, 1996; Swain *et al.*, 1997), by preventing the formation of DOX-Fe complexes and subsequent $OH^{\bullet}$ generation (Hasinoff *et al.*, 1997). In addition, DXZ has been identified as a significant anti-cancer drug where it inhibits the DNA enzyme, topoisomerase II, similarly to DOX's anti-cancer mechanism (Tetef *et al.*, 2001). However, it has been reported that DXZ treatment results in secondary malignancies in cancer survivors, therefore decreasing the efficacy of DOX (Tebbi *et al.*, 2007).

Polyphenols found in plants are rich sources of anti-oxidants and are known to decrease damage caused by ROS (Habauzit & Morand, 2012). Studies have shown

that the use of polyphenols, specifically flavonoids, in combination with DOX treatment, prevents DOX-induced toxicity. These effects are attributed to their anti-cancer and cardioprotective properties (Chung *et al.*, 2010; Huang, 2013). Flavonoids are believed to be both Fe-chelators and free radical scavengers. One of the most studied plant derived flavonoid is Quercetin, which is a potent flavonoid found in fruit and vegetables (Hertog *et al.*, 1993; Bravo, 1998; Jacobs *et al.*, 2010). It is known to have anti-inflammatory, anti-oxidant and cardioprotective properties, and has been reported to decrease lipid peroxidation when used in combination with DOX treatment (Matouk *et al.*, 2013). 7-mono-O-(β-hydroxyethyl)-rutoside (monoHER) is a semi-synthetic flavonoid. Its structure is similar to Quercetin's chemical structure, and *in vivo* studies have demonstrated its cardioprotective activities during chronic DOX treatment (Van Acker *et al.*, 1995, Van Acker *et al.,* 1997). Unfortunately, monoHER has negative effects on the cardiac glutathione system and, thus, its use in the clinical setting has failed to reproduce the same protective effects (Bruynzeel *et al.*, 2007). Due to the disappointing results obtained in clinical trials utilising anti-oxidants as an intervention to protect against DOX toxicity, targeting only oxidative stress in a condition that is multi-faceted will not suffice. This fact, therefore, indicates that more investigations are required to find effective therapies that act in ways other than what is currently established.

1.10 Ghrelin

1.10.1 Structure of ghrelin

Ghrelin is a 28-amino acid peptide that was originally isolated from both the rat and human stomach as an endogenous ligand for the growth hormone secretagogue receptor type 1-apha (GHS-R-1α) (Kojima *et al.*, 1999; Tomasetto *et al.*, 2000). Ghrelin is generated by the processing of preproghrelin, where the serine residue in the third position of desacyl ghrelin is octanoylated to form bioactive acylated ghrelin. The acetylated form acts as a ligand for the GHS-R-1α and throughout this study will merely be referred to as ghrelin. The unique modification at serine position 3 (serine-3) by a fatty acid, primarily *n*-octanoinc acid, permits its effects on the GHS-R-1α (Figure 1.8). Ghrelin is secreted in response to the nutritional status of the body, where during fasting, circulating ghrelin levels are high, and during feeding, ghrelin levels are low (Kageyama *et al.*, 2005; Kojima & Kangawa, 2005; Qader *et al.*, 2008). The

circulating ghrelin is mainly produced by the X/A-like cells of the oxyntic gastric mucosa and small intestine (Date *et al.*, 2000). A small amount of ghrelin has been shown to be produced in other organs of the body, including the pancreas (Leite-Moreira & Soares, 2007).

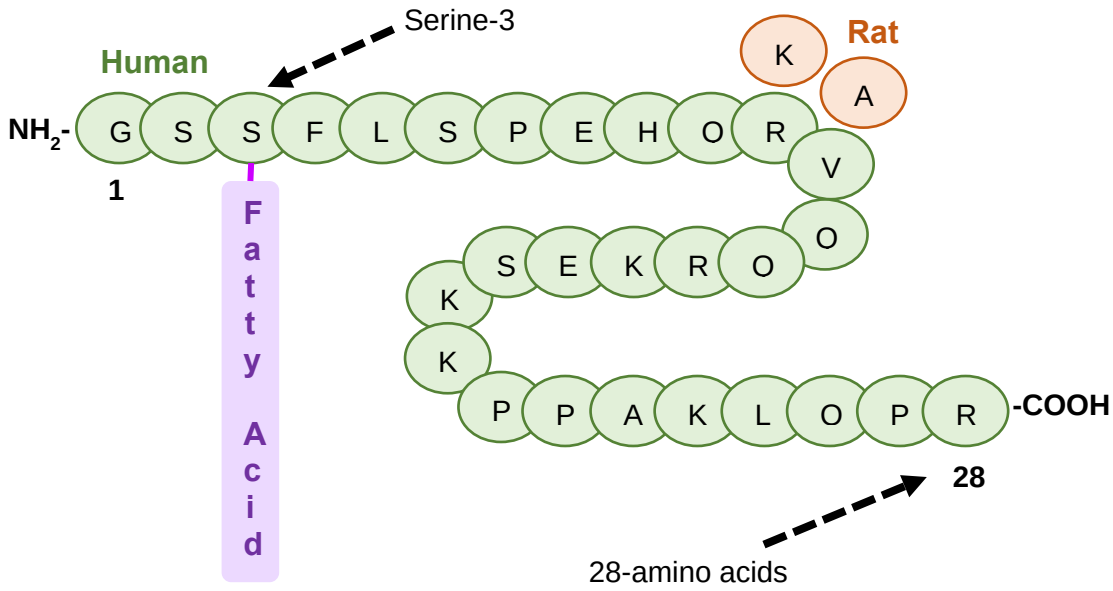

Figure 1.8: Structure of human and rat ghrelin molecules. Both human and rat ghrelin is 28-amino acid in length, where the unique modification of serine-3 by a fatty acid, mainly *n*-octanoic acid, allows it to bind to its receptor GHS-R-1α. Adapted from Kojima & Kangawa (2005).

Ghrelin cells, also termed epsilon-cells (ε-cells), are located in the pancreatic islets. In humans, these cells have been shown to be numerous in foetal and neonatal islets, and are observed in the islet periphery, while in the adult islets only a few ε-cells are visible (Wierup *et al.*, 2002). Furthermore, ε-cells comprise of approximately 10% of all islets in both foetal (15 - 26 weeks of gestation) and neonatal islets, while only approximately 1% are present in adult islets (Wierup *et al.*, 2014). Interestingly, in both humans and rodents, when comparing the foetal pancreas and the foetal stomach, the pancreas was found to possess more ε-cells, while very few X/A cells were found in the stomach, suggesting an inverse correlation between ε-cell and gastric X/A cell density (Wierup *et al.*, 2002; Wierup *et al.*, 2014). The density of ε-cells peaks at birth, while 40 days after birth (approximately six weeks old) these cells are occasionally

visible, and in adult islets they are rarely seen. Thus, the pancreas is suggested to be the main source of ghrelin during foetal development (Fak *et al.*, 2007; Walia *et al.*, 2009).

Studies have reported that ghrelin receptors are not only expressed in the central nervous system, particularly in the anterior pituitary and hypothalamus, but are also expressed in peripheral tissues, including the pancreatic islets, suggesting ghrelin has other effects within the body (Date *et al.*, 2002; Kageyama *et al.*, 2005; Işeri *et al.*, 2008; Chopin *et al.*, 2011). Ghrelin stimulates GH release by binding to GHS-R-1α in the pituitary gland, which causes an increase in intracellular Ca^{2+} and results in GH secretion (Date *et al.*, 2002). However, in addition to its effects on GH secretion, ghrelin has a wide variety of critical functions within the body as demonstrated in Figure 1.9 (Tschöp *et al.*, 2000; Wren *et al.*, 2001; Choi *et al.*, 2003; Zhang *et al.*, 2007; Delporte, 2013).

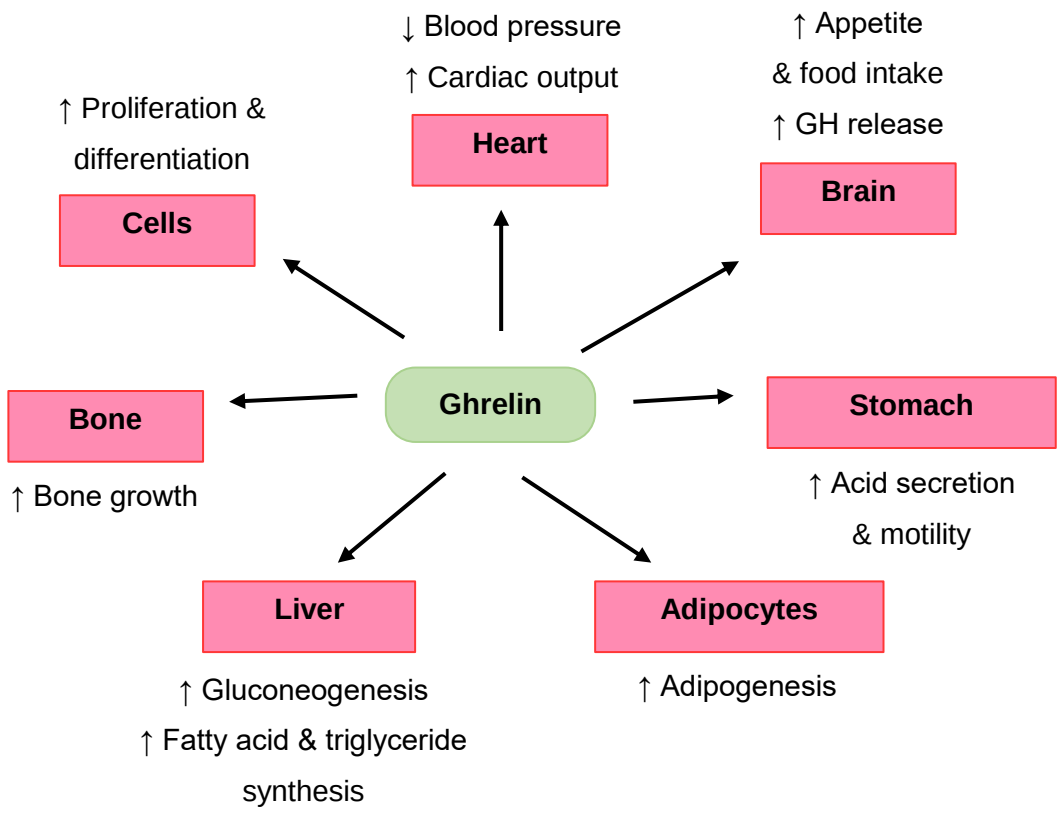

Figure 1.9: The main physiological effects of ghrelin within the body. Ghrelin has a wide variety of critical functions in the body, affecting several vital organs. Abbreviations: GH (growth hormone), ↑ (increases), ↓ (decreases).

1.10.2 The interactions between ghrelin and the pancreatic hormones

Whether ghrelin is involved in regulating hormonal secretion from the pancreas remains controversial. While some studies indicate that ghrelin inhibits insulin secretion in clonal β-cells, rodents and humans (Broglio *et al.*, 2001; Egido *et al.*, 2002; Kvist Reimer *et al.*, 2003), other studies indicate that ghrelin does in fact stimulate insulin secretion (Date *et al.*, 2002; Lee *et al.*, 2002; Cummings *et al.*, 2005). It is thought that these discrepancies may reflect differences in species and experimental design, such as doses administered and time of observation. Furthermore, both plasma ghrelin and insulin levels are glucose-dependant, in which high plasma glucose levels stimulate insulin secretion and suppress ghrelin secretion, indicating that plasma glucose is another important factor to consider in these studies (Kojima & Kangawa, 2005). Alternatively, insulin is suggested to inhibit ghrelin secretion, where an inverse correlation between ghrelin and insulin plasma levels exists (Korbonits *et al.*, 2004; Dezaki *et al.,* 2008). This inhibitory effect of insulin may explain the suppression of ghrelin secretion induced by high plasma glucose levels, and suggests that ghrelin's stimulatory effect on insulin secretion shown in some studies seems unlikely (Yin *et al.*, 2009; Wierup *et al.*, 2014). From a physiological perspective, this makes sense as plasma glucose levels are high after feeding, stimulating insulin secretion, both of which suppress ghrelin secretion. The opposite occurs during the fasted state when plasma glucose levels no longer stimulate insulin secretion, thus, the inhibition on ghrelin secretion is lifted (Tschöp *et al.,* 2000; Dornonville de la Cour *et al.*, 2001; Toshinai *et al.*, 2001). Regarding the effects of ghrelin on glucagon, somatostatin, and PP secretion, a study using perfused rat pancreas reported ghrelin had no effect on glucagon secretion, but inhibited somatostatin secretion (Egido *et al.*, 2002). In contrast, other studies have shown that ghrelin stimulated glucagon secretion in isolated islets, although this effect was not reflected in intact mice (Salehi *et al.*, 2004). Similarly in humans, ghrelin has been reported to stimulate somatostatin and PP secretion (Arosio *et al.*, 2003). Evaluating glucagon's effect on ghrelin secretion, it is suggested that glucagon stimulates ghrelin secretion as plasma glucagon levels increase during the fasted state (Yin *et al.*, 2009). In support of the above, Katayama *et al.* (2007) demonstrated that the exogenous administration of glucagon to experimental animals promotes ghrelin secretion. However, in contrast, the intramuscular injection of glucagon in humans reduces plasma ghrelin levels

potentially via the hypothalamic-pituitary axis (Arafat *et al.*, 2005, Arafat *et al.,* 2006). While additional research is necessary to understand the relationship between these hormones and their effects on one another, the beneficial effects of ghrelin should also be explored.

1.10.3 The protective effects of ghrelin during Doxorubicin treatment

Cachexia, or involuntary weight loss, is well-known to develop in cancer patients, and DOX has been associated with muscle atrophy and fat loss (De Lima Junior *et al.*, 2016), thus, ghrelin's appetite stimulating and adipogenesis effects in this context could be beneficial. A rodent study reported that during cachexia, ghrelin administration increased food intake, lean muscle mass and fat mass (Strassburg *et al.*, 2008), suggesting this to be a possible treatment therapy that could lead to improvements in the quality of life of patients undergoing chemotherapy. In addition, ghrelin has also been shown to have anti-oxidative, anti-inflammatory, anti-apoptotic and anti-fibrotic activities, which have been demonstrated in a variety of cells and tissues (Tong *et al.*, 2012; Yang *et al.*, 2013; Barazzoni *et al.*, 2014; Dobutovic *et al.*, 2014). Ghrelin has been shown to prevent DOX-induced apoptosis by reducing oxidative stress, ultimately leading to reduced fibrosis (Dixit *et al.*, 2004; Pei *et al.*, 2014; Wang *et al.*, 2014). Moreover, studies investigating the effects of ghrelin in fibrotic diseases showed that ghrelin reduces pro-inflammatory cytokine expression, including IL-6, IL-1β and TNF-α, and prevents macrophage infiltration, resulting in reduced collagen Type I, collagen Type II, fibronectin and α-SMA expression (Huang *et al.*, 2009; Li *et al.*, 2013; Sun *et al.*, 2015). However, while ghrelin's protective effects are demonstrated in several organs of the body, literature is lacking regarding its effects on the pancreas.

1.11 Problem statement

DOX is a potent chemotherapeutic agent that is used to treat a variety of different cancers and has contributed to the improved survival of patients. However, although effective, chronic DOX treatment is associated with off-target toxicity, particularly in cardiomyocytes. While literature has focused mainly on investigating the mechanisms involved in DOX-induced toxicity in the heart and other organs of the body, there are limited studies regarding the pancreas. Moreover, it is imperative that a therapeutic strategy is established that not only prevents DOX-induced toxicity, but also does not interfere with its anti-cancer effects in order to prolong survival of these cancer patients. Though anti-oxidants have been used in the clinical setting to reduce DOX-induced oxidative stress, they have yielded disappointing results. This brings us to ghrelin, a brain-gut peptide more commonly known for its appetite-inducing and GH-releasing effects. Ghrelin has been reported to exhibit beneficial properties in a variety of cells and tissues, including anti-oxidative, anti-apoptotic, anti-inflammatory and anti-fibrotic activities. However, studies are lacking with regards to investigating the protective effects of ghrelin in the pancreas.

1.12 Hypothesis and research aims

Although cells in the body have different functions, they all have similar cellular organelles that can be damaged by DOX treatment. Since oxidative stress and apoptotic cell death are believed to be the two major contributors to DOX-induced toxicity, this study hypothesised that DOX induces oxidative and apoptotic damage in pancreatic cells that will lead to the development of pancreatitis and fibrosis in the long term. In addition, ghrelin's protective effects against DOX-induced damage have been demonstrated in various organs, therefore, this study hypothesised that ghrelin will exhibit similar protective effects in the pancreas.

This study aimed to:

1. Investigate the effects of DOX treatment on the pancreas in a chronic model of DOX-induced toxicity by evaluating oxidative stress, apoptosis, inflammation and fibrosis.
2. Assess the potential of ghrelin to ameliorate these effects through its proposed anti-oxidant, anti-apoptotic, anti-fibrotic and anti-inflammatory effects.

CHAPTER 2: Materials & Methods

2.1 Ethical approval and animal care

Animals used in this study were treated adhering to the accepted standards for the use of animals in research and teaching as reflected in the South African National Standards 10386: 2008, and conformed to the guidelines for the care and use of laboratory animals implemented at Stellenbosch University. Approval for this study was obtained by the Animal Ethics Committees of Stellenbosch University (South Africa), (Ethics # SU- ACUD15-00038) (Appendix A).

Male Sprague Dawley rats (n = 32) were obtained at four weeks old and were allowed one week to acclimatize to the animal facility before the study commenced. As this study aimed to assess the effects of DOX on the pancreas using a model of chronic cardiotoxicity, often observed in survivors of childhood cancers, the age of the animals at the start of treatment were of equivalent age to late childhood in humans and early adulthood by the end of treatment. The rats were housed at 25 °C in sterile ventilated cages on a 12-hour light/dark cycle. Standard rat chow and tap water were provided ad libitum.

2.2 Experimental procedure

At five weeks, animals were randomly divided into vehicle (n = 7), ghrelin (n = 7), DOX (n = 9) and DOX+ghrelin (n = 9) treatment groups. The vehicle group was treated with 200 µl of physiological saline, the Ghrelin group received 100 µg/kg of ghrelin (G2869, LKT Laboratories, Inc., Minnesota, USA) three times a week, the DOX group received 2.5 mg/kg of DOX (D5794, LKT Laboratories, Inc., Minnesota, USA) once a week and the combination group received both treatments, respectively. All treatments were conducted via intraperitoneal injection using 25-gauge needle (HLSCDN-25, Lasec, Cape Town, South Africa) over a period of eight weeks. The cumulative dose of DOX for the duration of the study was thus 20 mg/kg, which, when translated to human doses, is clinically relevant. As DOX is a known cytotoxic agent, and very little is known about the adverse effects of ghrelin in this context, if any, animals were constantly monitored, weighed and food consumption recorded. No animals were lost as a result of the treatment (Appendix B).

2.3 Serum and tissue collection

A week after the last injection, animals were anaesthetised with a lethal dose (60 mg/kg) of sodium pentobarbitone (Euthapent, 130540, Kyron Laboratories, Johannesburg, South Africa). When the pedal reflex was no longer observed, a recognition and confirmation of death (Close *et al.*, 1996), the abdominal cavity was cut open and the pancreas was harvested from each animal. After weighing each pancreas, the organ was non-specifically divided into two sections, where one half was preserved in a 4% formaldehyde solution (100496, Merck Millipore, Massachusetts, USA) for histological analysis, and the other half was snap frozen in liquid nitrogen and stored at – 80 °C in for biochemical analysis.

At the time of euthanasia, blood was also collected from the thoracic cavity of each animal using a 10 ml sterile syringe upon removal of the heart. The blood was immediately placed into serum separation tubes (VGRV450470R, Lasec, Cape Town, South Africa), where after the tubes were inverted five times and placed on ice for 10 minutes to stand. The tubes were then centrifuged for 10 minutes at 4 000 rpm (1 400 x *g*) at 4 °C and the supernatant aliquoted into centrifuge tubes and stored at - 80 °C (Appendix C).

2.4 Metabolic parameters assessed in serum

MILLIPLEX® MAP Multiplex assay was used to analyse serum samples. The serum concentrations of glucagon, insulin, IL-6 and TNF-α were measured using a rat metabolic magnetic kit (RMHMAG-84K, Merck Millipore, Massachusetts, USA). Luminex xMAP® technology is based on beads (or microspheres) that are covalently coupled with a specific capture antibody and is used to detect multiple analytes from a single sample of a small volume. Each bead is distinctly coloured internally using two fluorescent dyes at discrete ratios. After cytokines in the serum bind to the anti-bodies on the beads, a biotinylated detection antibody is added and streptavidin-phycoerythrin conjugate, the fluorescently labelled reporter molecule, is added to complete the reaction (Houser, 2012). The Bio-Plex® MAGPIX™ Multiplex reader (MAGPIX13046704, BioRad, Johannesburg, South Africa) was then used to identify each bead and the fluorescent signal quantified using MAGPIX® with xPONENT® software. The assay was carried out as per the manufacturer's instructions.

In brief, a black 96-well plate was prewashed with Assay Buffer and serum matrix solution, where after the assay buffer, standards, quality controls, bead solution and samples were loaded into appropriate wells. The plate was sealed and incubated overnight (18 - 20 hours) with slight agitation at 4 °C to allow for binding of serum proteins to anti-bodies on the beads. This was followed by aspiration and washing steps using a Bio-Plex Pro™ Wash Station (BioRad, Johannesburg, South Africa). The plate was then incubated at room temperature with slight agitation firstly with the prepared Detection Antibodies, and then Streptavidin-Phycoerythrin was loaded into each well and the plate was incubated further. The solution in the wells were aspirated and washed as previously described, and incubated with MAGPIX® Drive Fluid (40-50013, Luminex) with slight agitation to resuspend the beads (Appendix D).

2.5 Histological analysis

2.5.1 Tissue processing and sectioning

The fixed pancreatic tissue samples were removed from the 4% formaldehyde solution and transferred onto labelled cassettes (Z672122, Sigma-Aldrich, St Louis, USA). The tissues were processed through a series of dehydration steps using a TissueTek® II automated tissue processing machine (4640B, Lab-Tek division, Miles Laboratories Inc, Naperville, Illinois, USA), and infiltrated with Paraplast® wax (A6330-4LB, Sigma-Aldrich, St Louis, USA) (Appendix E). After processing, tissues were embedding with melted paraffin wax (8002-74-2, Merck Millipore, Massachusetts, USA) onto a cassette (PLPS191023, Lasec, Cape Town, South Africa) using the Leica Modular Tissue Embedding Centre (EG1160, Lecia Biosystems, Wetzlar, Germany). Using a manual microtome (RM 2125 RT, Leica Biosystems, Wetzlar, Germany), 5 µm thick sections were prepared, carefully transferred onto appropriate microscope slides, and placed briefly into a 60 °C oven to ensure adhesion and drying of the sections.

2.5.2 Haematoxylin and eosin (H&E) staining

In histology, the H&E stain is the most widely used stain due to its ability to clearly display different structures of the tissue. Haematoxylin stains nuclei black by binding to the anionic DNA and RNA, while eosin stains the cytoplasm components in various shades pink due to its high affinity for positively charged cytoplasmic constituents (Bancroft & Gamble, 2008). A Leica Auto Stainer XL (ST5010, Leica Biosystems,

Wetzlar, Germany) was used for the H&E staining. The Mayer's Haematoxylin solution (SAAR2822001LC, Merck Millipore, Massachusetts, USA) was filtered and the Eosin solution (3801600E, Leica Biosystems, Wetzlar, Germany) was freshly prepared prior to sectioning. The 5 µm sections previously prepared were stained and the microscope slides (GLAS4S22M3000F, Lasec, Cape Town, South Africa) were mounted with coverslips (GLAS2C9M2250REC, Lasec, Cape Town, South Africa) using DPX mountant (06522, Sigma-Aldrich, St Louis, USA) and allowed to dry overnight (Appendix F).

Images were acquired with a 40 X objective lens on a E400 ECLIPSE microscope (Nikon Instruments, Japan) using a DS-Fi2 camera (Nikon Instruments, Japan) with NIS Elements version 4.10 software (Nikon, Japan), on a Dell desktop computer (Dell, United States of America) running Microsoft Windows 7 software (Microsoft, United States of America).

2.5.3 Masson's Trichrome staining

Masson's Trichrome stain is used in histology to stain collagenous connective tissue and, as its names implies, employs three dyes. The Masson Trichrome protocol used in this study was described by (Bancroft & Gamble, 2008), where collagen is stained green, cytoplasm is stained red while the nuclei are stained black. 5 µm sections were prepared as described previously and were transferred onto positively charged Histobond microscope slides (GLAS2S13M0810401, Lasec, Cape Town, South Africa). Following staining, the slides were mounted and allowed to dry. Sections of skin were used as positive control slides (Appendix G).

Images were obtained using the same microscope and software as indicated in section 2.5.2., and images were acquired at 4 X magnification. 20 images of random areas of the pancreas were captured for each treatment group. Images were brightened to make each colour stand out for easier differentiation and analysed using ImageJ software (Schneider *et al.*, 2012). The images were analysed as described by Bauman *et al.,* 2014 with modifications. Blue-green coloration, indicative of fibrosis, was separated by manual thresholding of hue (60 - 190), saturation (35 - 255), and brightness (10 - 255) values using ImageJ software. The value, or pixels, of the interstitial fibrotic areas (blue area) were represented as the percentage of the entire tissue (red area) analysed. This is illustrated by the equation below:

$$\%\ Fibrotic\ area = \frac{Blue\ Areas\ (Fibrotic\ Areas)}{Red\ Area\ (Entire\ Tissue)} \times 100$$

2.5.4 Immunohistochemical staining

In order to compare any significant changes observed in the serum glucagon and insulin levels of the animals between treatment groups, this study assessed the percentage of α- and β-cells within the islets of Langerhans. 5 µm sections were prepared as previously described. Positively charged Histobond microscope slides were again used for this stain where sections were deparaffinised, and rehydrated through a graded series of ethanol and stained using a Leica Bond-Max™ Immuno-Autostainer (ST5010, Lecia Biosystems, Wetzlar, Germany). Sequential double-staining was utilised for glucagon (ab10988, Abcam, Cambridge, United Kingdom) and insulin (ab7842, Abcam, Cambridge, United Kingdom) antibodies, using a Bond™ Polymer Refine Detection Kit (DS9800, Leica Biosystems, Wetzlar, Germany) and a Bond™ Polymer Refine Red Detection Kit (DS9390, Leica Biosystems, Wetzlar, Germany). In brief, sections were pre-treated with epitope-retrieval reagent in order to re-open the cross-linked and covered epitopes that occurred during fixation. Endogenous peroxidases were blocked using H_2O_2 in order to prevent background staining and to avoid obtaining false positives staining (Chen *et al.*, 2010). The Bond™ Polymer Refine Detection Kit is a horseradish peroxidase (HRP)-linked conjugate system, which converts the 3,3'-diaminobenzidine tetrahydrochloride hydrate (DAB) chromogen into a brown precipitate, while the Bond™ Polymer Refine Red Detection Kit is an alkaline phosphatase (AP)-linked conjugate system, which converts 3-amino-9-ethylcarbazole (AEC) into a red precipitate. This allows for the detection of tissue-bound Immunoglobulin G (IgG) primary antibodies and easy antigen differentiation. Both kits contain haematoxylin counterstains in order to visualise nuclei. Glucagon-secreting α-cells were stained brown, and insulin-secreting β-cells were stained red. After staining, tissues were mounted on slides, and cover slipped and allowed to dry (Appendix H).

Images were obtained using the same microscope and software as indicated in section 2.5.2. Twenty islets of Langerhans from each treatment group were randomly selected, and the number of α-cells and β-cells were manually counted using ImageJ

software. These results were presented as a percentage of α-cells and β-cells present in one islet per treatment group.

2.6 Oxidative stress analysis

DOX-induced oxidative stress suggested to be one of the main mechanisms by which DOX induces cell damage (Mizutani *et al.,* 2003), and are neutralised by endogenous enzymatic anti-oxidant systems. This study, therefore, employed the oxygen radical absorbance capacity (ORAC) assay that is indicative of the 'anti-oxidant power', SOD activity and glutathione (GSH: GSSG) assays to determine the influence of DOX and oxidative stress on the activity of these anti-oxidants. Furthermore, oxidative damage was measured by assessing the concentrations of conjugated dienes (CDs) and malondialdehyde (MDA), which are early and late markers of lipid peroxidation, respectively, using CDs and Thiobarbituric acid reactive substances (TBARS) assays.

2.6.1 Sample preparation

100 mg frozen pancreatic tissue samples were crushed using a chilled mortar and pestle and placed into chilled centrifuge tubes. For the ORAC, SOD, GSH, CDs and TBARS assays, tissues were incubated in 1 ml of cold 50 mM phosphate buffer (pH 7.5), whereas for the GSSG assay, 10 µl of 1-methyl-2-vinylpyridinium (M2VP) (69701, Sigma-Aldrich, St Louis, USA) was added in addition to the phosphate buffer. Tissues were homogenised on ice for approximately ten seconds using a POLYTRON™ PT 2100 benchtop homogeniser (Kinematica AG, Luzern, Switzerland) and the centrifuged for ten minutes at 12 000 rpm (13 300 x *g*). The supernatant was transferred into new chilled centrifuge tubes and frozen at – 80 °C until required (Appendix I). On the day the assays were performed, samples were thawed on ice and centrifuged at 14 000 rpm (16 000 x *g*) for ten minutes at 4 °C.

2.6.2 Assessment of the antioxidant capacity

The ORAC assay is the most widely used assay to determine the antioxidant status of samples, and is based on the ability of hydrophilic antioxidants in a sample to prevent peroxyl-radical-induced oxidation. Thus, the limitation of this assay, however, is its inability to measure hydrophilic antioxidants in the sample, including glutathione (Prior *et al.*, 2003). This assay, previously described by Ou *et al.*, 2001, employs fluorescent probe Fluorescein (F6377, Sigma-Aldrich, St Louis, USA) as the target, which

becomes oxidised after the addition of the peroxyl radical 2,2'-azobis (2-methylproprionamidine) dihydrochloride (AAPH, 440914, Sigma-Aldrich, St Louis, USA). Anti-oxidants present in the samples prevent the oxidation and subsequent fluorescent decay of Fluorescein until anti-oxidant activity is depleted. This activity is quantified over time by measuring the area under the curve (AUC). Trolox™ (238813, Sigma-Aldrich, St Louis, USA), a hydrophilic analog of vitamin E, is used as the reference antioxidant in this experiment, where the anti-oxidant capacity of each sample is represented as Trolox equivalents (µmol) per gram of tissue analysed.

The Fluoroskan Ascent™ Microplate Fluorometer (5210470, Thermo Fishcher Scientific, Massachusetts, USA) was set at 37 °C. Samples were prepared as previously described in 2.7.1., thawed on ice and centrifuged at 14 000 rpm (16 000 x *g*) for ten minutes to remove turbidity. 100 µl of 0.5 M Perchloric acid (PCA, 100514, Merck Millipore, Massachusetts, USA) was added to every 100 µl of sample into a new Eppendorf tube to precipitate the protein as the protein fraction in the sample is able to significantly mask and interfere with accurate anti-oxidant capacity measurements (Prior *et al.*, 2003). Standards and samples were loaded into appropriate wells of a black 96-well plate, and Fluorescein and AAPH were loaded into all wells. The fluorescence of the fluorescein molecule (excitation: 485 nm, emission: 538 nm) was measured every five minutes for two hours. The final ORAC values were calculated using the regression equation $y = ax^2 + bx = c$ between the Trolox concentration (µM) and the area under the curve (Appendix J).

2.6.3 Determination of the antioxidant status

2.6.3.1 SOD activity assay

The SOD enzyme is considered to be the first line of defence against ROS in cells (Houmani *et al.*, 2016), and this assay was thus employed in this study. The principle of the SOD assay is based under physiological conditions where 6-hydroxydopamine (6-HD) rapidly auto-oxidises and contributes to an increase in absorbance at 490 nm (Heikkila and Cabbat, 1976). Since SOD inhibits this auto-oxidation by consuming the $O_2^{\bullet -}$ produced, the activity of SOD can be measured by monitoring the auto-oxidation of 6-HD.

Samples were prepared as described previously in 2.7.1., thawed on ice and centrifuged at 14 000 rpm (16 000 x *g*) for ten minutes. Protein concentration was determined using the Direct Detect™ Infrared Spectrometer (DDHW00010-WW, Merck Millipore, Massachusetts, USA). This system determines protein concentration by measuring the absorbance of amide bonds in protein chains using infrared quantification. In brief, 2 µl of blank (SOD assay buffer) and samples were pipetted onto the transparent hydrophilic polytetrafluoroethylene (PTFE) membranes of the Direct Detect® Assay-free Cards (DDAC00010-GR, Merck Millipore, Massachusetts, USA) and placed into the Direct Detect® Infrared Spectrometer, where protein concentration was measured as mg/ml of protein. 6-HD (162957, Sigma-Aldrich, St Louis, USA) was prepared by dissolving it in PCA and loaded into all wells of a clear 96-well plate. The blank and samples were loaded into appropriate wells, after which diethylenetriaminepentaacetic acid (DETAPAC) (D6518, Sigma-Aldrich, St Louis, USA) was loaded into all wells and the plate was immediately place into plate reader. The absorbance of each sample was measured at 490 nm using the Multiskan™ Spectrum microplate spectrophotometer (51119200, Thermo Fisher Scientific, Massachusetts, USA) every minute for four minutes. The SOD activity in the samples was measured by comparing the values in each well to a linear calibration curve and results were expressed as Unit inhibition/mg of protein. One unit of SOD is defined as the amount of SOD required to exhibit 50% dismutation of the $O_2^{\bullet -}$ (Appendix K).

2.6.3.2 Glutathione assays

The anti-oxidant glutathione peroxidase (GPx) removes H_2O_2 by coupling its reduction (GSH) to H_2O_2 with the oxidation of glutathione (GSSG). Thus, GSH neutralises free radicals by donating an electron and forms GSSG. GSSG is recycled back to GSH by glutathione reductase (GR), which is NADPH-dependent (Asensi *et al.*, 1999; Noctor *et al.*, 2012). In the absence of oxidative stress, a higher GSH concentration with a relatively small GSSG concentration is present in cells. The ratio of GSH to GSSG, termed the glutathione status, is considered a good indicator of oxidative stress. The total glutathione (GSH_{total}) and GSSG concentrations in this study were measured using the method described by Asensi *et al.* (1999), in which the GSH concentration within the samples was calculated using the equation: $GSH = GSH_{total} - 2\ GSSG$. 5 5'-dithiobis-(2-nitrobenzoic acid) (DTNB, D8130, Sigma-Aldrich, St Louis, USA) has the ability to oxidise with GSH in a sample to produce both GSSG and 5-thio-2-

nitrobenzoic acid (TNB), which gives a yellow colour. This is then used to quantify the amount of GSH present in the sample. For the GSSG assay, the M2VP added during sample preparation binds to GSH, allowing only the GSSG concentration to be measured.

Samples were prepared as previously described, thawed on ice and centrifuged at 14 000 rpm (16 000 x *g*) for ten minutes. Samples for the GSH assay were diluted 0.5 X in assay buffer. Standards and samples were loaded into appropriate wells of a clear 96-well plate, and DTNB and GR (G3664, Sigma-Aldrich, St Louis, USA) were loaded into all wells, after which NADPH (N7505, Sigma-Aldrich) was added and the plate was immediately place into plate reader. The absorbance values of each sample were measured at 412 nm every 30 seconds for five minutes using the Multiskan^{TM} Spectrum microplate spectrophotometer (51119200, Thermo Fisher Scientific, Massachusetts, USA). The results for GSH and GSSG were then determined using the GSH standard (Appendix L).

2.7 Assessment of oxidative damage

It is well known that lipid peroxidation is involved in the pathogenesis of a variety of diseases and clinical conditions, including anthracycline-induced cardiotoxicity, inflammation and fibrosis. A variety of organelles contain membranes, such as mitochondria and the endoplasmic reticulum, therefore damage to these membranes can be detrimental to cell survival and function (Devasagayam *et al.,* 2003). Lipid peroxidation occurs when fatty acids present within membranes are oxidised and form lipid hydroperoxide (Botsoglou *et al.,* 1994). CDs are one of the initial products produced during lipid peroxidation, which can undergo further oxidation to form lipid peroxyl radicals, which can react with more membrane lipids and propagate lipid peroxidation. Lipid peroxyl radicals are unstable molecules and break down to form several products, including aldehydes such as MDA (Situnayake *et al.*, 1990; Devasagayam *et al.*, 2003). Therfore, CDs and MDA can be measured as early and late markers of lipid peroxidation respectively.

2.7.1 Conjugated dienes (CDs) assay

The concentration of CDs present in the pancreas was determined as described by Gul *et al* (Gül *et al.,* 2003). Samples were prepared as previously described, thawed

on ice and centrifuged at 14 000 rpm (16 000 x *g*) for ten minutes. A 2:1 solution of chloroform (102444, Merck Millipore, Massachusetts, USA) and methanol (106007, Merck Millipore, Massachusetts, USA) was added to each sample, followed by distilled water. This solution was vortexed and centrifuged at 12 000 rpm (13 300 x *g*) at 4 °C for ten minutes to separate the different phases. The bottom chloroform layer was transferred into new centrifuge tubes. As the chloroform layer contains a purified lipid extract (Bligh *et al.*, 1959), it was allowed to evaporate overnight at 4 °C. The following day, the remaining residue was reconstituted with cyclohexane (102822, Merck Millipore, Massachusetts, USA), vortexed and loaded into a clear 96-well ultra-violet (UV) plate for spectrophotometric analysis. The standard and samples were loaded into appropriate wells, where after the absorbance of each sample was measured at 234 nm using the Multiskan™ Spectrum microplate spectrophotometer (51119200, Thermo Fisher Scientific, Massachusetts, USA. CDs absorb maximally at 233 nm to 235 nm in UV light and, thus, this property is used as the basis for CD detection in biological samples (Situnayake *et al.*, 1990). The concentration of CDs was calculated using the formula below and expressed as µmol CDs /gram of tissue (Appendix M).

$$\frac{(Absorbance\ of\ the\ sample\ at\ 234\ nm) - (Absorbance\ of\ the\ blank\ at\ 234\ nm)}{extinction\ coefficient\ of\ 2.95\ x\ 10^4}$$

2.7.2 Thiobarbituric acid reactive substances (TBARS) assay

MDA reacts with two molecules of TBA to form a complex that gives a pink colour, which can be colorimetrically quantified to determine the concentration of MDA (Botsoglou *et al.*, 1994). Measuring the concentration of MDA is considered the most commonly used approach in estimating the amount of lipid peroxidation (Devasagayam, Boloor and Ramasarma, 2003).

Samples were prepared as previously described, thawed on ice and centrifuged at 14 000 rpm (16 000 x *g*) for ten minutes. Samples were added to 4 mM Butylated hydroxytoluene (BHT, B1378, Sigma-Aldrich, St Louis, USA) in order to prevent oxidation during sample processing. 0.2 M Ortho-Phosphoric acid (100573, Merck Millipore, Massachusetts, USA) and 0.11 M TBA was also added to assist in breaking up the tissues further. The reaction solutions were boiled in a 90 °C waterbath for 45

minutes and immediately cooled in an ice bath. Butanol and saturated salt solution were added to each sample and centrifuged at 14 000 rpm (16 000 x *g*) for 20 seconds to separate the phases, after which the top butanol phase and blank were transferred into appropriate wells of a clear 96-well plate. The absorbance was measured at 532 nm using the same spectrophotometer described in section 2.7.1. The concentration of MDA was determined by using the known extinction coefficient of the MDA-TBA complex (1.55 x 10^5 M/cm) and expressed as µmol/L of MDA (Appendix N).

2.8 Western blot analysis

2.8.1 Tissue lysate preparation and protein determination

Frozen pancreatic tissue samples were crushed using a chilled mortar and pestle. Protein was extracted with 300 µl of modified radio-immunoprecipitation (RIPA) buffer (pH 7.4) containing 50 mM Tris-HCl, 150 mM NaCl, 1mM Ethylenediaminetetraacetic acid (EDTA, EDS, Sigma-Aldrich, St Louis, USA), 1% Nonidet P 40 (NP-40, 74385, Sigma-Aldrich, St Louis, USA), 0.25% Na-deoxycholate (D6750, Sigma-Aldrich, St Louis, USA). The buffer was supplemented with 1 mM sodium fluoride (NaF, 106449, Merck Millipore, Massachusetts, USA), 1 mM sodium orthovanadate (Na_3VO_4, S6508, Sigma-Aldrich, St Louis, USA), 1 mM phenylmethylsulfonyl fluoride (PMSF, 93482, Sigma-Aldrich, St Louis, USA) and 1 x cOmplete™ protease inhibitor cocktail (11873580001, Roche, Basel, Switzerland) to inhibit phosphatase and protease activities. Tissue was homogenised in chilled centrifuge tubes for approximately ten seconds using a POLYTRON™ PT 2100 benchtop homogeniser (Kinematica AG, Luzern, Switzerland). Once the foam had subsided, lysates were centrifuged twice at 14 000 rpm (16 000 x g) at 4 °C for an hour and then again for 15 minutes, where the supernatant was transferred into new chilled centrifuge tubes after each centrifugation. Protein concentration was determined using Direct Detect™ Infrared Spectrometer as previously described.

2.8.2 Sample preparation

Following protein determination, 56.25 µg protein samples were prepared in Laemmli's sample buffer, boiled at 95 °C for five minutes and stored at - 80 °C until required. Prior to loading into polyacrylamide gels, samples were thawed on ice and boiled at 95 °C for an additional five minutes in order to denature and linearize proteins.

2.8.3 Sodium dodecyl sulfate-polyacrylamide gel electrophoresis (SDS-PAGE)

Proteins were separated by either 12% Stain-free® Fast-Cast® polyacrylamide gels or 15% polyacrylamide gels. The 12% gels were separated at 100 V for ten minutes and then 150 V for approximately one hour. The 15% gels were separated at 100 V for approximately two hours. The gels were then activated in the ChemiDoc™ XRS+ System with the Image Lab™ Software (Bio-Rad, Johannesburg, South Africa). Proteins were transferred onto low fluorescence polyvinylidene fluoride (LF PVDF) membranes Trans-Blot® Turbo™ Mini PVDF Transfer Packs (170-4156, Bio-Rad, Johannesburg, South Africa) using the TransBlot® Turbo™ Transfer System (Bio-Rad, Johannesburg, South Africa) for seven minutes at 15 V. Membranes were blocked for one hour in 5% fat-free milk made up in Tris-Buffered Saline-Tween®20 solution (TBS-T) at room temperature to prevent non-specific binding, and washed three times for five minutes in TBS-T. The membranes were incubated in primary antibody (Table 2.2) overnight at 4 °C with gentle agitation, after which the membranes were washed three times for five minutes in TBS-T and incubated for one hour in appropriate secondary antibody (Table 2.2) at room temperature. Membranes were washed three times for five minutes and incubated in Clarity™ Western ECL Substrate (1705061, Bio-Rad, Johannesburg, South Africa). Protein bands were detected using on the ChemiDoc™ XRS+ System with the Image Lab™ Software (Bio-Rad, Johannesburg, South Africa), and were normalised against total lane protein and quantified with the Image Lab™ Software (Appendix O and P).

2.8.4 Total protein loading controls

Although housekeeping proteins, including β-actin and Glyceraldehyde 3-phosphate dehydrogenase (GAPDH), have long been used as loading controls to ensure equal loading, BioRad Stain-free® technology has been shown to out-perform this traditional method (Rivero-Gutiérrez *et al.*, 2014). The traditional method relies on the assumption that these housekeeping proteins do not change under most circumstances (Aldridge *et al.*, 2008). The principle of BioRad Stain-free® technology lies in the polyacrylamide gel chemistry, in which a patented additive in the gel mixture reacts with tryptophan residues within proteins sequences, and can be visualised when exposed to UV radiation (Rivero-Gutiérrez *et al.*, 2014). This modern method was employed to ensure equal loading across all samples were maintained.

Table 2.1: Primary and secondary antibodies with their appropriate dilutions. Abbreviations: CST (Cell Signalling Technology), Cu/Zn SOD (copper/zinc superoxide dismutase), MnSOD (manganese superoxide dismutase), HRP (horseradish peroxidase)

Primary Antibody	Company	Dilution	Molecular Weight
Caspase 3	CST (9662)	1:1000	17, 19, 35
SOD1 (Cu/Zn SOD)	CST (71G8)	1:1000	18
SOD2 (Mn SOD)	CST (13141)	1:1000	22
Secondary Antibody			
HRP-Linked	CST (7074)	1:10 000	
HRP-Linked	CST (7076S)	1:10 000	

2.9 Statistical analysis

GraphPad Prism software version 5.0.3 (GraphPad Inc., San Diego, CA) was used for statistical analysis of the data. All data were tested for normality after which the appropriate tests were performed. Comparisons between the different treatment groups were performed by either one-way analysis of variance (ANOVA) or two-way ANOVA where applicable, followed by the Fischer's Least Squared Difference (LSD) post-hoc tests. All statistical tests were performed in consultation with an experienced biostatistician (Prof Daan Nel, Stellenbosch Statistical Consultation Centre, Stellenbosch University, South Africa). All data are represented as mean ± standard error of mean (SEM). A *p*-value <0.05 was considered statistically significant.

CHAPTER 3: Results

3.1 Food consumption, body and pancreatic weights of the animals

As ghrelin is a known appetite stimulant, food consumption was monitored throughout the eight weeks of treatment. Surprisingly and most unexpectedly, the saline treated animals (vehicle) actually consumed more food than the ghrelin treated group (Figure 3.1). DOX affected appetite as food consumed by DOX treated animals was significantly reduced (152.95 ± 10.23 g, $p<0.05$) from 4 weeks of treatment when compared to vehicle (185.30 ± 6.98 g), and this was maintained throughout the treatment duration (Figure 3.1). While ghrelin in the combination group modestly increased food consumption throughout this study when compared to the DOX group only, this was not statically significant. Moreover, following eight weeks of treatment, animals in the combination group consumed significantly less food (162.44 ± 18.46 g) when compared to vehicle (197.38 ± 8.85 g) which shows that ghrelin prevented loss of appetite induced by DOX until the eighth week of treatment.

This study then went on to evaluate the change in body weight of the animals from the start of the study to the end of eight weeks of treatment. All animals gained weight by the end of the study (Figure 3.2 and Table 3.1). However, the change in body weight of the DOX treated animals was significantly lower (186.88 ± 10.35 g, $p<0.0001$) when compared to the vehicle group (304.61 ± 22.62 g) which correlates with the reduced food intake observed (Figure 3.1). Ghrelin alone did not cause a change in body weight when compared to the vehicle, but in combination with DOX it modestly increased body weight when compared to the DOX group, although this increase was not statistically significant. Furthermore, the change in body weight of the animals in the combination group was significantly lower (231.01 ± 8.21 g, $p<0.01$) than the vehicle. Thus, the food consumption data obtained throughout the treatment duration echoes the change in body weight seen at the end of the study, and highlights that while ghrelin in the presence of DOX prevented loss of appetite throughout the duration of treatment, it was unable to prevent the animals from losing weight. In addition, pancreatic weight was recorded after the duration of treatment and expressed as a ratio to final body weight, however, no significant changes were observed between the groups (Table 3.2).

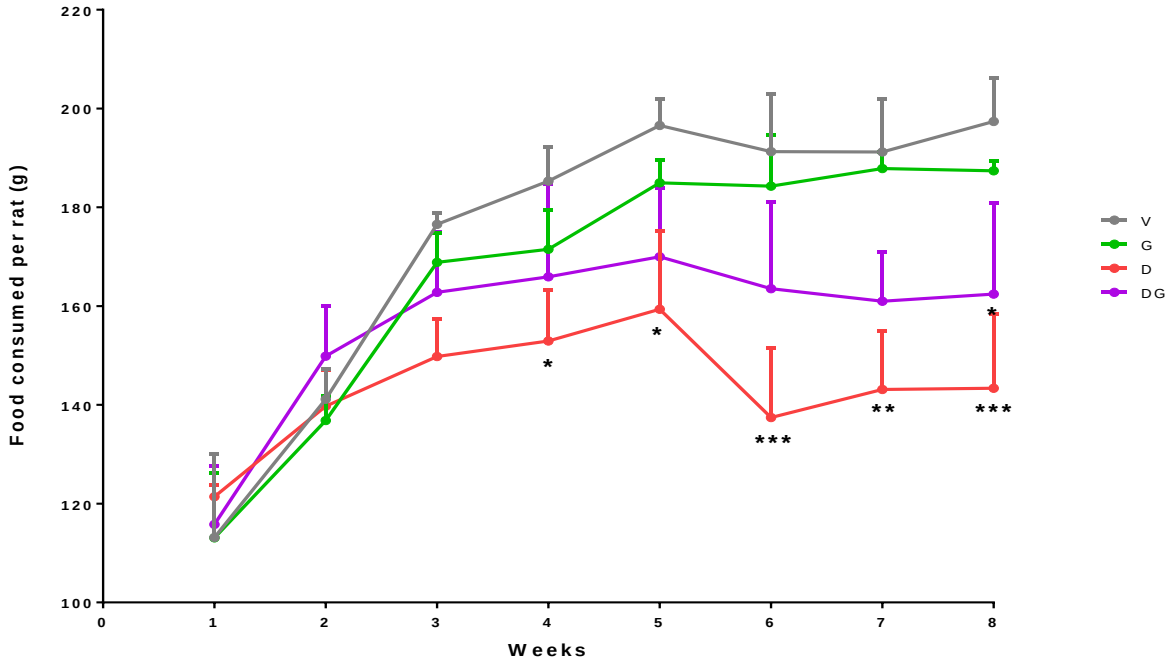

Figure 3.1: Food consumed by animals throughout treatment duration. Experimental animals were treated with saline, ghrelin, DOX and DOX+ghrelin and were assessed on the ninth week following treatment. Values are expressed as mean ± SEM (n = 7 - 9), *p<0.05, **p<0.01, ***p<0.001 vs V. Abbreviations: V (vehicle), G (ghrelin), D (DOX), DG (DOX+ghrelin).

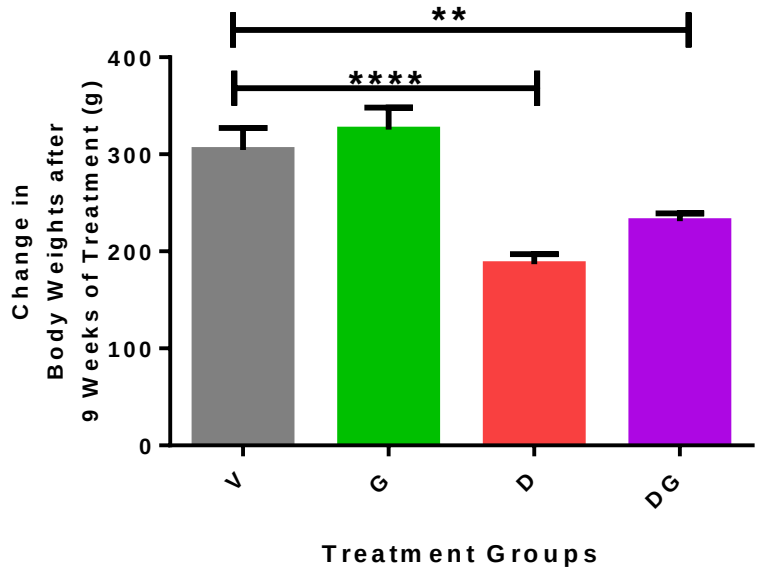

Figure 3.2: Change in body weight of animals between treatment groups following eight weeks of treatment. Experimental animals were treated with saline, ghrelin, DOX and DOX+ghrelin and were assessed on the ninth week following treatment. Values are expressed as mean ± SEM (n = 7 - 9), **p<0.01, **** p<0.0001 vs V. Abbreviations: V (vehicle), G (ghrelin), D (DOX), DG (DOX+ghrelin).

Table 3.1: The average initial and final body weight (grams) of animals in each treatment group after eight weeks of treatment. Experimental animals were treated with saline, ghrelin, DOX and DOX+ghrelin and were assessed on the ninth week following treatment. Values are expressed as mean ± SEM (n = 7 - 9). Abbreviations: V (vehicle), G (ghrelin), D (DOX), DG (DOX+ghrelin).

Treatment Groups	Initial Body Weight (g)	Final Body Weight (g)
V	115.90 ± 24.87	420.50 ± 16.44
G	82.81 ± 9.71	408.20 ± 21.30
D	97.39 ± 6.55	281.40 ± 9.78
DG	85.27 ± 9.87	316.30 ± 7.09

Table 3.2: Average ratio of pancreatic weight to final body weight. Experimental animals were treated with saline, ghrelin, DOX and DOX+ghrelin and were assessed on the ninth week following treatment. Values are expressed as mean ± SEM (n = 7 - 9). Abbreviations: V (vehicle), G (ghrelin), D (DOX), DG (DOX+ghrelin), AU (arbitrary units).

Treatment groups	V	G	D	DG
Pancreatic weight: Body weight (AU)	0.003 ± 0.0001	0.004 ± 0.0003	0.004 ± 0.0001	0.003 ± 0.0001

3.2 Hormonal and inflammatory cytokine evaluation

Considering that the pancreas regulated circulating blood glucose levels in the body with the help of insulin and glucagon, this study determined the circulating levels of these hormones in the serum of non-fasted animals. Although not significant, there was a trend towards an increase in the insulin levels of both groups of DOX treated animals when compared to the vehicle (Figure 3.3A), suggesting that DOX may have the ability to influence insulin secretion from the pancreas. Glucagon serum concentrations in the DOX and ghrelin treated groups were similar to that of the vehicle group, while the combination of both DOX and ghrelin also trended towards an increase, however, this was not statistically significant (Figure 3.3B). In the same

serum samples, inflammatory markers including TNF-α and IL-6 were also analysed but the concentration of both cytokines was unfortunately below the detectable range (1 – 62 pg/ml) of the multiplex kit utilised (data not shown). As inflammation plays an integral role in pancreatitis, these results do not imply that no changes occurred, but rather a more sensitive technique should have been applied.

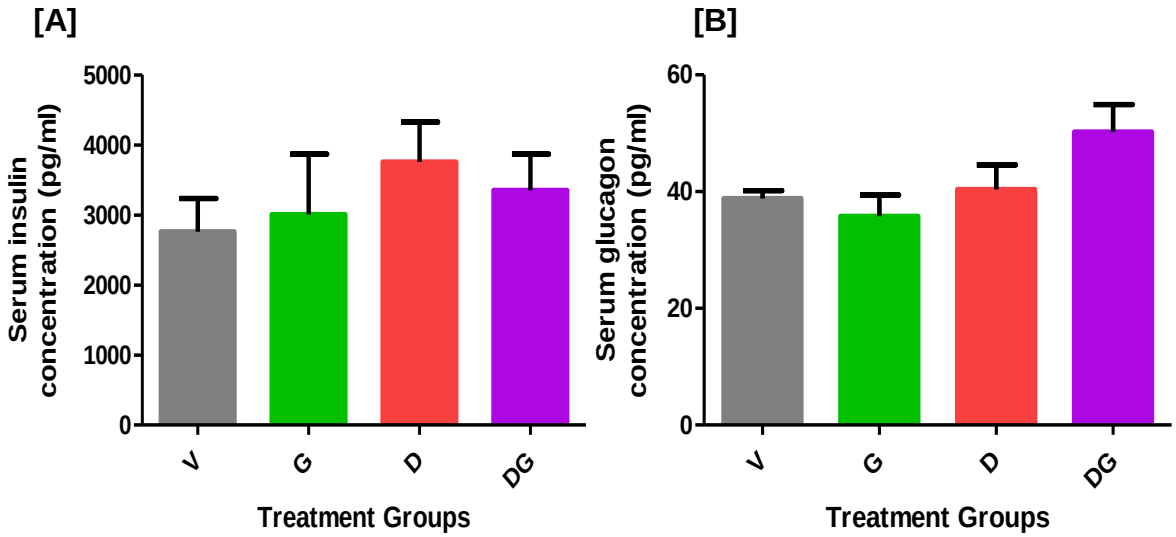

Figure 3.3: Serum [A] insulin and [B] glucagon concentrations of animals between treatment groups following eight weeks of treatment. Experimental animals were treated with saline, ghrelin, DOX and DOX+ghrelin and were assessed on the ninth week following treatment. Values are expressed as mean ± SEM (n = 7 - 9). Abbreviations: V (vehicle), G (ghrelin), D (DOX), DG (DOX+ghrelin).

3.3 Histomorphological changes induced by DOX and ghrelin treatment

In an effort to determine the potential structural modifications induced by DOX and ghrelin within the islets of Langerhans, H&E staining was conducted. There were no noticeable changes observed between both the endocrine and exocrine tissue between treatment groups. The islets present with an ovoid shape and this was relatively maintained throughout the various treatment groups without any major modifications. However, it should be noted that the islets in the groups treated with DOX did appear to be smaller and irregularly shaped when compared to the vehicle group (Figure 3.4). Even though the islets displayed in this figure seem to be quantified, this was not the case in this study.

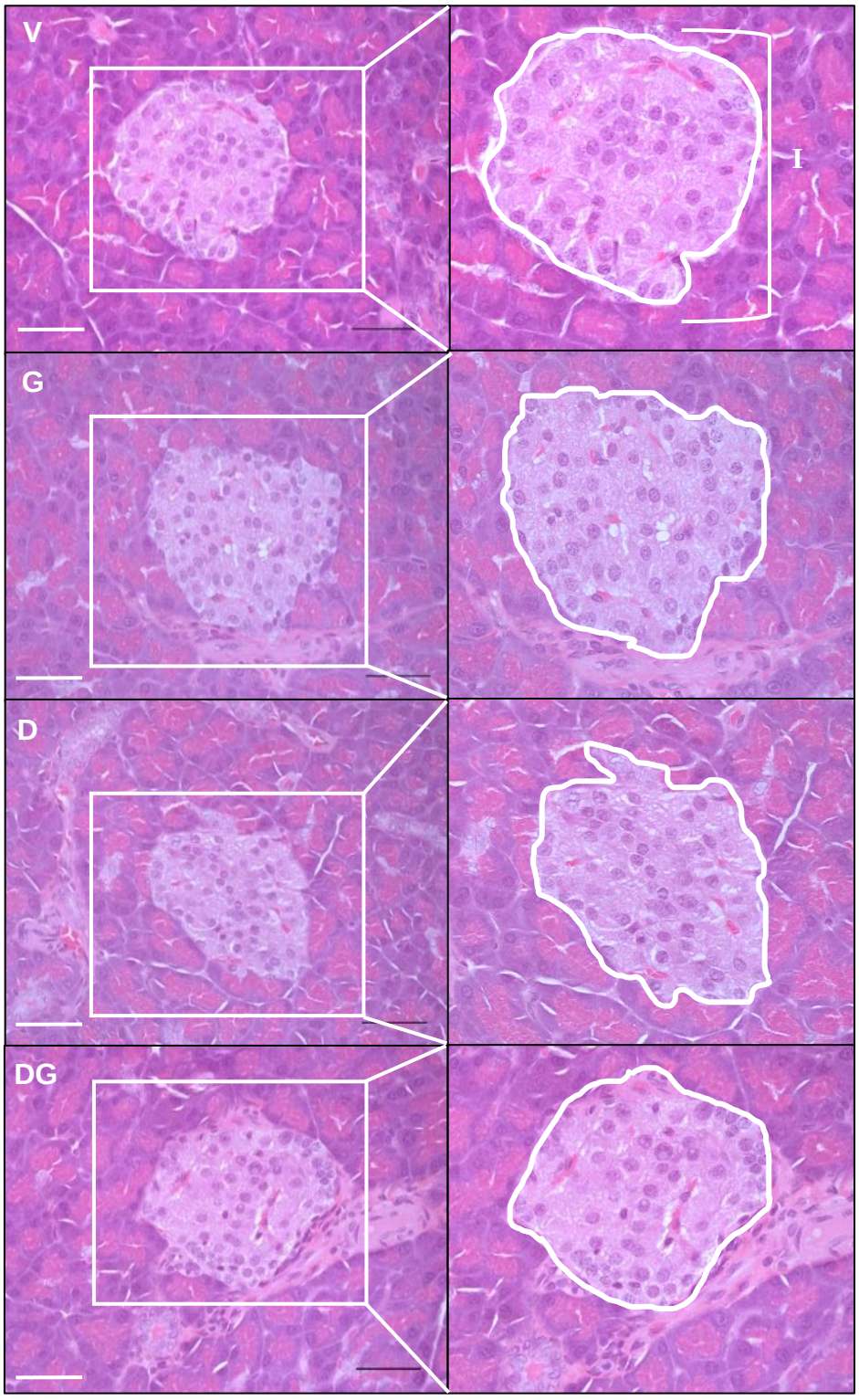

Figure 3.4: Representative H&E photomicrographs of the islets of Langerhans between treatment groups following eight weeks of treatment. Images were enlarged (right) and the islets encircled in order to assess islet shape. Experimental animals were treated with saline, ghrelin, DOX and DOX+ghrelin and were assessed on the ninth week following treatment. Images on left: Magnification = 40 X, Scale bar = 50 µm, n = 7 – 9. Abbreviations: V (vehicle), G (ghrelin), D (DOX), DG (DOX+ghrelin), I (Islet of Langerhans).

3.4 DOX and ghrelin's effect on collagen deposition

The Masson's Trichrome stain was employed to establish fibrosis within the pancreas and the representative images of collagen deposition are presented in Figure 3.5A. Both the vehicle and ghrelin groups showed relatively small amounts of collagenous tissue (blue areas), while a noticeable amount of collagen was observed in the DOX treated group when compared to the vehicle. The combination group displayed less collagen deposition versus the DOX group. To quantify these observations and statistically compare differences between groups, 20 random areas of the pancreas in each treatment group were imaged and analysed using Image J software. The collagenous areas (blue areas) were quantified and expressed as a percentage of the area of the entire tissue (red area). DOX was shown to induce significant collagenous tissue deposition (4.80 ± 0.78%, $p<0.0001$) when compared to the Vehicle group (1.14 ± 0.14%). Ghrelin significantly reduced the amount of collagen deposition in the combination group (2.22 ± 0.39%, $p<0.001$) when compared to the DOX group (Figure 3.5B), therefore confirming its known anti-fibrotic effects.

[A]

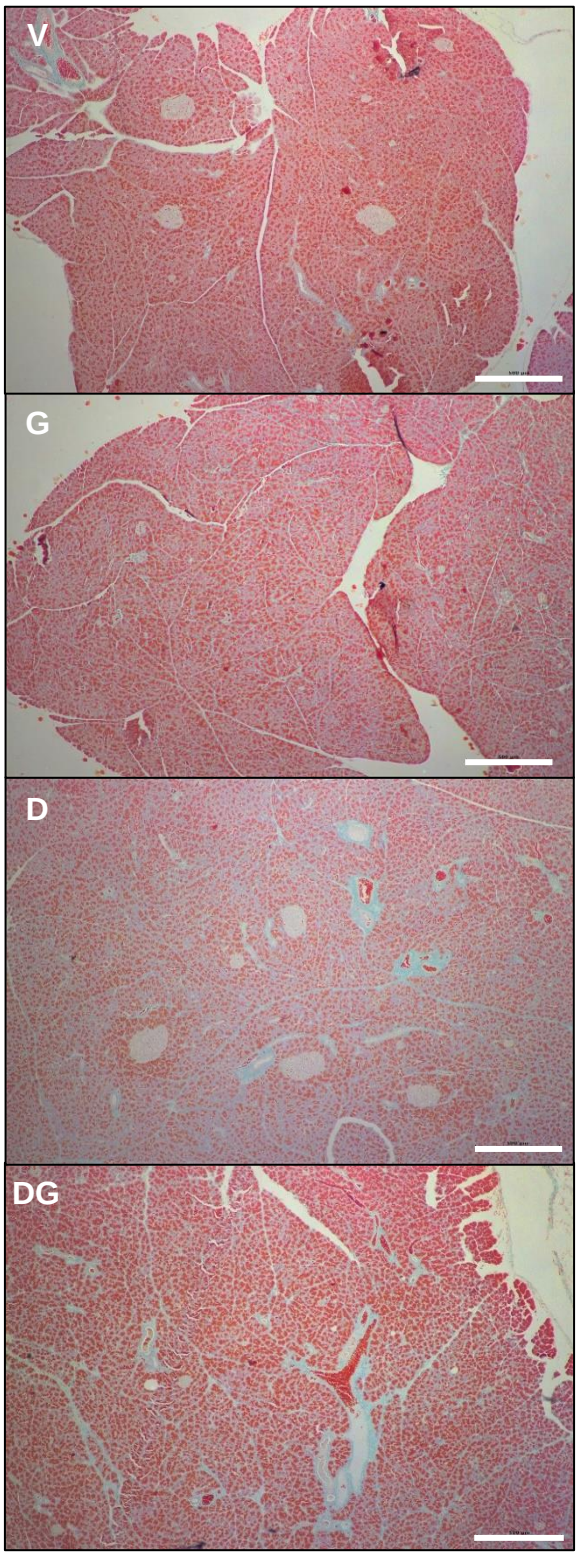

Figure 3.5: [A] Representative images of collagen deposition (blue-stained) in the pancreas between treatment groups following eight weeks of treatment. Experimental animals were treated with saline, ghrelin, DOX and DOX+ghrelin and were assessed on the ninth week following treatment. Magnification = 4 X, Scale bar = 50 µm, n = 7 – 9. Abbreviations: V (vehicle), G (ghrelin), D (DOX), DG (DOX+ghrelin).

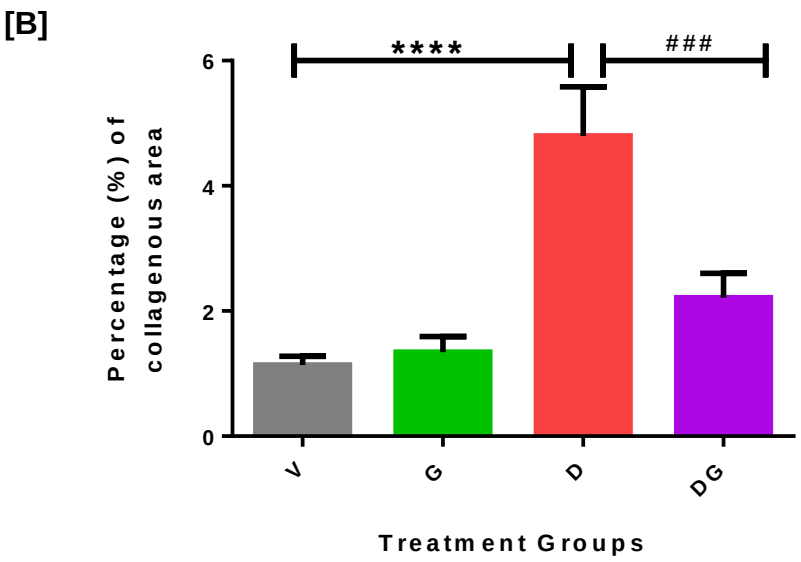

Figure 3.5: [B] Quantitative analysis of collagen content between treatment groups following eight weeks of treatment. Experimental animals were treated with saline, ghrelin, DOX and DOX+ghrelin and were assessed on the ninth week following treatment. Values are expressed as mean ± SEM (n = 7 - 9), **** p<0.0001 vs V, ###p<0.001 vs DG. Abbreviations: V (vehicle), G (ghrelin), D (DOX), DG (DOX+ghrelin).

3.5 Immunohistochemical evaluation of the islet composition

Immunohistochemistry was employed to establish the percentage of glucagon-secreting α-cells and insulin-secreting β-cells within each islet. Sequential double staining was utilised, where the α-cells were stained brown, and the β-cells were stained red/pink. Representative images of immunohistochemical stains are shown in Figure 3.6A. This study observed no significant changes to the number of α- and β-cells following manual quantification of the images (Figure 3.6B & Figure 3.6C).

Collectively, all the different histological techniques used in this study displayed no structural differences between treatment groups, other than collagen deposition. This may suggest that either the model of chronic DOX treatment used in this study was not severe enough to produce significant changes, or the changes were too subtle to be detected overall.

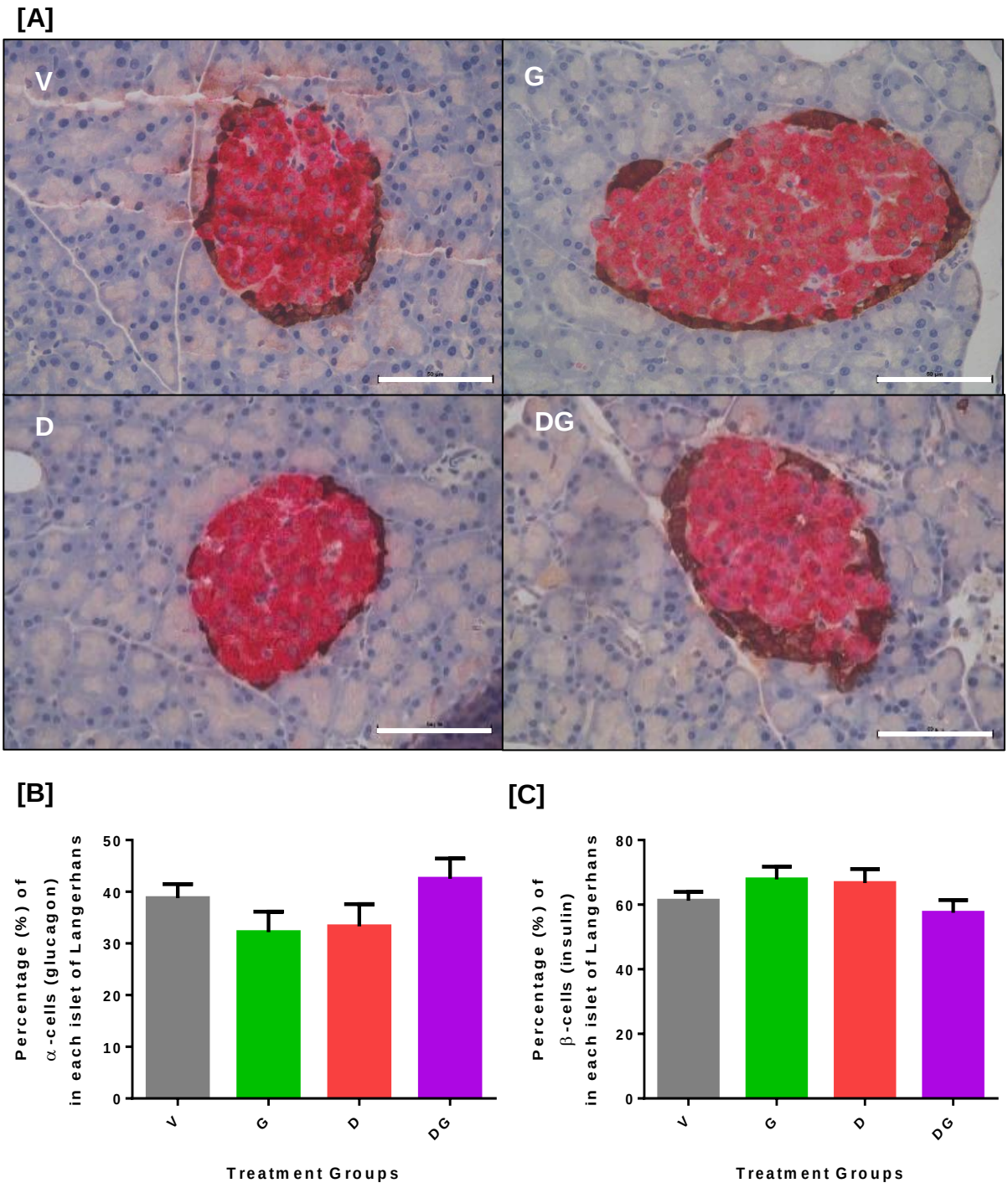

Figure 3.6: [A] Representative immunohistochemical photomicrographs of the islets of Langerhans, and the percentage of [B] α-cells and [C] β-cells within each islet of Langerhans between treatment groups following eight weeks of treatment. Experimental animals were treated with saline, ghrelin, DOX and DOX+ghrelin and were assessed on the ninth week following treatment. [A] Magnification = 40 X, Scale bar = 50 µm, n = 4 – 5. [B] Values are expressed as mean ± SEM (n = 7 – 9). Abbreviations: V (vehicle), G (ghrelin), D (DOX), DG (DOX+ghrelin).

3.6 Investigating the effects of chronic DOX and ghrelin treatments on oxidative stress

The major mechanism by which DOX is believed to cause damage to other organs is by the generation of free radicals which induce oxidative damage and, if severe enough, eventually lead to apoptosis. While anti-oxidant enzymes maintain the balance of free radicals in cells, oxidative damage may result if the generation of free radical exceeds the ability of anti-oxidants to protect cells (Rahman, 2007). Therefore, this study measured the anti-oxidant capacity, anti-oxidant status, as well as oxidative damage for a holistic evaluation of oxidative stress in the different treatment groups.

3.6.1 Anti-oxidant capacity

The oxidative radical absorbance capacity (ORAC) was measured to establish DOX and ghrelin's effects on the anti-oxidant capacity of the pancreas. As indicated in Figure 3.7, DOX significantly increased (0.51 ± 0.028 µmol TE/g, $p<0.01$) the anti-oxidant capacity when compared to the vehicle (0.37 ± 0.05 µmol TE/g). Ghrelin, either alone or in the presence of DOX, did not lead to any considerable changes when compared to the vehicle and DOX treated groups, respectively. Moreover, this figure illustrates that the anti-oxidant capacity of the combination group was significantly higher (0.47 ± 0.01 µmol TE/g) than the vehicle group. Taken together, these results suggest that DOX induces oxidative stress which raises the anti-oxidant capacity of the pancreas while ghrelin reduces the DOX-induced oxidative stress and, thus, the consequent increase in anti-oxidant capacity.

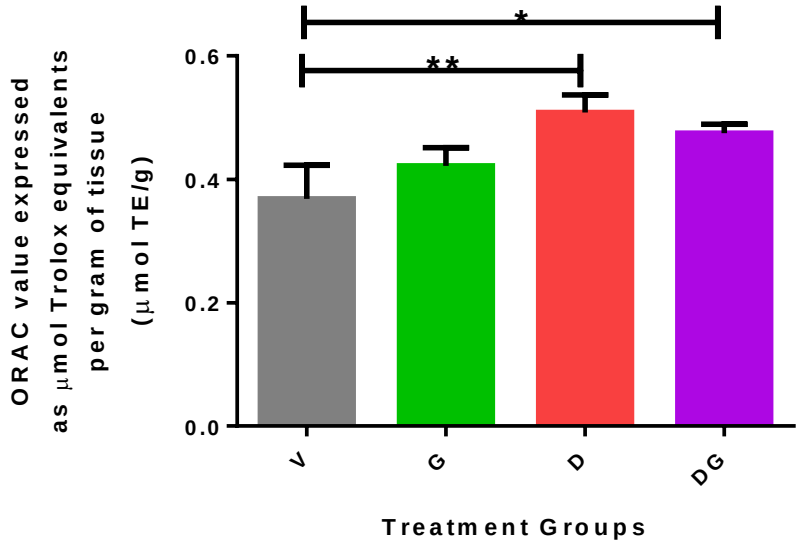

Figure 3.7: Anti-oxidant capacity of the pancreas between treatment groups following eight weeks of treatment. Experimental animals were treated with saline, ghrelin, DOX and DOX+ghrelin and were assessed on the ninth week following treatment. Values are expressed as mean ± SEM (n = 7 - 9), ** p<0.01 vs V. Abbreviations: V (vehicle), G (ghrelin), D (DOX), DG (DOX+ghrelin), µmol TE/g (µmol of Trolox equivalent/gram of tissue).

3.6.2 Superoxide dismutase activity and expression

To further evaluate the effects of the different treatment regimens on specific anti-oxidants, SOD activity and expression was determined. SOD was assessed as it is the most abundant anti-oxidant in the pancreas, and DOX is known to produce ROS in the form of $O_2^{\bullet -}$, which are dismutated by SOD. DOX reduced (1.49 ± 0.18 U/mg, p<0.01) the overall activity of these enzymes when compared to the vehicle (2.31 ± 0.28 U/mg) (Figure 3.8A). No changes in SOD activity were observed with ghrelin treatment, either alone or in combination with DOX, when compared to vehicle and DOX treated groups, respectively. However, SOD activity in the combination group was significantly reduced (1.54 ± 0.12 U/mg) when compared to the vehicle. These results indicate that DOX is inhibiting the activity of SOD, while treatment with ghrelin is preventing the inhibitory effect of DOX on SOD activity.

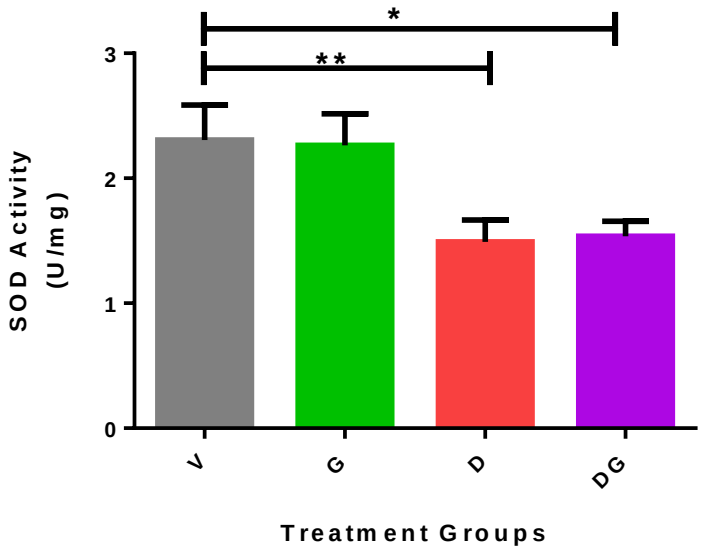

Figure 3.8: [A] SOD activity in the pancreas between treatment groups following eight weeks of treatment. Experimental animals were treated with saline, ghrelin, DOX and DOX+ghrelin and were assessed on the ninth week following treatment. Values are expressed as mean ± SEM (n = 7 - 9), ** p<0.01 vs V. Abbreviations: V (vehicle), G (ghrelin), D (DOX), DG (DOX+ghrelin), U/mg (unit inhibition/mg of protein).

When observing protein expression of the two SOD isoforms, including SOD1 (copper Zinc/CuZnSOD) and SOD2 (manganese/MnSOD), different expression patterns were observed. SOD1 is mainly cytosolic and while no changes observed were statistically significant across treatment groups, there was a gradual decline in its expression (Figure 3.9B). SOD2, on the other hand, is mainly mitochondrial and DOX did not appear to affect its expression when compared to the vehicle group. Alternatively, although not statistically significant, ghrelin modestly increased SOD2 expression both alone and in the presence of DOX when compared to vehicle and DOX treated groups, respectively (Figure 3.9C). It is therefore likely that both DOX and ghrelin influence expression of SOD enzymes depending on their localisation.

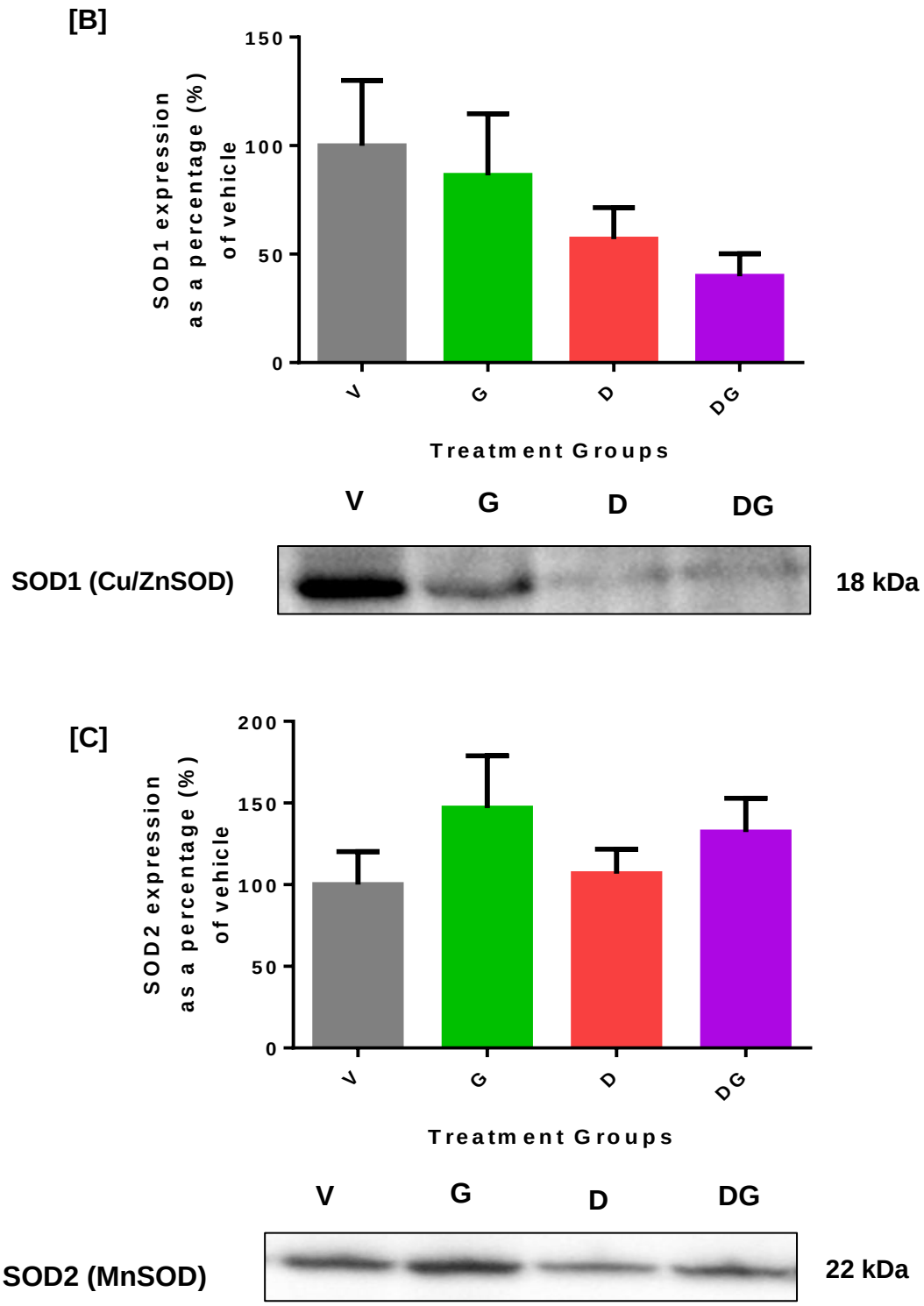

Figure 3.8: Western blot analysis of [B] SOD1 and [C] SOD2 protein levels between treatment groups following eight weeks of treatment. Experimental animals were treated with saline, ghrelin, DOX and DOX+ghrelin and were assessed on the ninth week following treatment. Values are expressed as mean ± SEM (n = 7 - 9). Abbreviations: V (vehicle), G (ghrelin), D (DOX), DG (DOX+ghrelin).

3.6.3 Glutathione assays

Considering that the ORAC assay does not measure glutathione levels, as well as the fact that SOD dismutates $O_2^{\bullet -}$ into H_2O_2 which is then targeted by GPx, this study utilised glutathione assays to measure the levels of both the reduced (GSH) and oxidised (GSSG) forms of glutathione. GPx removes H_2O_2 by coupling its reduction (GSH) to H_2O_2 with the oxidation of glutathione (GSSG). As indicated in Table 3.3, no changes were observed in any of the treatment groups when GSH, GSSG and the ratio (GSH: GSSG) between the two were evaluated, thus demonstrating that neither DOX nor ghrelin treatment had any considerable effect on GPx activity in the pancreas.

Table 3.3: Glutathione content in the pancreas between treatment groups following eight weeks of treatment. Experimental animals were treated with saline, ghrelin, DOX and DOX+ghrelin and were assessed on the ninth week following treatment. Values are expressed as mean ± SEM (n = 6 - 9). Abbreviations: V (vehicle), G (ghrelin), D (DOX), DG (DOX+ghrelin), AU (arbitrary unit).

Treatment Group	Vehicle	Ghrelin	DOX	DOX+Ghrelin
GSH (µmol/g)	102.7 ±1.42	89.55 ±4.31	95.15 ±5.05	90.62 ±6.178
GSSG (µmol/g)	23.81 ±1.05	25.47 ±0.80	24.95 ±1.715	26.89 ±2.345
GSH: GSSG (AU)	4.357 ±0.1876	3.55 ±0.2662	4.068 ±0.4733	3.721 ±0.5162

3.6.4 Assessment of lipid peroxidation

Lipid peroxidation is the most widely used indicator of free radical production. Unsaturated fatty acids, present in the cell membranes and other organelles, are a common target for free radicals. When fatty acids are oxidised, they produce lipid hydroperoxides, in which conjugated dienes (CDs) are one of the initial products generated that undergo further oxidation to form malondialdehyde (MDA). The results presented in Figure 3.9A & B show no significant changes between treatment groups,

which demonstrates that neither DOX nor ghrelin treatment resulted in oxidative damage of the pancreas following eight weeks of treatment.

Taken together, the oxidative stress analyses used in this study indicate that while there was a degree of free radical production, the ROS produced was not significant to induce oxidative damage in the form of lipid peroxidation.

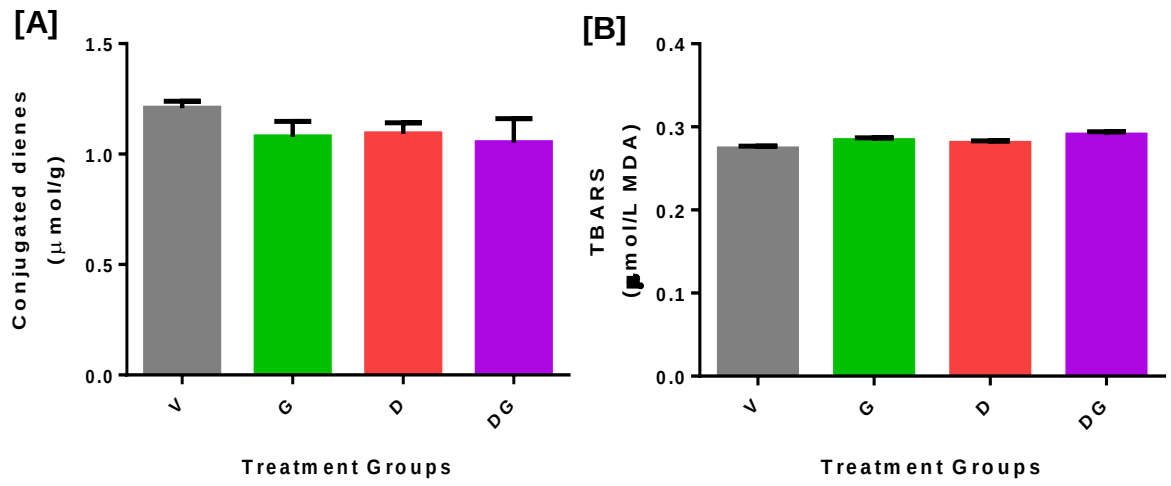

Figure 3.9: Assessment of lipid peroxidation in which [A] conjugated dienes and [B] malonaldehyde concentrations were measured in the pancreas between treatment groups following eight weeks of treatment. Experimental animals were treated with saline, ghrelin, DOX and DOX+ghrelin and were assessed on the ninth week following treatment. Values are expressed as mean ± SEM (n = 3 - 5). Abbreviations: V (vehicle), G (ghrelin), D (DOX), DG (DOX+ghrelin), µmol/g (µmol conjugated dienes/gram of tissue), µmol/L MDA (µmol/L of malonaldehyde).

3.7 Evaluation of apoptosis during DOX and ghrelin treatment

When oxidative stress exceeds the anti-oxidant capacity, apoptotic cell death is stimulated. This study illustrated that while total caspase-3 expression did not change between the treatment groups, the expression of the cleaved form of caspase-3 produced considerable changes although not statistically significant (Figure 3.10). DOX treatment resulted in increased cleaved caspase-3 expression, though in the presence of ghrelin, its expression was reduced. These results indicate that while DOX is a potent cytotoxic agent, ghrelin is anti-apoptotic and thus, protective.

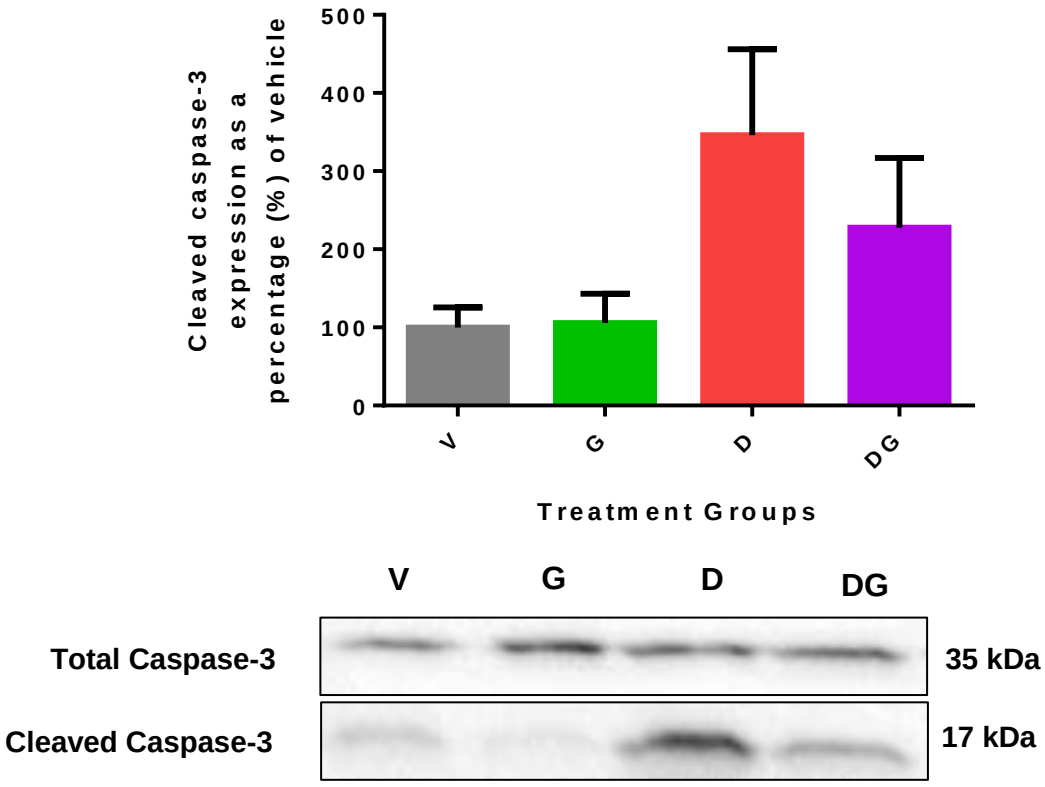

Figure 3.10: Western blot analysis of both total and cleaved caspase-3 protein levels between treatment groups following eight weeks of treatment. Experimental animals were treated with saline, ghrelin, DOX and DOX+ghrelin and were assessed on the ninth week following treatment. Values are expressed as mean ± SEM (n = 7 - 9). Abbreviations: V (vehicle), G (ghrelin), D (DOX), DG (DOX+ghrelin).

Chapter 4: Discussion

The pancreas is one of the most important organs in the body as it aids in digestion and glucose metabolism due to the presence of exocrine and endocrine tissues, respectively. It is similar to other organs in that it is prone to injury induced either by extracellular or intracellular stimuli. DOX, a potent chemotherapeutic agent known for its clinical efficiency against rapidly multiplying cells, remains one of the most widely used anti-cancer agents for the treatment of a variety of cancers. However, DOX's clinical use is limited due to its cumulative, dose-dependent toxicity, particularly in cardiomyocytes. This has led to literature predominately focusing on the underlying mechanisms involved in DOX's toxicity in the heart and other organs, while studies are lacking regarding DOX's effects on the pancreas. Therefore, the influence of DOX on the pancreas was investigated in this study. Furthermore, as there is no cure for DOX toxicity, there is no consensus nor guidelines established in the literature as to how this condition should be managed. Thus, this study further evaluated the properties of ghrelin, a brain-gut hormone best known for its appetite stimulating effects, which could be of potential benefit in this context. Furthermore, since DOX toxicity is associated with oxidative stress, apoptosis, inflammation and fibrosis, this study investigated ghrelin's previously demonstrated protective properties in this context.

4.1 DOX prevents weight gain while ghrelin promotes appetite

One of the most striking features of a cancer patient undergoing chemotherapy is not only hair loss but also weight loss, and considering that ghrelin promotes appetite, its use as an adjuvant therapy in this study was promising. As indicated in Figures 3.1 and 3.2, DOX treated animals ate significantly less food and consequently gained less weight, when compared to their control (vehicle) counterparts, and thereby the growth of these animals was stunted. The inclusion of ghrelin as part of the treatment regimen appears to prevent this from occurring, albeit insignificantly so. These results are in accordance with other *in vivo* studies that showed that ghrelin administration during a cachexic state not only stimulated appetite, increased body weight and adiposity, it also protected the skeletal muscles from wasting (Strassburg *et al.*, 2008; Reano *et al.,* 2014; Tschöp *et al.*, 2000). Although the exact mechanisms underlying ghrelin's orexigenic effects are still unknown, what is known is that ghrelin acts through the

hypothalamic-pituitary axis to promote appetite. When ghrelin is produced by the oxyntic gastric mucosa, it is released into circulation where it travels to the anterior pituitary gland and exerts its effects (Date *et al.*, 2002; Chopin *et al.*, 2011). In addition, ghrelin induces the release of GH from the pituitary to promote adipogenesis, proliferation and differentiation of cells, as well as the stimulation of bone growth (Zhang *et al.*, 2007; Delporte, 2013). The above effects could thus be attributed to the increase in food consumption which promotes energy production and increased body weight, as well as the independent effects of GH. As there are no known toxic effects of ghrelin even at supraphysiological doses, it may be a promising agent that could be used alongside DOX to prevent cachexia and improve quality of life of patients.

4.2 Neither DOX nor ghrelin alters pancreatic insulin and glucagon secreting cells

Insulin secreted by pancreatic β-cells promotes the uptake of glucose, fatty acids and amino acids from the blood into peripheral tissues, including skeletal muscle and adipocytes, whereas glucagon secreted by pancreatic α-cells induces glucose production through the promotion of glycogenolysis and gluconeogenesis (Jiang & Zhang, 2003; Rafacho *et al.*, 2014). Therefore, in the post-prandial state, circulating insulin levels are high and ghrelin levels are low in order to decrease circulating blood glucose levels. When insulin binds to its receptor (IR) or insulin-like growth factor-1(IGF-1R), which are expressed at the cell surface of peripheral tissues, cytoplasmic insulin receptor substrate (IRS) proteins transmit signals from these receptors to induce a cellular response. This occurs by IRS becoming phosphorylated at the tyrosine residues and leads to the activation of the phosphatidylinositol-4,5-bisphosphate 3-kinase (PI3K)/Akt pathway, which triggers glucose transporter 4 (GLUT-4) to translocate to the cell membrane, facilitating glucose uptake into the cell (Shaw, 2011). In the fasted state however, both glucagon and ghrelin levels are high in order to increase blood glucose levels. Even though our results show that there were no changes in the circulating levels of both insulin and glucagon in any of the treatment groups (Figure 3.3A & B), the levels of insulin were ±70 fold higher than glucagon levels. As these animals were not fasted when blood was collected, it is thus likely that the high insulin levels observed were as a result of the animals being in a fed state. Since the link between the use of chemotherapeutic drugs and the development of diabetes remains to be elucidated and the fact that previous studies

have reported that DOX treatment inhibits glucose-stimulated insulin secretion in isolated rat β-cells (Dispenzieri & Loprinzi, 1997; Geetha *et al.*, 1999), this study merely aimed to evaluate DOX's effects on insulin and glucagon secretion and to assess the role of ghrelin within this context. To investigate this further, fasted serum levels of insulin, glucagon and ghrelin should be taken before, during and after treatment with DOX.

Damage to α- and β-cells can lead to pancreatic disorders such as diabetes (Bachmann *et al.* 2011; Steer, 2012). Numerous experimental studies have shown that DOX is highly toxic to rodent islets and induces apoptotic cell death of β-cells (Zhang *et al.*, 2007; Heart *et al.,* 2016). In our study, ghrelin did not appear to induce any obvious morphological changes to the islets of Langerhans, which all displayed a relatively normal ovoid shape (Figure 3.4). Although the islets of Langerhans in the DOX treated group appeared to be smaller and irregularly shaped, these changes were minor. To support our findings, Saleh & Ali (2005) also illustrated that DOX stimulates atrophy of pancreatic cells. Furthermore, the number of α- and β-cells contained within each islet in this study remained the same (Figure 3.6 A-C). Considering all of the above, the model used to simulate chronic DOX toxicity had no significant effect on glucagon and insulin secretion as well as the number of α- and β-cells within the islets. It is likely that our insignificant results were due to the concentration, frequency and duration of DOX treatment compared to other studies. Whereas this study treated animals with DOX once weekly (2.5 mg/kg) over eight weeks resulting in a cumulative dose of 20 mg/kg, Saleh & Ali (2015) treated their animals with a dose of 15 mg/kg for 30 days.

4.3 Ghrelin ameliorates DOX-induced fibrosis

Despite DOX being listed as one of the drugs associated with the development of pancreatitis, the mechanisms involved remain unknown (Trivedi & Pitchumoni, 2005; Kaurich, 2008). Pancreatitis, as mentioned previously can be categorised as acute pancreatitis, which is associated with inflammation, and chronic pancreatitis, in which fibrosis is a hallmark characteristic (Bachmann *et al.,* 2011; Lankisch *et al.*, 2015). During acute pancreatitis, obstruction or damage to the pancreatic ducts can result in the leakage of pancreatic digestive enzymes from acinar cells, resulting in damage to the pancreatic tissue and the stimulation of an inflammatory response (Jones &

Gorges, 1997). Serum TNF-α and IL-6 levels can be used as early markers for the detection of acute pancreatitis, however considering the half-life of these cytokines, peak serum concentrations are difficult to detect. The serum levels of TNF-α and IL-6 in this study were below the detectable range (data not shown).

Prolonged and continuous inflammation within the pancreas can progress to fibrosis often associated with chronic pancreatitits (Steer, 2012; French & Charnely, 2016). Although the mechanisms involved have yet to be fully determined, persistent activation of pancreatic stellate cells have been reported in both human and experimental studies, where these cells are responsible for collagen synthesis (Haber *et al.*, 1999; Kozak *et al.*, 2016). Following pancreatic injury, platelets secrete pro-fibrotic cytokines PDGF and TGF-β1 which recruit white blood cells to the injured site. PDGF triggers proliferation of pancreatic stellate cells, while TGF-β1 stimulates these cells to produce collagen, consequently replacing damaged cells with fibrotic tissue (Kishi *et al.*, 2003). In this study, treatment with DOX induced significant collagen deposition indicative of fibrosis (Figure 3.5A & B), while co-treatment with ghrelin reduced collagen deposition. In support of our observations, various studies have shown the anti-fibrotic effects of ghrelin administration in different contexts. Reduced type I and III collagen deposition following ghrelin administration has previously been demonstrated in injured rat kidneys (Sun *et al.*, 2015) and following a myocardial infarction (Huang *et al.*, 2009), which reduced overall fibrosis. These event are thought to occur through ghrelin's anti-inflammatory effects which have been shown to downregulate pro-inflammatory cytokine expression in human monocytes (Dixit *et al.*, 2004). Therefore, this study proposes that by reducing the expression levels of pro-inflammatory and pro-fibrotic cytokines, ghrelin exhibits similar protective effects in the pancreas during DOX treatment and thereby reduces collagen deposition.

4.4 DOX induces SOD anti-oxidant activity

As a result of inflammation, ROS generation cannot be avoided and has been implicated in playing a role in damaging pancreatic parenchyma, leading to fibrosis (Angelino *et al.*, 2015). In this context, DOX is a potent inducer of oxidative stress due to its chemical structure having the ability to be oxidised and reduced, and thereby producing ROS (Minotti *et al.*, 2004). This study demonstrates that the pancreas in response to DOX treatment elevates its anti-oxidant capacity (Figure 3.7). Although

this response was expected, it is a clear indication that this organ is attempting to protect itself against DOX-induced ROS generation.

SOD is the most abundant anti-oxidant found in the pancreas and DOX is particularly known to produce ROS in the form of $O_2^{\bullet -}$ (Grankvist *et al.,* 1981; Kalyanaraman *et al.*, 2002). Therefore, to determine the presence of $O_2^{\bullet -}$, SOD activity was measured (Figure 3.8A). Our findings show that in both DOX treated groups, SOD anti-oxidant activity was significantly reduced. Although it is known that persistent or high levels of ROS can reduce anti-oxidant activity (Poljsak *et al.*, 2013), it is relatively unknown that DOX can influence the expression of SOD enzymes in the pancreas (Figure 3.8B & C). While SOD1, which is mainly cytosolic, was reduced in all treatment groups when compared to the vehicle, mitochondrial SOD2 was elevated in both ghrelin treated groups. Despite these results being insignificant, there is a clear distinction in differential effects that both ghrelin and DOX have on the SOD isoforms. Whereas SOD1 appeared to be severely affected by DOX treatment and unaffected by ghrelin, SOD2 remained unchanged in the presence of DOX, its expression increased in the presence of ghrelin.

The role of SOD is to dismutate $O_2^{\bullet -}$ to form H_2O_2, which is removed by catalase and GPx. However, H_2O_2 removal is influenced by where it is produced. While H_2O_2 produced by enzymes in peroxisomes is usually disposed of by catalase, H_2O_2 produced in the mitochondria is removed by GPx. GPx removes H_2O_2 by coupling its reduction to H_2O_2 with the oxidation of glutathione (Weydert & Cullen, 2010). This study did not observe any noteworthy changes in the status of glutathione levels in its reduced (GSH) nor oxidised (GSSG) forms (Table 3.3). This result was not particularly surprising considering that SOD activity was reduced, and thus H_2O_2 was not produced to influence the GSH levels in a significant manner.

We also found no changes in the early and late markers of lipid peroxidation, the main molecular mechanism involved in oxidative damage to cell structures and the toxicity that leads to cell death. (Figure 3.9A & B). The first step in the initiation of lipid peroxidation is the production of a fatty acid radical by ROS such as $OH^{\bullet}$ or hydroperoxyls ($HOO^{\bullet}$) radicals. As these fatty acid radicals are not very stable, they react with O_2 to produce a peroxyl fatty acid radical. This newly formed radical is also not stable, and reacts with another fatty acid radical to produce a different fatty acid

radical and lipid peroxides. If, however, the peroxyl fatty acid radical reacts with itself, then cyclic peroxide is produced. This cycle continues in a chain reaction until two radicals react with one another to produce a non-radical (Botsoglou *et al.*, 1994; Devasagayam *et al.*, 2003). Yet to produce $OH^{\bullet}$, $O_2^{\bullet-}$ would have to react with H_2O_2 in the presence of transition metals such as Fe; whereas to form $HOO^{\bullet}$, hydrogen atoms are donated to O_2 or, O_2 donates to $OH^{\bullet}$ or, protons are donated to $O_2^{\bullet-}$ (Halliwell, 2006; Valko *et al.*, 2006). Considering that $OH^{\bullet}$ are the most reactive of all ROS, and no H_2O_2 was detected in this study (indirectly measured by GSH levels) it is plausible to speculate that there was an insufficient of amount ROS generated to induce lipid peroxidation in this study. However, $OH^{\bullet}$ radicals have been observed in isolated rat islets (Armanna *et al.*, 2007), but whether they are upregulated in animal models of inflammatory diseases and make a significant contribution to the disease pathology by aggravating tissue injury, remains to be resolved.

4.5 Anti-apoptotic effects of ghrelin against DOX-induced cell death

Apoptotic cell death triggered by either oxidative stress, inflammation or DOX treatment directly, is a relevant event that occurs in this context (Sawyer *et al.*, 1999; Kotamraju *et al.*, 2000). It is well known that caspase-mediated apoptosis involves the cleavage of initiator and executioner caspases resulting in their activation (Poirier *et al.*, 2002; Chaitanya *et al.*, 2010). In this study, DOX considerably increased cleaved caspase-3 protein expression, but in the presence of ghrelin, this protein was reduced (Figure 3.10). Since the results from the oxidative stress analysis suggest that the amount of ROS was not sufficient to cause lipid peroxidation, and the inflammatory cytokines were undetectable, this study proposes that this ROS could have contributed to activating the intrinsic apoptotic pathway. There are a few ways in which this can be achieved. Firstly, p53-mediated apoptosis involves transcriptional regulation of target genes and is dependent on the Apaf-1/caspase-9 pathway, which results in cytochrome c release (Kim *et al.*, 2006), though the exact mechanism remains elusive. Secondly, cytochrome c has a high affinity for cardiolipin, and once a shift in the oxidation state of cardiolipin changes as a result of ROS, cytochrome c is released (Paradies *et al.*, 2014). Finally, the disruption of Ca^{2+} homeostasis within the ER or mitochondria are also known to be apoptogenic (Zhang *et al.*, 2012; Williams *et al.*, 2013). All of the above events culminate in the initiation of the caspase cascade as a result of cytochrome c leakage. The anti-apoptotic effect of ghrelin observed from our

findings is in agreement with other studies where ghrelin prevented apoptosis from taking place in kidney cells and cardiomyocytes (Sun *et al.*, 2015; Wang *et al.*, 2014). This study therefore proposes that ghrelin exhibits its effects by protecting mitochondria to prevent cytochrome c release so that apoptosis can be averted.

CHAPTER 5: Conclusion

DOX forms an integral part of the current chemotherapeutic treatment regimens due to its potency in treating various cancers. As a result of this characteristic, DOX remains one of the most widely used anti-neoplastic agents leading to improved survival rates of cancer patients. However, DOX's efficacy is a double-edged sword where prolonged treatment is associated with off-target toxicity, particularly in cardiomyocytes. While literature over the years predominantly focused on DOX-induced cardiotoxicity, very few studies regarding the effects of DOX on the pancreas are available. Although the exact mechanisms underlying DOX's toxicity is yet to be elucidated, it is known that these mechanisms are distinct to its anti-neoplastic activities. This creates the possibility that an adjuvant treatment strategy can be investigated to reduce DOX's off-target toxicity without interfering with its efficacy. Due to the disappointing and inconclusive results obtained in clinical trials utilising anti-oxidants to target DOX-induced oxidative stress, a solution to this problem is yet to be found. Bearing the above in mind, this study approached this multi-faceted problem by investigating the benefits of a hormone with multi-faceted effects in this context. Ghrelin is a natural hormone most well-known for its appetite inducing and GH releasing effects. In addition, it has previously been shown to reduce oxidative stress, apoptosis, inflammation and fibrosis, all of which contribute to DOX toxicity. Our findings reveal that while ghrelin prevented weight loss by inducing food intake, and reduced both collagen deposition (indicative of fibrosis) and DOX-induced apoptosis in pancreatic tissue, it had no effect on oxidative stress overall and no definitive conclusions can be drawn with regards to inflammation (Figure 5.1A & B). Overall, while results are promising, further investigations are necessary to decipher the potential of ghrelin as an adjuvant treatment regimen in the context of DOX-induced pancreatic injury.

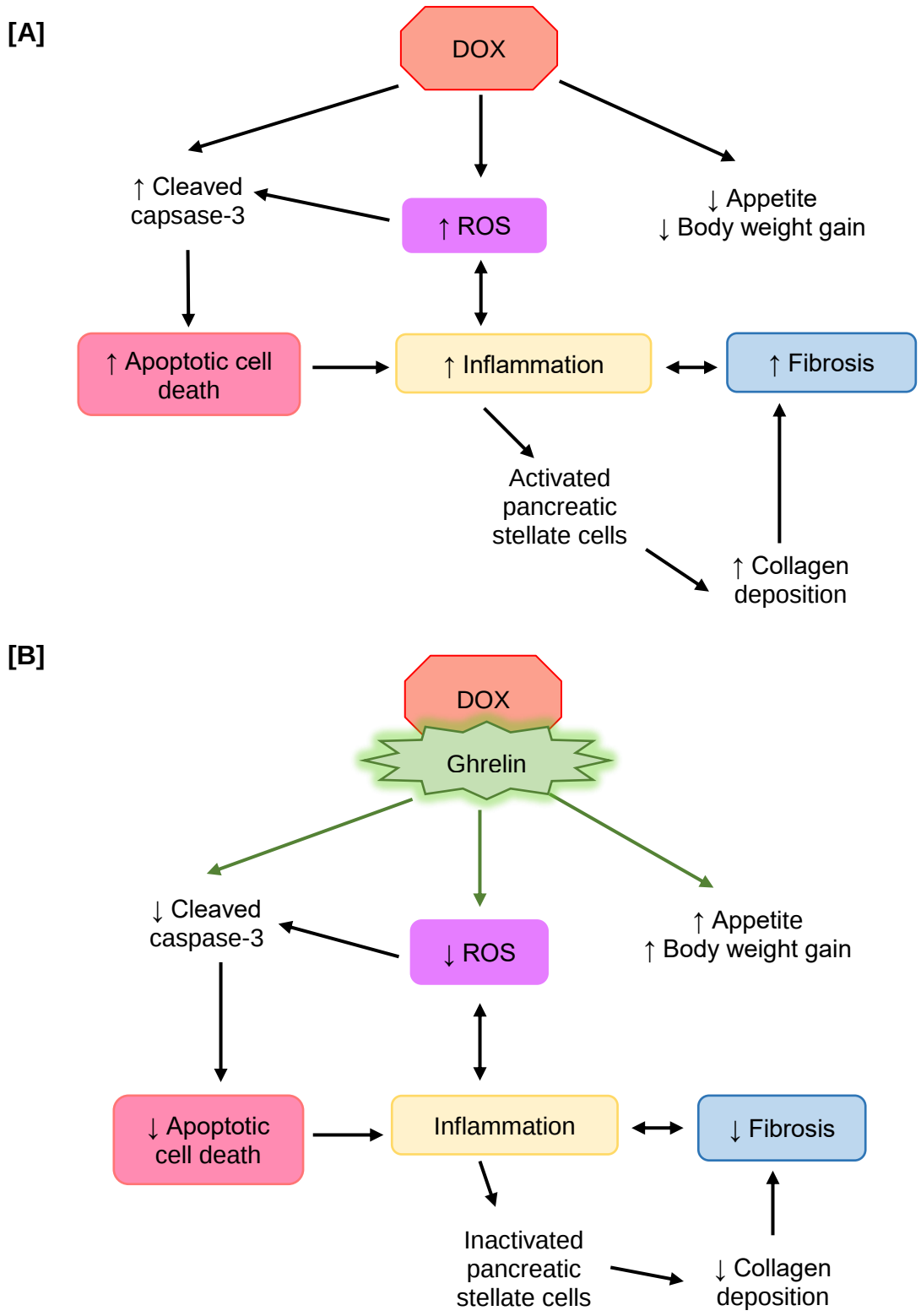

Figure 5.1: The proposed mechanisms of action of DOX and ghrelin on pancreatic tissue. A summary of the main findings indicating the possible effects of DOX alone [**A**] and DOX co-treated with ghrelin [**B**]. Abbreviations: ROS (reactive oxygen species), DOX (Doxorubicin), ↑ (increases), ↓ (decreases).

5.1 Limitations and future direction

As far as we are aware, this study is one of very few studies investigating the effects of DOX treatment on the pancreas in a model simulating chronic DOX-induced cardiotoxicity. The fact that clinically relevant dosages of DOX were used in this study further strengthens its originality and highlights its importance in reducing the gap that exists in the literature. While ghrelin's beneficial properties have been demonstrated in other organs, it has been relatively unknown whether the same effects would be observed in the pancreas. Due to the fact that there are limited studies available to support the results obtained in this study, we suggest that a larger sample size be utilised to strengthen the obvious trends observed. This will not only ensure a better understanding of DOX's effects on the pancreas, but also the role that ghrelin plays in this context. As there was a long period from the time that blood was collected to the time of analysis, and the fact that inflammatory cytokines have a short half-life, in hind sight blood should be have been collected between 12 and 24 hours after the last dose of DOX and ghrelin and immediately analysed. In addition, to measure circulating hormones of the pancreas, the animals should be fasted for at least 24 hours, and ghrelin could be included as part of the analysis. The size of the islets in the different treatment groups could also be measured to give an indication as to whether the islets are undergoing atrophy. Finally, GPx and apoptotic activity assays should be taken into account to supplement the protein expression already obtained.

The future recommendations of this study are vast as there are a multitude of questions to be answered. If funding constraints are not considered, additional animals could be included in the study design where some are sacrificed after 24 hours, one week, five weeks and at the end of the treatment protocol. With an increase in sample size, fasted blood samples could be collected after each treatment dosage and serum levels of insulin, glucagon, ghrelin, somatostatin and pancreatic polypeptide could be determined to indicate any changes that occurred over eight weeks of treatment. To determine pancreatitis, serum lipase and amylase enzymes as well as CRP levels could be measured as a possible indication of pancreatitis as these are all elevated during this condition. With the analysis of protein expression *via* Western blotting, a better approach would be to separate the cellular fractions (mitochondrial, cytosolic and membrane). This would enable improved understanding of the molecular events that take place and also how ghrelin induces its actions. Furthermore, desmin and α-

SMA fluorescent staining could be performed to understand the role of pancreatic stellate cells in contributing to fibrosis. As DOX treatment is known to induce gender specific changes, a female cohort could be added since DOX is one of the main treatments for breast cancer. Finally, since the aim of this study was to investigate the whether ghrelin can counteract DOX's cytotoxic effects, it is important to establish the effect of ghrelin on cancer cell proliferation and survival.

REFERENCES

Aldridge, G. M., Podrebarac, D. M., Greenough, W. T. & Weiler, I. J. (2008) 'The use of total protein stains as loading controls: an alternative to high-abundance single protein controls in semi-quantitative immunoblotting', *Journal of Neuroscience Methods*, 172(2), pp. 250–254.

Ali, M. K., Ewer, M. S., Gibbs, H. R., Swafford, J. & Graff, K. (1994) 'Late doxorubicin associated cardiotoxicity in children', *Cancer*, 74, pp. 182–188.

Altavilla, D., Famulari, C., Passaniti, M., Galeano, M., Macrì, A., Seminara, P., Minutoli, L., Marini, H., Calò, M., Venuti, F. S., Esposito, M. & Squadrito, F. (2003) 'Attenuated Cerulein-Induced Pancreatitis in Nuclear Factor–κB–Deficient Mice', *Laboratory Investigation*, 83(12), pp. 1723–1732.

Altavilla, D., Saitta, A., Guarini, S., Galeano, M., Squadrito, G., Cucinotta, D., Santamaria, L., Mazzeo, A., Campo, G., Ferlito, M., Minutoli, L., Barzani, C., Bertolini, A., Caputi, A. & Squadrito, F. (2001) 'Oxidative stress causes nuclear factor kappa B activation in acute hypovolemic hemorrhagic shock', *Free Radical Biology and Medicine*, 10, pp. 1055–1066.

Angelino, E., Reano, S., Ferrara, M., Agosti, E., Graziani, A. & Filigheddu, N. (2015) 'Antifibrotic activity of acylated & unacylated ghrelin', *International Journal of Endocrinology*. Hindawi Publishing Corporation, pp. 1–9.

De Angelis, A., Urbanek, K., Cappetta, D., Piegari, E., Ciuffreda, L. P., Rivellino, A., Russo, R., Esposito, G., Rossi, F. & Berrino, L. (2016) 'Doxorubicin cardiotoxicity and target cells: a broader perspective', *Cardio-Oncology*, 2, pp. 2.

Arafat, A., Perschel, F., Otto, B., Weickert, M., Rochlitz, H., Schofl, C., Spranger, J., Mohlig, M. & Pfeiffer, A. (2006) 'Glucagon suppression of ghrelin secretion is exerted at hypothalamus–pituitary level', *The Journal of Clinical Endocrinology & Metabolism*, 91(9), pp. 3528–3533.

Arafat, M., Otto, B., Rochlitz, H., Tschöp, M., Bähr, V., Möhlig, M., Diederich, S., Spranger, J. & Pfeiffer, A. (2005) 'Glucagon inhibits ghrelin secretion in humans', *European Journal of Endocrinology*, 153(3), pp. 397–402.

Arimura, A. & Fishback, J. (1981) 'Somatostatin: regulation of secretion', *Neuroendocrinology*, 33(4), pp. 246–256.

Armanna, B., Hansona, M. S., Hatcha, E., Steffena, A. & Fernandeza, L. A. (2007) 'Quantification of Basal and Stimulated ROS Levels as Predictors of Islet Potency and Function', *American Journal of Transplantation*, 7, pp. 38–47.

Arosio, M., Ronchi, C. L., Gebbia, C., Cappiello, V., Beck-peccoz, P. & Peracchi, M. (2003) 'Stimulatory Effects of Ghrelin on Circulating Somatostatin and Pancreatic Polypeptide Levels', *The Journal of Clinical Endocrinology & Metabolism*, 88(2), pp. 701–704.

Arunachalam, S., Tirupathi Pichiah, P. B. & Achiraman, S. (2013) 'Doxorubicin treatment inhibits PPARγ and may induce lipotoxicity by mimicking a type 2 diabetes-like condition in rodent models', *FEBS Letters*, 587, pp. 105–110.

Asakawa, A., Inui, A., Yuzuriha, H., Ueno, N., Katsuura, G., Fujimiya, M., Fujino, M. A., Niijima, A., Meguid, M. M. & Kasuga, M. (2003) 'Characterization of the Effects of Pancreatic Polypeptide in the Regulation of Energy Balance', *Gastroenterology*, 124(5), pp. 1325–1336.

Asensi, M., Sastre, J., Pallardo, F. V., Lloret, A., Lehner, M., Garcia-De-La Asuncion, J. & Viña, J. (1999) 'Ratio of reduced to oxidized glutathione as indicator of oxidative stress status and DNA damage', *Methods in Enzymology*, 299(1978), pp. 267–276.

Bachmann, K., Izbicki, J. R. & Yekebas, E. F. (2011) 'Chronic pancreatitis: Modern surgical management', *Langenbeck's Archives of Surgery*, 396(2), pp. 139–149.

Badalov, N., Baradarian, R., Iswara, K., Li, J., Steinberg, W. & Tenner, S. (2007) 'Drug-Induced Acute Pancreatitis: An Evidence-Based Review', *Clinical Gastroenterology and Hepatology*, 5(6), pp. 648–661.

Baeurle, P. & Baichwal, V. (1995) 'NF-kappa B as a frequent target for immunosuppressive and anti- inflammatory molecules', *Advances in Immunology*, 65, pp. 111–260.

Bancroft, J. D. & Gamble, M. (2008) *Theory and Practice of Histological Techniques*. Philadelphia: Churchhill Livingstone Elsevier.

Barazzoni, R., Semolic, A., Cattin, M. R., Zanetti, M. & Guarnieri, G. (2014) 'Acylated ghrelin limits fat accumulation and improves redox state and inflammation markers in the liver of high-fat-fed rats', *Obesity,* 22, pp. 170–177.

Barrett-Lee, P. J., Dixon, J. M., Farrell, C., Jones, A, Leonard, R., Murray, N., Palmieri, C., Plummer, C. J., Stanley, A. & Verrill, M. W. (2009) 'Expert opinion on the use of anthracyclines in patients with advanced breast cancer at cardiac risk.', *Annals of Oncology,* 20(5), pp. 816–827.

Bauman, T. M., Nicholson, T. M., Abler, L. L., Eliceiri, K. W., Huang, W., Vezina, C. M. & Ricke, W. A. (2014) 'Characterization of fibrillar collagens and extracellular matrix of glandular benign prostatic hyperplasia nodules', *PLoS ONE*, 9(10), pp. 1–9.

Beckman, K. B. & Ames, B. N. (1998) 'The Free Radical Theory of Aging Matures', *Physiological Reviews*, 78(2), pp. 547–581.

De Beer, E. L., Bottone, A. E. & Voest, E. E. (2001) 'Doxorubicin and mechanical performance of cardiac trabecular after acute and chronic treatment: a review', *European Journal of Pharmacology*, 415, pp. 1–11.

Bernaba, B. N., Chan, J. B., Lai, C. K. & Fishbein, M. C. (2010) 'Pathology of late-onset anthracycline cardiomyopathy.', *Cardiovascular Pathology : The Official Journal of the Society for Cardiovascular Pathology*, 19(5), pp. 308–311.

Berthiaume, J., Oliveira, P. J., Fariss, M. W. & B., W. K (2005) 'Dietary vitamin E decreases doxorubicin-induced oxidative stress without preventing mitochondrial dysfunction', *Cardiovascular Toxicology*, 5, pp. 257–276.

Biondo, L., Lima Junior, E., Souza, C., Cruz, M., Cunha, R., Alonso-Vale, M., Oyama, L., Nascimento, C., Pimentel, G., Dos Santos, R., Lira, F. & Rosa Neto, J. (2016) 'Impact of doxorubicin treatment on the physiological functions of white adipose tissue', *PloS*

One, 11(3), pp. 1-14

Bligh, E.G., & Dyer, W. J. (1959) 'A rapid method of total lipid extraction and purification', *Canadian Journal of Biochemistry and Physiology*, 37(21), pp. 911–917.

Bosco, D., Armanet, M., Morel, P., Niclauss, N., Sgroi, A., Muller, Y. D., Giovannoni, L. & Berney, T. (2010) 'Unique Arrangement of α- and β-Cells in Human Islets of Langerhans', *Diabetes*, 59, pp. 1202–1210.

Botsoglou, N. A., Fletouris, D. J., Papageorgiou, G. E., Vassilopoulos, V. N., Mantis, A. J. & Trakatelliss, A. G. (1994) 'Rapid, Sensitive, and Specific Thiobarbituric Acid Method for Measuring Lipid Peroxidation in Animal Tissue, Food, and Feedstuff Samples', *Journal of Agriculture and Food Chemistry*, 42(1983), pp. 1931–1937.

Bravo, L. (1998) 'Polyphenols: chemistry, dietary sources, metabolism, and nutritional significance', *Nutrition Reviews*, 56, pp. 317–333.

Bredehorst, R., Panneerselvam, M. & Vogel, C. (1987) 'Doxorubicin Enhances Complement Susceptibility of Human Melanoma Cells by Extracellular Oxygen Radical Formation', *The Journal of Biological Chemistry*, 262(5), pp. 2034–2041.

Brissova, M., Fowler, M. J., Nicholson, W. E., Chu, A., Hirshberg, B., Harlan, D. M. & Powers, A. C. (2005) 'Assessment of Human Pancreatic Islet Architecture and Composition by Laser Scanning Confocal Microscopy', *Journal of Histochemistry & Cytochemistry*, 53(9), pp. 1087–1097.

Broglio, F., Arvat, E., Benso, A., Gottero, C., Muccioli, G., Papotti, M., Van de Lely, A., Deghenghi, R. & Ghigo, E. (2001) 'Ghrelin, a natural GH secretagogue produced by the stomach, induces hyperglycemia and reduces insulin secretion in humans', *Journal of Clinical Endocrinology & Metabolism*, 86(10), pp. 5083–5086.

Brookes, P. S., Parker, N., Buckingham, J. A., Vidal-Puig, A., Halestrap, A. P., Gunter, T. E., Nicholls, D. G., Bernardi, P., Lemasters, J. J. & Brand, M. D. (2008) 'UCPs--unlikely calcium porters', *Nature Cell Biology*, 10(11), pp. 1235–1237.

Bruynzeel, A. M. E., Niessen, H. W. M., Bronzwaer, J. G. F., Van der Hoeven, J. J. M., Berkhof, J., Bast, A., Van der Vijgh, W. J. & Van Groeningen, C. J. (2007) 'The effect of monohydroxyethylrutoside on doxorubicin-induced cardiotoxicity in patients treated for metastatic cancer in a phase II study', *British Journal of Cancer*, 97(8), pp. 1084–1089.

Cabrera, O., Berman, D. M., Kenyon, N. S., Ricordi, C., Berggren, P. & Caicedo, A. (2006) 'The unique cytoarchitecture of human pancreatic islets has implications for islet cell function', *Proceedings of the National Academy of Sciences of the United States of America*, 103(7), pp. 2234–2339.

Caroni, P., Villani, F. & Carafoli, E. (1981) 'The cardiotoxic antibiotic doxorubicin inhibits the Na+/Ca2+ exchange of dog heart sarcolemmal vesicles', *FEBS Letters*, 130(2), pp. 184–186.

Chandra, J., Samali, A. & Orrenius, S. (2000) 'Triggering and modulation of apoptosis by oxidative stress', *Free Radical Biology and Medicine*, 29, pp. 323–333.

Chen, X., Cho, D. & Yang, P. (2010) 'Double staining immunohistochemistry', *North*

American Journal of Medical Sciences, 2(5), pp. 241–245.

Choi, K., Roh, S., Hong, Y., Shrestha, Y., Hishikawa, D., Chen, C., Kojima, K., Kangawa, K. & Sasaki, S. (2003) 'The role of ghrelin and growth hormone secretagogue receptor on rat adipogenesis', *Endocrinology*, 144, pp. 754–759.

Chopin, L., Walpole, C., Seim, I., Cunningham, P., Murray, R., Whiteside, E., Josh, P. & Herington, A. (2011) 'Molecular and Cellular Endocrinology Ghrelin and Cancer', *Molecular and Cellular Endocrinology*, 340, pp. 65–69.

Chung, S., Yao, H., Caito, S., Hwang, J.-W., Arunachalam, G. & Rahman, I. (2010) 'Regulation of SIRT1 in cellular functions: role of polyphenols', *Archives of biochemistry and biophysics*, 501, pp. 79–90.

Close, B., Banister, K., Baumans, V., Bernoth, E.-M., Bromage, N., Bunyan, J., Erhardt, W., Flecknell, P., Gregory, N. & Hackbarth, H. (1996) 'Recommendations for euthanasia of experimental animals: Part 1', *Laboratory Animals*, 30, pp. 293–316.

Crompton, M. (2000) 'Bax, Bid and the permeabilization of the mitochondrial outer membrane in apoptosis.', *Current Opinion in Cell Biology*, 12, pp. 414–419.

Cummings, D., Foster-Schubert, K. & Overduin, J. (2005) 'Ghrelin and energy balance: focus on current controversies', *Current Drug Targets*, 6, pp. 153–169.

Date, Y., Kojima, M., Hosoda, H., Sawaguchi, A., Mondal, M., Suganuma, T., Matsukura, S., Kangawa, K. & Nakazato, M. (2000) 'Ghrelin, a novel growth hormone-releasing acylated peptide, is synthesized in a distinct endocrine cell type in the gastrointestinal tracts of rats and humans', *Endocrinology*, 141, pp. 4255–4426.

Date, Y., Nakazato, M., Hashiguchi, S., Dezaki, K., Mondal, M. S., Hosoda, H., Kojima, M., Kangawa, K., Arima, T., Matsuo, H., Yada, T. & Matsukura, S. (2002) 'Ghrelin is present in pancreatic α-cells of humans and rats and stimulates insulin secretion', *Diabetes*, 51, pp. 124–129.

Davies, K. J. & Doroshow, J. H. (1986) 'Redox cycling of anthracyclines by cardiac mitochondria. I. Anthracycline radical formation by NADH dehydrogenase', *Journal of Biological Chemistry*, 261, pp. 3060–3067.

Delporte, C. (2013) 'Structure and physiological actions of ghrelin', *Scientifica*, 2013, pp. 1–25.

Devasagayam, T. P. A., Boloor, K. K. & Ramasarma, T. (2003) 'Methods for estimating lipid peroxidation: An analysis of merits and demerits', *Indian Journal of Biochemistry and Biophysics*, 40(5), pp. 300–308.

Dezaki, K., Sone, H. & Yada, T. (2008) 'Ghrelin is a physiological regulator of insulin release in pancreatic islets and glucose homeostasis', *Pharmacology & Therapeutics*, 118, pp. 239–249.

Dispenzieri, A. & Loprinzi, C. L. (1997) 'Chemotherapy-induced insulin-dependent diabetes mellitus', *Journal of Clinical Oncology*, 15, pp. 1287.

Dixit, V., Schaffer, E., Pyle, R., Collins, G., Sakthivel, S., Palaniappan, R., Lillard, J. J. & Taub, D. (2004) 'Ghrelin inhibits leptin- and activation-induced proinflammatory

cytokine expression by human monocytes and T cells', *Journal of Clinical Investigation*, 114, pp. 57–66.

Dobutovic, B., Sudar, E., Tepavcevic, S., Djordjevic, J., Djordjevic, A., Radojcic, M. & Isenovic, E. R. (2014) 'Effects of ghrelin on protein expression of antioxidative enzymes and iNOS in the rat liver', *Archives of Medical Science*, 10(4), pp. 806–816.

Dornonville de la Cour, C., Bjorkqvist, M., Sandvik, A., Bakke, I., Zhao, C., Chen, D. & Hakanson, R. (2001) 'A-like cells in the rat stomach contain ghrelin and do not operate under gastrin control', *Regulatory Peptides*, 99, pp. 141–150.

Egido, E., Rodriguez-Gallardo, J., Silvestre, R. & Marco, J. (2002) 'Inhibitory effect of ghrelin on insulin and pancreatic somatostatin secretion', *European Journal of Endocrinology*, 146, pp. 241–244.

El-Gohary, Y. & Gittes, G. K. (2012) 'Embryologic development of the liver , biliary tract , and pancreas', in Jarnagin, W.R. (ed.). *Blumgart's Surgery of the Liver, Pancreas and Biliary Tract*, New York: Elsevier Inc., pp. 18–30.

El-Missiry, M., Othman, A., Amer, M. & Add el-Aziz, M. (2001) 'Attenuation of the acute adriamycin-induced cardiac and hepatic oxidative toxicity by N-(2-mercaptopropionyl) glycine in rats', *Free Radical Research*, 35, pp. 575–581.

Elayat, A. A., El-naggar, M. M. & Tahir, M. (1995) 'An immunocytochemical and morphometric study of the rat pancreatic islets', *Journal of Anatomy*, 186, pp. 629–637.

Ellerby, L. M. & Bredesen, D. E. (2000) 'Measurement of cellular oxidation, reactive oxygen species, and antioxidant enzymes during apoptosis', *Methods in enzymology*, 322(1996), pp. 413–21.

Erlandersen, S., Hegre, O., Parsons, J. A., McEvoy, R. & Elde, R. (1976) 'Pancreatic Islet Cell Hormones Distribution of Cell Types in the Islet and Evidence for the Presence of Somatostatin and Garstin within the D Cell', *The Journal of Histochemistry and Cytochemistry*, 24(7), pp. 883–897.

Ezquer, F., Gutiérrez, J., Ezquer, M., Caglevic, C. & Salgado, H. C. (2015) 'Mesenchymal stem cell therapy for doxorubicin cardiomyopathy : hopes and fears', *Stem Cell Research & Therapy*, 6(116), pp. 1–9.

Fak, F., Friis-Hansen, L., Westrom, B. & Wierup, N. (2007) 'Gastric ghrelin cell development is hampered and plasma ghrelin is reduced by delayed weaning in rats', *Journal of Endocrinology*, 192, pp. 345–352.

Farhat, B., Almelkar, A., Ramachandran, K., Williams, S. J., Huang, H. H., Zamierowski, D., Novikova, L. & Stehno-Bittel, L. (2013) 'Small human islets comprised of more β-cells with higher insulin content than large islets', *Islets*, 5(2), pp. 87–94.

Feng, J. P., Yuan, X. L., Li, M., Fang, J., Xie, T., Zhou, Y., Zhu, Y. M., Luo, M., Lin, M. & Ye, D. W. (2013) 'Secondary diabetes associated with 5-fluorouracil-based chemotherapy regimens in non-diabetic patients with colorectal cancer: results from a single-centre cohort study', *Colorectal Disease*, 15, pp. 27–33.

Fischer, U., Janicke, R. & Schulze-Osthoff, K. (2003) 'Many cuts to ruin: a comprehensic

update on caspase substrates', *Cell Death Differentiation*, 10, pp. 76–100.

French, J. J. & Charnely, R. (2016) 'Chronic pancreatitis', *Surgery*, 34(6), pp. 301–306.

Geetha, N., Lali, V. S., Hussain, B. M. & Nair, M. K. (1999) 'Insulin dependent diabetes mellitus induced by chemotherapy and granulocyte, macrophage–colony stimulating factor', *Journal of the Association of Physicians of India*, 47, pp. 835.

Gersell, D., Gingerich, R. & Greider, M. (1979) 'Reginal distribution and concentration of pancreatic polypeptide in the human and canine pancreas', *Diabetes*, 28, pp. 11–15.

Gewirtz, D. A. (1999) 'A Critical Evaluation of the Mechanisms of Action Proposed for the Antitumor Effects of the Anthracycline Antibiotics Adriamycin and Daunorubicin', *Biochemical Pharmacology*, 57(98), pp. 727–741.

Ghigo, A., Li, M. & Hirsch, E. (2016) 'New signal transduction paradigms in anthracycline-induced cardiotoxicity', *Biochimica et Biophysica Acta - Molecular Cell Research*, 1863(7), pp. 1916–1925.

Ghosh, S., May, M. & Kopp, E. (1998) 'NF-κB and Rel proteins: Evolutionarily conserved mediators of immune response', *Annual Review of Immunolgy*, 16, pp. 225–260.

Goodman, J. & Hochstein, P. (1977) 'Generation of free radicals and lipid peroxidation by redox cycling of Adrimycin and Daunomycin', *Biochemical and Biophysical Research Communitcations*, 77(2), pp. 797–803.

Goormaghtigh, E., Brasseur, R., Huart, P. & Ruysschaert, J. M. (1987) 'Study of the adriamycin-cardiolipin complex structure using attenuated total reflection infrared spectroscopy', *Biochemistry*, 26, pp. 1789–1794.

Goormaghtigh, E., Huart, P., Praet, M., Brasseur, R. & Ruysschaert, J. (1990) 'Structure of the adriamycin-cardiolipin complex. Role in mitochondrial toxicity', *Biophysical Chemistry*, 35, pp. 247–257.

Granger, J. & Remick, D. (2005) 'Acute pancreatitis: Models, Markers, and Mediators', *Shock*, 24, pp. 45–51.

Grankvist, K., Marklund, S. & Taljedal, I. (1981) 'CuZn-superoxide dismutase, Mn-superoxide dismutase, catalase and glutathione peroxidase in pancreatic islets and other tissues in the mouse', *Biochemical Journal*, 199, pp. 393–398.

Gukovsky, I., Gukovskaya, A., Blinman, T., Zaninovic, V. & Pandol, S. (1998) 'Early NF-κB activation is associated with hormone-induced pancreatitis', *American Journal of Physiology*, 275, pp. G1402–1414.

Gül, M., Atalay, M. & Hänninen, O. (2003) 'Endurance training and glutathione-dependent antioxidant defense mechanism in heart of the diabetic rats', *Journal of Sports Science and Medicine*, 2(2), pp. 52–61.

Guo, S. & DiPietro, L. (2010) 'Factors affecting wound healing', *Journal of Denatal Research*, 89(3), pp. 219–229.

Gustafsson, Å. B. & Gottlieb, R. A. (2003) 'Mechanisms of apoptosis in the heart', *Journal of Clinical Immunology*, 23, pp. 447–459.

Habauzit, V. & Morand, C. (2012) 'Evidence for a protective effect of polyphenols-containing foods on cardiovascular health: an update for clinicians', *Therapeutic Advances in Chronic Disease*, 3, pp. 87–106.

Haber, P. S., Keogh, G. W., Apte, M. V, Moran, C. S., Stewart, N. L., Crawford, D. H., Pirola, R. C., McCaughan, G. W., Ramm, G. A. & Wilson, J. S. (1999) 'Activation of pancreatic stellate cells in human and experimental pancreatic fibrosis', *American Journal of Pathology*, 155(4), pp. 1087–1095.

Hall, M., Young, D., Waters, J., Rowan, A., Chanty, A., Edwards, D. & Clark, I. (2003) 'The comparative role of activator protein 1 and Smad factors in the regulation of Timp-1 and MMP-1 gene expression by transforming growth factor-β1', *Journal of Biological Chemistry*, 278(12), pp. 10304–10313.

Halliwell, B. (2006) 'Reactive species and antioxidants. Redox biology is a fundamental theme of aerobic life', *Plant physiology*, 141, pp. 312–322.

Hampton, M. B., Fadeel, B. & Orrenius, S. (1998) 'Redox regulation of the caspases during apoptosis', *Annals of the New York Academy of Sciences*, 854, pp. 328–335.

Harake, D., Franco, V. I., Henkel, J. M., Miller, T. L. & Lipshultz, S. E. (2012) 'Cardiotoxicity in Childhood Cancer Survivors', *Future Cardiology*, 8(4), pp. 647–670.

Hasinoff, B. B., Kuschak, T. I., Creighton, A. M., Fattman, C. L., Allan, W. P., Thampatty, P. & Yalowich, J. C. (1997) 'Characterization of a Chinese hamster ovary cell line with acquired resistance to the bisdioxopiperazine dexrazoxane (ICRF-187) catalytic inhibitor of topoisomerase II', *Biochemical Pharmacology*, 53(12), pp. 1843–1853.

Hattori, S., Hattori, Y., Banba, N., Kasai, K. & Shimoda, S. (1995) 'Pentamethyl-hydroxychromane, vitamin E derivative, inhibits induction of nitric oxide by bacterial lipopolysaccharide', *Biochemistry and Molecular Biology International*, 35, pp. 177–183.

Hauge-evans, A. C., King, A. J., Carmignac, D., Richardson, C. C., Robinson, I. C. A. F., Low, M. J., Christie, M. R., Persaud, S. J. & Jones, P. M. (2009) 'Somatostatin secreted by islet δ-cells fulfills multiple roles as a paracrine regulator of islet function', *Diabetes*, 58, pp. 403–411.

Heart, E. A., Karandrea, S., Liang, X., Balke, M. E., Beringer, P. A., Bobczynski, E. M., Burgos, D. Z. B., Richardson, T. & Gray, J. P. (2016) 'Mechanisms of doxorubicin toxicity in pancreatic β-cells', *Toxicological Sciences*, 152(2), pp. 395–405.

Heikkila, R. E. & Cabbat, F. (1976) 'A sensitive assay for superoxide dismutase based on the autoxidation of 6-hydroxydopamine', *Analytical Biochemistry*, 75(2), pp. 356–362.

Hertog, M. G., Hollman, P. C., Katan, M. B. & Kromhout, D. (1993) 'Intake of potentially anticarcinogenic flavonoids and their determinants in adults in the Netherlands', *Nutrition and Cancer*, 20, pp. 21–29.

Von Hoff, D. D., Layard, M. W., Basa, P., Davis, H. L., Von Hoff, A. L., Rozencweig, M. & Muggia, F. M. (1979) 'Risk factors for doxorubicin-induced congestive heart failure', *Annals of Internal Medicine*, 91(5), pp. 710–717.

Houmani, H., Rodríguez-Ruiz, M., Palma, J. M., Abdelly, C. & Corpas, F. J. (2016) 'Modulation of superoxide dismutase (SOD) isozymes by organ development and high long-term salinity in the halophyte Cakile maritima', *Protoplasma*, 253(3), pp. 885–894.

Houser, B. (2012) 'Bio-Rad's Bio-Plex® suspension array system, xMAP technology overview', *Archives Of Physiology And Biochemistry*, 118(4), pp. 192–196.

Huang, C., Yuan, M., Huang, H., Wu, G., Liu, Y., Yu, S., Li, H. & Wang, T. (2009) 'Ghrelin inhibits postinfarct myocardial remodeling and improves cardiac function through anti-inflammation effect', *Peptides*, 30(12), pp. 2286–2291.

Huang, S. (2013) 'Inhibition of PI3K/Akt/mTOR signaling by natural products', *Anti-Cancer Agents in Medicinal Chemistry*, 13, pp. 967–970.

Imondi, A. R., Torre, P., Della Mazué, G., Mazuã, G., Sullivan, M., Robbins, L., Hagerman, L. M., Podestà, A. & Pinciroli, G. (1996) 'Relationship of Dexrazoxane for Prevention of Doxorubicin-induced Cardiotoxicity in Mice,Rats and Dogs', *Cancer Research*, 56(18), pp. 4200–4204.

Işeri, S. Ö., Şener, G., Saglam, B., Ercan, F., Gedik, N. & Yeğen, B. Ç. (2008) 'Ghrelin alleviates biliary obstruction-induced chronic hepatic injury in rats', *Regulatory Peptides*, 146, pp. 73–79.

Jacobs, H., Moalin, M., Bast, A., Van der Vijgh, W. J. F. & Haenen, G. R. M. M. (2010) 'An essential difference between the flavonoids monoHER and quercetin in their interplay with the endogenous antioxidant network', *PloS One*, 5(11), p. e13880.

Jiang, G. and Zhang, B. B. (2003) 'Glucagon and regulation of glucose metabolism', *American Journal of Physiology- Endocrinology Metabolism*, 284, pp. E671–E678.

Jones, B. and Gorges, G. (1997) 'Physiology and pathophysiology of apoptosis in epithelial cells of the liver, pancreas, and intestine', *American Physiological Society*, 273, pp. G1174–G1188.

Kageyama, H., Funahashi, H., Hirayama, M., Takenoya, F., Kita, T., Kato, S., Sakurai, J., Lee, E. Y., Inoue, S., Date, Y., Nakazato, M., Kangawa, K. & Shioda, S. (2005) 'Morphological analysis of ghrelin and its receptor distribution in the rat pancreas', *Regulatory Peptides*, 126, pp. 67–71.

Kaiser, A. M., Saluja, A., Sengupta, A., Saluja, M. & Steer, M. L. (1995) 'Relationship between severity, necrosis, and apoptosis in five models of experimental acute pancreatitis', *American Journal of Physiology*, 269(38), C1295–C1304.

Kalyanaraman, B., Joseph, J., Kalivendi, S., Wang, S., Konorev, E. & Kotamraju, S. (2002) 'Doxorubicin-induced apoptosis: Implications in cardiotoxicity', *Molecular and Cellular Biochemistry*, 234, pp. 119–124.

Katayama, T., Shimamoto, S., Oda, H., Nakahara, K., Kangawa, K. & Murakami, N. (2007) 'Glucagon receptor expression and glucagon stimulation of ghrelin secretion in rat stomach', *Biochemical and Biophysical Research Communitcations*, 357, pp. 865–870.

Kaufmann, S., Desnoyers, S., Ottaviano, Y., Davidson, N. & Poirier, G. (1993) 'Specific

proteolytic cleavage of poly(ADP-ribose) polymerase: an early marker of chemotherapy-induced apoptosis', *Cancer Research*, 53, pp. 3976–3985.

Kaurich, T. (2008) 'Drug-induced acute pancreatitis', *Baylor University Medical Center Proceedings*, 21, pp. 77–81.

Keizer, H. G., Pinedo, H. M., Schuurhuis, G. J. & Joenje, H. (1990) 'Doxorubicin (Adriamycin): A criticial review of free radical-dependent mechanisms of cytotoxicity', *Pharmacology & Therapeutics*, 47, pp. 219–231.

Kim, A., Miller, K., Jo, J., Kilimnik, G., Wojcik, P. & Hara, P. (2009) 'Islet architechture A comparative study', *Islets*, 1(2), pp. 129–136.

Kim, S.Y., Kim, S.J., Kim, B.J., Rah, S.Y., Chung, S.M., Im, M. J. & Kim, U.H. (2006) 'Doxorubicin-induced reactive oxygen species generation and intracellular Ca2+ increase are reciprocally modulated in rat cardiomyocytes', *Experimental & Molecular Medicine*, 38(5), pp. 525–545.

Kishi, S., Takeyama, Y., Ueda, T., Yasuda, T., Shinzeki, M., Kuroda, Y. & Yokozaki, H. (2003) 'Pancreatic duct obstruction itself induces expression of α smooth muscle actin in pancreatic stellate cells', *Journal of Surgical Research*, 114, pp. 6–14.

Koh, T. & DiPietro, L. (2011) 'Inflammation and wound healing: the role of the macrophage', *Expert Reviews in Molecular Medicine*, 13, p. e23.

Kojima, M., Hosoda, H., Date, Y., Nakazato, M., Matsuo, H. & Kangawa, K. (1999) 'Ghrelin is a growth-hormone-releasing acylated peptide from stomach', *Nature*, 402, pp. 656–660.

Kojima, M. & Kangawa, K. (2005) 'Ghrelin : Structure and Function', *Physiological Reviews*, 85, pp. 495–522.

Kojima, S., Uneo, N., Asakawa, A., Sagiyama, K., Naruo, T., Mizuno, S. & Inui, A. (2007) 'A role for pancreatic polypeptide in feeding and body weight regulation', *Peptides*, 28(2), pp. 459–463.

Korbonits, M., Goldstone, A., Gueorguiev, M. & Grossman, A. (2004) 'Ghrelin – a hormone with multiple functions', *Frontiers in Neuroendocrinology*, 25, pp. 27–68.

Kostrzewa-Nowak, D., Paine, M. J., Wolf, C. R. and Tarasiuk, J. (2005) 'The role of bioreductive activation of doxorubicin in cytotoxic activity against leukaemia HL60-sensitive cell line and its multidrug-resistant sublines', *British Journal of Cancer*, 93, pp. 89–97.

Kotamraju, S., Konorov, E., Joseph, J. & Kalyanaraman, B. (2000) 'Doxorubicin-induced apoptosis in endothelial cells and cardiomyocytes is ameliorated by nitrone spin traps and epsilon. Role of reactive oxygen and nitrogen species', *Journal of Biological Chemistry*, 275, pp. 33585–33592.

Kozak, A., Talar-Wojnarowska, R., Kaczka, A., Borkowska, A., Czupryniak, L., Małecka-Panas, E. & Gąsiorowska, A. (2016) 'Utility of different serum fibrosis markers in diagnosing patients with chronic pancreatitis and pancreatic adenocarcinoma', *World Journal of Gastrointestinal Oncology*, 8(8), pp. 635–41.

Kroemer, G., Zamzami, N. & Susin, S. (1997) 'Mitochondrial control of apoptosis', *Immunology Today*, 18, pp. 44–51.

Krown, K. A., Page, M. T., Nguyen, C., Zechner, D., Gutierrez, V., Comstock, K. L., Glembotski, C.C., Quintana, P. J. & Sabbadini, R. A. (1996) 'Tumor necrosis factor alpha-induced apoptosis in cardiac myocytes. Involvement of the sphingolipid signaling cascade in cardiac cell death', *Journal of Clinical Investigation*, 98, pp. 2854–2865.

Kvist Reimer, M., Pacini, G. & Ahren, B. (2003) 'Dose-dependent inhibition by ghrelin of insulin secretion in the mouse', *Endocrinology*, 144, pp. 916–921.

Lankisch, P. G., Apte, M. and Banks, P. A. (2015) 'Acute pancreatitis', *The Lancet*, 86(9988), pp. 85–96.

Lassmann, V., Vague, P., Vialettes, B. & Simon, M. (1980) 'Low plasma levels of pancreatic polypeptide in obesity', *Diabetes*, 29, pp. 428–430.

Leandro, J., Dyck, J., Poppe, D., Shore, R., Airhart, C., Greenberg, M., Gilday, D., Smallhorn, J. & Benson, L. (1994) 'Cardiac dysfunction late after cardiotoxic therapy for childhood cancer', *The American Journal of Cardiology*, 74(11), pp. 1152–1156.

Lee, H., Wang, G., Englander, E., Kojima, M. & Greeley Jr, G. (2002) 'Ghrelin, a new gastrointestinal endocrine peptide that stimulates insulin secretion: enteric distribution, ontogeny, influence of endocrine, and dietary manipulations.', *Endocrinology*, 143, pp. 185–190.

De Leers, M. & Goormaghtigh, E. (1985) 'Adriamycin effects on insulin secretion, Ca2+ movements and glucose oxidation in pancreatic islet cells', *Pharmacological Research Communications*, 17(3), pp. 227–232.

Leite-Moreira, A. & Soares, J. (2007) 'Physiological, pathological and potential therapeutic roles of ghrelin', *Drug Discovery Today*, 12, pp. 276–288.

Li, J., Zhou, R., Zhang, J. & Li, Z. (2014) 'Calcium signaling of pancreatic acinar cells in the pathogenesis of pancreatitis', *World Journal of Gastroenterology*, 20(43), pp. 16146–16152.

Li, Y., Hai, J., Li, L., Chen, X., Peng, H., Cao, M. & Zhang, Q. (2013) 'Administration of ghrelin improves inflammation, oxidative stress, and apoptosis during and after non-alcoholic fatty liver disease development', *Endocrine*, 43(2), pp. 376–386.

De Lima Junior, E. A., Yamashita, A. S., Pimentel, G. D., De Sousa, L. G. O., Santos, R. V. T., Goncalves, C. L., Streck, E. L., de Lira, F. S. & Rosa Neto, J. C. (2016) 'Doxorubicin caused severe hyperglycaemia and insulin resistance, mediated by inhibition in AMPk signalling in skeletal muscle', *Journal of Cachexia, Sarcopenia and Muscle*, 7(5), pp. 615–625.

Lipshultz, S. E., Alvarez, J. A. & Scully, R. E. (2008) 'Anthracycline associated cardiotoxicity in survivors of childhood cancer', *Heart*, 94(4), pp. 525–533.

Liu, J., Mao, W., Ding, B. & Liang, C. (2008) 'ERKs/p53 signal transduction pathway is involved in doxorubicin-induced apoptosis in H9c2 cells and cardiomyocytes', *American Journal of Physiology*, 295(5), pp. H1956–1965.

Lomovskaya, N., Otten, S. L., Doi-Katayama, Y., Fonstein, L., Liu, X. C., Takatsu, T., Inventi-Solari, A., Filippini, S., Torti, F., Colombo, A. L. & Hutchinson, C. R. (1999) 'Doxorubicin overproduction in Streptomyces peucetius: Cloning and characterization of the dnrU ketoreductase and dnrV genes and the doxA cytochrome P-450 hydroxylase gene', *Journal of Bacteriology*, 181, pp. 305–318.

Matouk, A. I., Taye, A., Heeba, G. H. & El-Moselphy, M. A. (2013) 'Quercetin augments the protective effect of losartan against chronic doxorubicin cardiotoxicity in rats', *Environmental Toxicology and Pharmacology*, 36, pp. 443–450.

Matull, W. R., Pereira, S. P. & O'Donohue, J. W. (2006) 'Biochemical markers of acute pancreatitis', *Journal of Clinical Pathology*, 59(4), pp. 340–344.

Meneghin, A. & Hogaboam, C. (2007) 'Infectious disease, the innate immune response, and fibrosis', *Journal of Clinical Investigation*, 117(3), pp. 530–538.

Midgley, A., Rogers, M., Hallett, M., Clayton, A., Bowen, T., Phillips, A. & Steadman, R. (2013) 'Transforming growth factor-β1(TGF-β1)-stimulated fibroblast to myofibroblast differentiation is mediated by hyaluronan (HA)-facilitated epidermal growth factor receptor (EGFR) and CD44 co- localization in lipid rafts', *Journal of Biological Chemistry*, 288(21), pp. 14824–14838.

Minotti, G., Menna, P., Salvatorelli, E., Cairo, G. & Gianni, L. (2004) 'Anthracyclines: Molecular Advances and Pharmacologic Developments in Antitumor Activity and Cardiotoxicity', *Pharmacological Reviews*, 56(2), pp. 185–229.

Misiti, F., Giardina, B., Mordente, A. & Clementi, M. E. (2003) 'The secondary alcohol and aglycone metabolites of doxurubicin alter metabolism of human erythrocytes', *Brazilian Journal of Medical and Biological Research*, 36(12), pp. 1643–1651.

Mizutani, H., Oikawa, S., Hiraku, Y., Murata, M., Kojima, M. & Kawanishi, S. (2003) 'Distinct mechanisms of site-specific oxidative DNA damage by doxorubicin in the presence of copper(II) and NADPH-cytochrome P450 reductase', *Cancer Science*, 94(8), pp. 686–691.

Mizutani, H., Tada-Oikawa, S., Hiraku, Y., Kojima, M. & Kawanishi, S. (2005) 'Mechanism of apoptosis induced by doxorubicin through the generation of hydrogen peroxide', *Life Sciences*, 76(13), pp. 1439–1453.

Montaigne, D., Hurt, C. & Neviere, R. (2012) 'Mitochondria death/survival signaling pathways in cardiotoxicity induced by anthracyclines and anticancer-targeted therapies', *Biochemistry Research International*, 2012, p. 951539

Moore, K., Dalley, A. F. & Agur, A. M. R. (2008) *Clinically Orientated Anatomy*. Philadelphia: Lippincott Williams & Wilkins.

Moulin, M., Piquereau, J., Mateo, P., Fortin, D., Rucker-Martin, C., Gressette, M., Lefebvre, F., Gresikova, M., Solgadi, A., Veksler, V., Garnier, A. & Ventura-Clapier, R. (2015) 'Sexual dimorphism of doxorubicin-mediated cardiotoxicity potential role of energy metabolism remodeling', *Circulation: Heart Failure*, 8, pp. 98–108.

Myers, C. (1998) 'The role of iron in doxorubicin-induced cardiomyopathy', *Seminars in Oncology*, 25(4), pp. 10–4.

Nagata, S. (1997) 'Apoptosis by Death Factor', *Cell*, 88(3), pp. 355–365.

Nakamura, T., Ueda, Y., Juan, Y., Katsuda, S., Takahashi, H. & Koh, E. (2000) 'Fas-mediated apoptosis in Adriamycin-induced cardiomyopathy in rats: in vivo study', *Circulation*, 102, pp. 572–578.

Nitobe, J., Yamaguchi, S., Okuyama, M., Nozaki, N., Sata, M., Miyamoto, T., Takeishi, Y., Kubota, T. & Tomoike, T. (2003) 'Reactive oxygen species regulate FLICE inhibitory protein (FLIP) and susceptibility to Fas-mediated apoptosis in cardiac myocytes', *Cardiovascular Research*, 57, pp. 119–128.

Noctor, G., Mhamdi, A., Chaouch, S., Han, Y., Neukermans, J., Marquez-Garcia, B., Queval, G. & Foyer, C. H. (2012) 'Glutathione in plants: An integrated overview', *Plant, Cell and Environment*, 35(2), pp. 454–484.

Octavia, Y., Tocchetti, C. G., Gabrielson, K. L., Janssens, S., Crijns, H. J. & Moens, A. L. (2012) 'Doxorubicin-induced cardiomyopathy: From molecular mechanisms to therapeutic strategies', *Journal of Molecular and Cellular Cardiology*, 52(6), pp. 1213–1225.

Oliveira, M. S., Melo, M. B., Carvalho, J. L., Melo, I. M., Lavor, M. S., Gomes, D. A., Goes, A. M. & Melo, M. M. (2013) 'Doxorubicin cardiotoxicity and cardiac function improvement after stem cell therapy diagnosed by strain echocardiography', *Journal of Cancer Science and Therapy*, 5(2), pp. 52–57.

Olson, H. M., Young, D. M., Prieur, D. J., LeRoy, A. F. & Reagan, R. L. (1974) 'Electrolyte and morphologic alterations of myocardium in adriamycin-treated rabbits', *The American Journal of Pathology*, 77(3), pp. 439–454.

Olson, R. D., Mushlin, P. S., Brenner, D. E., Fleischer, S., Cusack, B. J., Chang, B. K. & Boucek, R. J. J. (1988) 'Doxorubicin cardiotoxicity may be caused by its metabolite, Doxorubicinol', *Proceedings of the National Academy of Sciences of the United States of America*, 85, pp. 3585–3589.

Ou, B., Hampsch-Woodill, M. & Prior, R. L. (2001) 'Development and Validation of an Improved Oxygen Radical Absorbance Capacity Assay Using Fluorescein as the Fluorescent Probe', *Journal of Agriculture and Food Chemistry*, 49(10), pp. 4619–4626.

Parrish, A., Freel, C. & Kornbluth, S. (2013) 'Cellular mechanisms controlling caspase activation and function', *Cold Spring Harbour Perspectives in Biology*, 5(6), pp. 1-24.

Pei, X. M., Yung, B.Y., Yip, S. P., Ying, M., Benzie, I. F. & Siu, P. (2014) 'Desacyl ghrelin prevents doxorubicin-induced myocardial fibrosis and apoptosis via the GHSR-independent pathway', *The American Journal of Physiology-Endocrinology and Metabolism*, 306(3), pp. e311–323.

Pereira, G. G. C., Silva, A. M., Diogo, C. V, Carvalho, F. S., Monteiro, P. & Oliveiraalo, P. J. (2011) 'Drug-induced Cardiac Mitochondrial Toxicity and Protection: From Doxorubicin to Carvedilol.', *Current Pharmaceutical Design*, 17(20), pp. 2113–2129.

Petrov, V., Fagard, R. & Lijnen, P. (2002) 'Stimulation of collagen production by transforming growth factor-β1 during differentiation of cardiac fibroblasts to

myofibroblasts', *Hypertension*, 39(2), pp. 258–263.

Poirier, M. G., Eroglu, S. & Marko, J. F. (2002) 'The bending rigidity of mitotic chromosomes.', *Molecular biology of the cell*, 13(6), pp. 2170–2179.

Poljsak, B., Šuput, D. & Milisav, I. (2013) 'Achieving the balance between ROS and antioxidants: When to use the synthetic antioxidants', *Oxidative Medicine and Cellular Longevity*, 2013, pp. 1–11.

Prior, R. L., Hoang, H., Gu, L., Wu, X., Bacchiocca, M., Howard, L., Hampsch-Woodill, M., Huang, D., Ou, B. & Jacob, R. (2003) 'Assays for hydrophilic and lipophilic antioxidant capacity (oxygen radical absorbance capacity (ORAC)) of plasma and other biological and food samples', *Journal of Agricultural and Food Chemistry*, 51(11), pp. 3273–3279.

Puri, S., Folias, A. E. & Hebroks, M. (2015) 'Plasticity and Dedifferentiation within the Pancreas: Development, Homeostasis, and Disease', *Cell Stem Cell*, 16, pp. 18–31.

Qader, S., Håkanson, R., Rehfeld, J. F., Lundquist, I. & Salehi, A. (2008) 'Proghrelin-derived peptides influence the secretion of insulin , glucagon , pancreatic polypeptide and somatostatin : A study on isolated islets from mouse and rat pancreas', *Regulatory Peptides*, 146, pp. 230–237.

Rafacho, A., Ortsater, H., Nadal, A. & Quesada, I. (2014) 'Glucocorticoid treatment and endocrine pancreas function : implications for glucose homeostasis , insulin resistance and diabetes', *Journal of Endocrinology*, 223(3), pp. R49-R62.

Raghuwansh, P., Dawra, R. K. & Saluja, A. (2013) 'New Insights into the Pathogenesis of Pancreatitis', *Current Opinion in Gastroenterolgy*, 29(5), pp. 523–530.

Rahman, K. (2007) 'Studies on free radicals, antioxidants, and co-factors', *Clinical Interventions in Aging*, 2 (2), pp. 219–236.

Reano, S., Graziani, A. & Filigheddu, N. (2014) 'Acylated and unacylated ghrelin administration to blunt muscle wasting', *Current Opinion in Clinical Nutrition and Metabolic Care*, 17(3), pp. 236–240.

Rivero-Gutiérrez, B., Anzola, A., Martínez-Augustin, O. & De Medina, F. S. (2014) 'Stain-free detection as loading control alternative to Ponceau and housekeeping protein immunodetection in Western blotting', *Analytical Biochemistry*, 467, pp. 1–3.

Robertson, R. P. & Harmon, J. S. (2007) 'Pancreatic Islet β-cell and Oxidative Stress: the Importance of Glutathione Peroxidase', *FEBES Letters*, 581(19), pp. 3743–3748.

Sadler, T. W. & Langman, J. (2006) *Langman's Medical Embryology*. Philadelphia: Lippincott Williams & Wilkins.

Saelens, X., Festjens, N., Van de Wallle, L., Van Gurp, M., Van Loo, G. & Vandenabeele, P. (2004) 'Toxic proteins released from mitochondria in cell death', *Oncogene*, 23, pp. 2861–2874.

Saleh, H. S. & Ali, H. N. (2015) 'Tocotrienol Mitigating Adverse Effect of Doxorubicin on Pancreas Tissue in Male Rats', *Journal of Advanced Biomedical & Pathobiology Research*, 5(2), pp. 23–31.

Salehi, A., Dornonville de la Cour, C., Hakanson, R. & Lundquist, I. (2004) 'Effects of ghrelin on insulin and glucagon secretion : a study of isolated pancreatic islets and intact mice', *Regulatory Peptides*, 118, pp. 143–150.

Salvador, V. B., Singh, M., Witek, P. & Peress, G. (2014) 'Cyclophosphamide and Doxorubicin-induced acute pancreatitis in a patient with breast cancer', *British Journal of Medical Practitioners*, 7(3), p. 727.

Sandoval, D., Gukovskaya, A., Reavey, P., Gukovsky, S., Sisk, A., Braquet, S., Pandol, S. J. & Poucell-Hatton, S. (1996) 'The role of neutrophils and platelet-activating factor in mediating experimental pancreatitis', *Gastroenterology*, 111(4), pp. 1081–1091.

Sawyer, D., Fukazawa, R., Arstall, M. & Kelly, R. (1999) 'Daunorubicin-induced apoptosis in rat cardiac myocytes is inhibited by dexrazoane', *Circulation Research*, 84, pp. 257–265.

Schneider, C. A., Rasband, W. S. & Eliceiri, K. W. (2012) 'NIH Image to ImageJ: 25 years of image analysis', *Nature Methods*, 9(7), pp. 671–675.

Schreck, R., Rieber, P. & Baeuerle, P. (1991) 'Reactive oxygen intermediates as apparently widely used messengers in the activation of NF-kB transcription factor and HIV-1', *EMBO Journal*, 10, pp. 2247–2258.

Sereno, M., Brunello, A., Chiappori, A., Barriuso, J., Casado, E., Belda, C., De Castro, J., Feliu, J. & González-Barón, M. (2008) 'Cardiac toxicity: old and new issues in anticancer drugs', *Clinical & Translational Oncology*, 10, pp. 35–46.

Shaw, L. M. (2011) 'The insulin receptor substrate (IRS) proteins: At the intersection of metabolism and cancer', *Cell Cycle*, 10(11), pp. 1750–1756.

Sherwood, L. (2001) *Human Physiology: from cells to systems*. China: Brooks/Cole, Centerage Learning.

Shivakumar, P., Ran, M., Reddy, A. & Anjaneyulu, Y. (2012) 'A study on the toxic effects of doxorubicin on the histology of certain organs', *Toxicology International*, 19(3), p. 241.

Shroff, A., Mamalis, A. & Jagdeo, J. (2014) 'Oxidative stress and skin fibrosis', *Current Pathobiology Reports*, 2(4), pp. 257–267.

Sies, H. & Packer, L. (2004) 'Quinones and Quinone Enzymes, Part A', *Methods in Enzymology*. Amsterdam: Elsevier Academic Press.

Šimůnek, T., Štěrba, M., Popelová, O., Adamcová, M., Hrdina, R. & Gerši, V. (2009) 'Anthracycline-induced cardiotoxicity: Overview of studies examining the roles of oxidative stress and free cellular iron', *Pharmacological Reports*, 61, pp. 154–171.

Singal, P. K., Iliskovic, N., Li, T. & Kumar, D. (1997) 'Adriamycin cardiomyopathy: pathophysiology and prevention.', *FASEB Journal ,* 11(12), pp. 931–936.

Situnayake, R. D., Crump, B. J., Zezulka, A. V, Davis, M., McConkey, B. & Thurnham, D. I. (1990) 'Measurement of conjugated diene lipids by derivative spectroscopy in heptane extracts of plasma', *Annals of Clinical Biochemistry*, 27, pp. 258–266.

Steer, M. (2012) 'Pancreatic physiology and functional assessment', in Jarnagin, W.R. (ed.). *Blumgart's Surgery of the Liver, Biliary Tract, and Pancreas*. New York: Elsevier Inc., pp. 65–73.

Steiner, D. J., Kim, A., Miller, K. & Hara, M. (2010) 'Pancreatic islet plasticity: Interspecies comparison of islet architecture and composition', *Islets*, 2(3), pp. 135–145.

Steinle, A., Weidenbach, H., Wagner, M., Adler, G. & Schmid, R. (1999) 'NF-kB/Rel activation in cerulein pancreatitis', *Gastroenterology*, 116, pp. 420–430.

Štěrba, M., Popelová, O., Lenčo, J., Fučíková, A., Brčáková, E., Mazurová, Y., Jirkovskỳ, E., Šimůnek, T., Adamcová, M., Mičuda, S., Stulík, J. & Geršl, V. (2011) 'Proteomic insights into chronic anthracycline cardiotoxicity', *Journal of Molecular and Cellular Cardiology*, 50(5), pp. 849–862.

Strassburg, S., Anker, S., Castaneda, T., Burget, L., Erez-Tilve, D., Pfluger, P., Nogueiras, R., Halem, H., Dong, J., Culler, M., Datta, R. & Tschöp, M. (2008) 'Long-term effects of ghrelin and ghrelin receptor agonists on energy balance in rats', *American Physiological Society*, 295, pp. E78–84.

Suda, T., Takahashi, T., Golstein, P. & Nagata, S. (1993) 'Molecular cloning and expression of the Fas ligand, a novel member of the tumor necrosis factor family', *Cell*, 75(6), pp. 1169–1178.

Sun, G., Ding, R., Li, M., Guo, Y., Fan, L., Yue, L., Li, L. & Zhao, M. (2015) 'Ghrelin attenuates renal fibrosis and inflammation of obstructive nephropathy', *The Journal of Urology*, 193(6), pp. 2107–2015.

Swain, S. M., Whaley, F. S., Gerber, M. C., Weisberg, S., York, M., Spicer, D., Jones, S. E., Walder, S., Desai, A., Vogel, C., Speyer, J., Mittelman, A., Reddy, S., Pendergrass, K., Velez-Gardcoa, E., Ewer, M. S., Biachine, J. R. & Gams, R. A. (1997) 'Cardioprotection with dexrazoxane for doxorubicin-containing therapy in advanced breast cancer', *Journal of Clinical Oncology*, 15(4), pp. 1318–1332.

Tacar, O., Sriamornsak, P. & Dass, C. R. (2013) 'Doxorubicin: An update on anticancer molecular action, toxicity and novel drug delivery systems', *Journal of Pharmacy and Pharmacology*, 65(2), pp. 157–170.

Tebbi, C. K., London, W. B., Friedman, D., Villaluna, D., De Alarcon, P. A., Constine, L. S., Mendenhall, N. P., Sposto, R., Chauvenet, A. & Schwartz, C. L. (2007) 'Dexrazoxane-associated risk for acute myeloid leukemia/myelodysplastic syndrome and other secondary malignancies in pediatric Hodgkin's disease', *Journal of Clinical Oncology*, 25, pp. 493–500.

Tetef, M. L., Synold, T. W., Chow, W., Leong, L., Margolin, R., Morgan, R., Raschko, J., Shibata, S., Somlo, G., Yen, Y., Groshen, S., Johnson, K., Lenz, H. J., Gandara, D. & Doroshow, J. H. (2001) 'Phase I trial of 960hour continuous infusion of dexrazoxane in patients with advanced malignancies', *Clinical Cancer Research*, 7(6), pp. 1569–1576.

Tewari, M., Quan, L., O'Rourke, K., Desnoyers, S., Zeng, Z. & Beidler, D. (1995) 'Yama/CPP32 beta, a mammalian homolog of CED-3, is a CrmA-inhibitable protease that cleaves the death substrate poly(ADP-ribose) polymerase', *Cell*, 81, pp. 801–809.

Tolosa, L., Morlá, M., Iglesias, A., Busquets, X., Lladó, J. & Olmos, G. (2005) 'IFN-γ prevents TNF-α-induced apoptosis in C2C12 myotubes through down-regulation of TNF-R2 and increased NF-κB activity', *Cell Signalling*, 17, pp. 1333–1342.

Tomasetto, C., Karam, S., Ribieras, S., Masson, R., Lefebvre, O., Staub, A., Alexander, G., Chenard, M. & Rio, M. (2000) 'Identification and characterization of a novel gastric peptide hormone: the motilin-related peptide', *Gastroenterology*, 119, pp. 395–405.

Tong, X., Wu, D., Wang, X., Chen, H., Chen, J., Wang, X., Wang, X., Gan, L., Guo, Z., Shi, G., Zhang, Y. & Jiang, W. (2012) 'Ghrelin protects against cobalt chloride-induced hypoxic injury in cardiac H9c2 cells by inhibiting oxidative stress and inducing autophagy', *Peptides*, 38(2), pp. 217–227.

Tonsi, A. F., Bacchion, M., Crippa, S., Malleo, G., Bassi, C., Bacchion, M., Crippa, S. & Malleo, G. (2009) 'Acute pancreatitis at the beginning of the 21st century : The state of the art', *World Journal of Gastroenterology*, 15(24), pp. 2945–2959.

Toshinai, K., Mondal, M., Nakazato, M., Date, Y., Murakami, N., Kojima, M., Kangawa, K. & Matsukura, S. (2001) 'Upregulation of ghrelin expression in the stomach upon fasting, insulin-induced hypoglycemia, and leptin administration', *Biochemical and Biophysical Research Communications*, 281, pp. 1220–1225.

Trivedi, C. D. & Pitchumoni, C. S. (2005) 'Drug-induced pancreatitis: an update.', *Journal of Clinical Gastroenterology*, 39(8), pp. 709–716.

Tsang, W., Chau, S. P., Kong, S., Fung, K. & Kwok, T. (2003) 'Reactive oxygen species mediate doxorubicin induced p53-independent apoptosis', *Life Sciences*, 73, pp. 2047–2058.

Tschöp, M., Smiley, D. L. & Heiman, M. L. (2000) 'Ghrelin induces adiposity in rodents', *Nature*, 407(6806), pp. 908–913.

Tsuchitani, M., Sato, J. & Kokoshima, H. (2016) 'A comparison of the anatomical structure of the pancreas in experimental animals.', *Journal of toxicologic pathology*, 29(3), pp. 147–154.

Tsujimoto, Y. (1998) 'Role of Bcl-2 family proteins in apoptosis: apoptosomes or mitochondria?', *Genes Cells*, 3, pp. 697–707.

Uhe, A., Szmukler, G., Collier, G., Hansky, J., O'Dea, K. & Young, G. (1992) 'Potential regulators of feeding behavior in anorexia nervosa', *The American Journal of Clinical Nutrition*, 55(28), pp. 28–32.

Valko, M., Rhodes, C. J., Moncol, J., Izakovic, M. & Mazur, M. (2006) 'Free radicals, metals and antioxidants in oxidative stress-induced cancer', *Chemico-Biological Interactions*, 160, pp. 1–40.

Van Acker, S. A., Boven, E., Kuiper, K., Van den Berg, D. J., Grimbergen, J. A., Kramer, K., Bast, A. & Van der Vijgh, W. J. (1997) 'Monohydroxyethylrutoside, a dose-dependent cardioprotective agent, does not affect the antitumor activity of doxorubicin', *Cancer Research*, 3(10), pp. 1747–1754.

Van Acker, S. A., Kramer, K., Grimbergen, J. A., Van den Berg, D. J., Van der Vijgh, W. J. & Bast, A. (1995) 'Monohydroxyethylrutoside as protector against chronic

doxorubicin-induced cardiotoxicity', *British Journal of Pharmacology*, 115(7), pp. 1260–1264.

Walia, P., Asadi, A., Kieffer, T., Johnson, J. & Chanoine, J. (2009) 'Ontogeny of ghrelin, obestatin, preproghrelin, and prohormone convertases in rat pancreas and stomach.', *Pediatric Research*, 65, pp. 39–44.

Wang, S., Kotamraju, S., Konorev, E., Kalivendi, S., Joseph, J. & Kalyanaraman, B. (2002) 'Activation of nuclear factor-kappaB during doxorubicin-induced apoptosis in endothelial cells and myocytes is pro-apoptotic: the role of hydrogen peroxide', *The Biochemical Journal*, 36, pp. 729–740.

Wang, X., Wang, X., Chen, H., Wu, D., Chen, J., Wang, X., Li, R., He, J., Mo, L., Cen, X., Wei, Y. & Jiang, W. (2014) 'Ghrelin inhibits doxorubicin cardiotoxicity by inhibiting excessive autophagy through AMPK and p38-MAPK', *Biochemical Pharmacology*, 88(3), pp. 334–350.

Warpe, V. S., Mali, V. R., Arulmozhi, S., Bodhankar, S. L. & Mahadik, K. R. (2015) 'Cardioprotective effect of ellagic acid on doxorubicin induced cardiotoxicity in wistar rats', *Journal of Acute Medicine*, 5, pp. 1–8.

Weiss, R. B. (1992) 'The anthracyclines: will we ever find a better doxorubicin?', *Seminars in Oncology*, 19(6), pp. 670–86.

Weydert, C. J. & Cullen, J. J. (2010) 'Measurement of superoxide dismutase, catalase and glutathione peroxidase in cultured cells and tissue', *Nature Protocols*, 5, pp. 51–66.

Wieczorek, G., Pospischil, A. & Perentes, E. (1998) 'A comparative immunohistochemical study of pancreatic islets in laboratory animals (rats, dogs, minipigs, nonhuman primates)', *Experimental and Toxicologic Pathology*, 50(3), pp. 151–172.

Wierup, N., Sundler, F. & Heller, R. S. (2014) 'The islet ghrelin cell', S*ociety for Endocrinology*, 52, pp. R35–49.

Wierup, N., Svensson, H., Mulder, H. & Sundler, F. (2002) 'The ghrelin cell: a novel developmentally regulated islet cell in the human pancreas', *Regulatory Peptides*, 107, pp. 63–69.

Williams, G. S. B., Boyman, L., Chikando, A. C., Khairallah, R. J. & Lederer, W. J. (2013) 'Mitochondrial calcium uptake', *Proceedings of the National Academy of Sciences of the United States of America*, 110(26), pp. 10479–10486.

Wook, K., Jennifer L., F., Shinb, Y.-K., Okunc, E., Kim, J. S., Rappd, P. R. & Egan, J. M. (2014) 'Pancreatic Polypeptide Inhibits Somatostatin Secretion', *FEBS Letters*, 588(17), pp. 3233–3239.

Wren, A., Small, C., Abbott, C., Dhillo, W., Seal, L., Cohen, M., Batterham, R., Taheri, S., Stanley, S., Ghatei, M. & Bloom, S. (2001) 'Ghrelin causes hyperphagia and obesity in rats', *Diabetes*, 50, pp. 2540–2547.

Wulczyn, F., Krapmann, D. & Scheidereit, C. (1996) 'The NF-kB/Rel and I-kB gene families: Mediators of immune response and inflammation', *Journal of Molecular*

Medicine, 74, pp. 749–769.

Wynnand, T. & Ramalingam, T. (2012) 'Mechanisms of fibrosis: therapeutic translation for fibrotic disease', *Nature Medicine*, 18(7), pp. 1028–1040.

Yamamoto, M., Otani, M. & Otsuki, M. (2006) 'A new model of chronic pancreatitis in rats.', *American journal of physiology. Gastrointestinal and Liver Physiology*, 291(4), pp. G700–G708.

Yamanaka, S., Tatsumi, T., Shiraishi, J., Mano, A., Keira, N., Matoba, S., Asayama, J., Fushiki, S., Fliss, H. & Nakagawa, M. (2003) 'Amlodipine inhibits doxorubicin-induced apoptosis in neonatal rat cardiac myocytes', *Journal of the American College of Cardiology*, 41, pp. 870–878.

Yang, D., Liu, Z., Zhang, H. & Luo, Q. (2013) 'Ghrelin protects human pulmonary artery endothelial cells against hypoxia-induced injury via PI3-kinase/Akt', *Peptides*, 42, pp. 112–117.

Yee, K. S. & Vousden, K. H. (2005) 'Complicating the complexity of p53', *Carcinogenesis,* 26, pp. 1317–1322.

Yeh, E. T. H., Tong, A. T., Lenihan, D. J., Yusuf, S. W., Swafford, J., Champion, C., Durand, J.-B., Gibbs, H., Zafarmand, A. A. & Ewer, M. S. (2009) 'Cardiovascular Complications of Cancer Therapy', *Journal of the American College of Cardiology*, 24, pp. 2231–2247.

Yi, X., Bekeredjian, R., DeFilippis, N. J., Siddiquee, Z., Fernandez, E. & Shohet, R. V (2006) 'Transcriptional analysis of doxorubicin-induced cardiotoxicity.', *American journal of physiology. Heart and Circulatory Physiology*, 290(3), pp. H1098-1102.

Yin, X., Li, Y., Xu, G., An, W. & Zhang, W. (2009) 'Ghrelin fluctuation, what determines its production?', *Acta Biochimica et Biophysica Sinica*, 41(3), pp. 188–197.

Yonehara, S. (1989) 'A cell-killing monoclonal antibody (anti-Fas) to a cell surface antigen co-downregulated with the receptor of tumor necrosis factor', *Journal of Experimental Medicine*, 169(5), pp. 1747–1756.

Zafar, M. & Mughal, A. (2002) 'Distribution of cell types of the islets of Langerhans in the pancreas of the albino rats.', *The Professional*, 9, pp. 71–76.

Zhang, S., Liu, X., Bawa-Khalfe, T., Lu, L.S., Lyu, Y.L., Liu, L.F. & Yeh, E.T.H. (2012) 'Identification of the molecular basis of doxorubicin-induced cardiotoxicity', *Nature Medicine*, 18(11), pp. 1639–1642.

Zhang, Y. W., Shi, J., Li, Y. J. & Wei, L. (2009) 'Cardiomyocyte death in doxorubicin-induced cardiotoxicity', *Archivum Immunologiae et Therapiae Experimentalis*, 57(6), pp. 435–445.

Zhang, Y., Ying, B., Shi, L., Fan, H., Yang, D., Xu, D., Wei, Y., Hu, X., Zhang, Y., Zhang, X., Wang, T., Liu, D., Dou, L., Chen, G., Jiang, F. & Wen, F. (2007) 'Ghrelin inhibits cell apoptosis induced by lipotoxicity in pancreatic β-cell line', *Toxicology*, 237, pp. 194–202.

Zheng, Z., Pavlidis, P., Chua, S., D'Agati, V. & Gharavi, A. (2006) 'An ancestral haplotype

defines susceptibility to doxorubicin nephropathy in the laboratory mouse', *Journal of the American Society of Nephrology*, 17, pp. 1796–1800.

APPENDICES

APPENDIX A: Ethical clearance letter

UNIVERSITEIT•STELLENBOSCH•UNIVERSITY
jou kennisvennoot • your knowledge partner

Approved with Stipulations

Date: 29-Apr-2016

PI Name: Goldswain, Toni T Protocol #: SU-ACUD15-00038

Title: Investigating the role of the RISK and SAFE pathways, through ghrelin stimulation, in an in vivo rat model of chronic Doxorubicin-induced cardiotoxicity.

Dear Toni Goldswain, the Response to Modifications submission was reviewed on 26-Apr-2016 by Research Ethics Committee: Animal Care and Use via committee review procedures and was approved on condition that the following stipulations are adhered to:

1. South African Veterinary Council authorisation for Dr Bester is not addressed in the response to modification. Sodium Pentobarbital is a scheduled substance, the committee recommend a suitable person be responsible for euthanasia using this substance. By suitable, referring to a person registered with SAVC or alternatively authorised by SAVC to do this procedure.

Applicants are reminded that they are expected to comply with accepted standards for the use of animals in research and teaching as reflected in the South African National Standards 10386: 2008. The SANS 10386: 2008 document is available on the Division for Research Developments website www.sun.ac.za/research.

As provided for in the Veterinary and Para-Veterinary Professions Act, 1982. It is the principal investigator's responsibility to ensure that all study participants are registered with or have been authorised by the South African Veterinary Council (SAVC) to perform the procedures on animals, or will be performing the procedures under the direct and continuous supervision of a SAVC-registered veterinary professional or SAVC-registered para-veterinary professional, who are acting within the scope of practice for their profession.

Please remember to use your protocol number, SU-ACUD15-00038 on any documents or correspondence with the REC: ACU concerning your research protocol.

Any event not consis10t with routine expected outcomes that results in any unexpected animal welfare issue (death, disease, or prolonged distress) or human health risks (zoonotic disease or exposure, injuries) must be reported to the committee, by creating an Adverse Event submission within the system.

If you have any questions or need further help, please contact the REC: ACU secretariat at WABEUKES@SUN.AC.ZA or 0218089003.

Sincerely,

Winston Beukes

REC: ACU Secretariat

Research Ethics Committee: Animal Care and Use

APPENDIX B: Preparation of ghrelin and Doxorubicin

Materials & Reagents:

- Ghrelin, rat (G2869, LKT® Laboratories, Inc., St. Paul, Minnesota, USA)
- Doxorubicin Hydrochloride (D5794, LKT® Laboratories, Inc., St. Paul, Minnesota, USA)
- Physiological Saline
- Syringes
- Gloves

Ghrelin Preparation:

- Resuspended 5 mg of ghrelin in 5 ml of sterile saline to yield a stock solution of 1 mg/ml = 1 µg/µl. Vortexed solution thoroughly.
- Animal dose = 100 µg/kg

  = 0.1 µg/g

For example:

Animal weight: 118.1 g

= 118.1 g x 0.1 µg/g

= 11.81 µg ghrelin

Stock = 1 µg/ µL

Therefore, $\frac{1\ \mu g}{1\ \mu l} = \frac{11.81\ \mu g}{x}$

x = 11.81 µl ghrelin stock (1 µg/ µl) in 200 µl saline (200 µl is the injection volume)

But, to account for bubble and wastage, multiplied by 2:

11.81 µl x 2 = 23.62 µl ghrelin in 376.38 µl saline.

Vortex solution thoroughly and injected animals with 200 µl

DOX Preparation:

- Resuspended 50 mg of DOX in 12.5 ml of sterile saline to yield a stock solution of 4 mg/ml = 4 µg/µl. Vortexed solution thoroughly.
- Animal dose = 2.5 mg/kg

  = 2.5 µg/g

For example:

Animal weight: 118.1 g

= 118.1 g x 2.5 µg/g

= 295.25 µg DOX

Stock = 4 µg/ µL

Therefore, $\frac{4\ \mu g}{1\ \mu l} = \frac{295.25\ \mu g}{X}$

x = 73.8125 µl DOX stock (4 µg/ µl) in 200 µl saline (200 µl is the injection volume)

But, to account for bubble and wastage, multiplied by 2:

73.8125 µl x 2 = 147.625 µl ghrelin in 252.375 µl saline

Vortex solution thoroughly and injected animals with 200 µl.

APPENDIX C: Serum collection

- After the last injection (eight weeks), the animals were transported to the Cape Peninsula University of Technology (CPUT)

- Following a week of acclimatisation, the animals were weighed and anaesthetised with a lethal dose of sodium pentobarbitone (60 mg/kg), (Euthapent, 130540, Kyron Laboratories, Johannesburg, South Africa), which was injected intraperitoneally
- When pedal reflex was no longer observed, the abdominal cavity was cut open and blood was aspirated from the thoracic cavity, using a sterile syringe, while the heart was being removed from the abdominal cavity
- Collected blood was placed into serum separation tubes (VGRV450470R, Lasec, Cape Town, South Africa) without anti-coagulant
- Serum tubes were immediately placed on ice and blood was allowed to clot for 15 - 20 minutes
- Serum tubes were then centrifuged for 10 minutes at 4 000 rpm (1 400 *x g*) at 4 °C.
- The serum was then aliquoted into centrifuge tubes and stored at – 80 °C

APPENDIX D: Metabolic parameters analysis

Reagents Supplied in Milliplex® MAP Kit:

Reagents	Catalogue number	Volume	Quality
Rat Metabolic Hormone Standard	RMH-8084	Lyophilized	1 vial
Rat Metabolic Hormone Quality Controls 1 and 2	RMH-6084	Lyophilized	2 vials
Set of one 96-well black plate with 2 sealers	-	-	1 plate 2 sealers
Assay Buffer	LE-ABGLP	30 ml	1 bottle
Serum Matrix	LRGT-SM	1 ml	1 bottle
Bead Diluent	LE-BD	3.5 ml	1 bottle
10 X Wash Buffer	L-WB	60 ml	1 bottle
Rat Metabolic Hormone Detection Antibodies	RMH-1084	5.5 ml	1 bottle
Mixing Bottle	-	-	1 bottle

Preparation of Reagents for Immunoassay:

- Preparation of Antibody-Immobilized Beads:
    - Vortexed antibody-bead vials for 1 minute
    - Added 150 µl from each of the 6 beads vials to the Mixing Bottle. Then added 2100 µl Bead Diluent to make a final volume of 3 ml
    - Vortexed beads well
- Preparation of Quality Controls:
    - Added 250 µl deionised water to Quality Control 1 and Quality Control 2
    - Mixed and vortexed well
    - Allowed vial to sit for 5 – 10 minutes
    - Vortexed and transferred to labelled Centrifuge tubes
- Preparation of Wash Buffer:
    - Allowed 10 X wash buffer to come to room temperature and mixed to bring all salts into solution
    - Diluted 60 ml of 10 X Wash Buffer with 540 ml deionized water
- Preparation of Serum Matrix
    - Added 1 ml of deionised water to bottle containing lyophilized serum Matric
    - Mixed well and allowed at least 10 minutes for complete reconstitution
- Preparation of Rat Metabolic Hormone Standard
    - Added 250 µl deionised water to the Rat Metabolic Hormone Standard
    - Mixed well and vortexed for 10 seconds
    - Allowed to sit for 5 - 10 minutes, and then vortexed and transferred this standard to the centrifuge tubes labelled Standard 7
    - The preparation of the working standards was as follows:

Standard Tube	Volume of Deionised Water to add (µl)	Volume of Standard to add (µl)
S7	250	0
S6	200	100 of S7
S5	200	100 of S6
S4	200	100 of S5
S3	200	100 of S4
S2	200	100 of S3
S1	200	100 of S2

- After performing three times serial dilutions, the standard tubes had the following concentrations for constructing standard curves:

Standard Tube	Glucagon, TNFα (pg/ml)	IL-6, Insulin, (pg/ml)
1	14	69
2	41	206
3	124	617
4	370	1 852
5	1 111	5 556
6	3 333	16 667
7	10 000	50 000

Method:

- The serum centrifuge tubes were thawed to room temperature
- The centrifuge tubes were centrifuged at 3000 rpm (800 *x g*) for 5 minutes at 4 °C.
- Added 200 µl of Assay Buffer to each well and swirled plated around in order to pre-wet the plate with Assay Buffer
- Contents were decanted
- Added 25 µl of Serum Matrix Solution to blank, standard, and quality control wells

- Added 25 µl of Assay Buffer to blank and sample wells
- Added 25 µl of Standard and Quality Control solutions to appropriate wells
- Added 25 µl samples to appropriate wells
- Added 25 µl of Beads Solution to each well
- Sealed the plate with plate sealed and covered in foil
- Placed plate on Orbit™ P4 Digital Shaker (serial number 14061102, Labnet International, Inc., North America) at 550 rpm and incubated overnight at 4 °C.
- Plate con10ts were removed and washed three times with Wash Buffer using a Bio-Plex Pro™ Wash Station (BioRad, Johannesburg, South Africa)
- Added 50 µl of Detection Antibodies to each well
- Sealed the plate with plate sealed and covered in foil
- Placed the plate shaker at 600 rpm and incubated for 30 minutes at room temperature
- Added 50 µl of Streptavidin-Phycoerythrin to each well
- Sealed the plate with plate sealed and covered in foil
- Placed the plate shaker at 600 rpm and incubated for 30 minutes at room temperature
- Plate con10ts were removed and washed three times as previously described
- Added 100 µl of MAGPIX® Drive Fluid (40-50013, Luminex) to each well
- Placed the plate shaker at 600 rpm for 5 minutes to resuspend the beads
- Placed the plate into Bio-Plex® MAGPIX™ Multiplex reader (MAGPIX13046704, BioRad, Johannesburg, South Africa)
- Results were acquired results using Manager™ MP (BioRa, Johannesburg, South Africa) and analysed using BioPlex Manager™ Software version 6.1 (BioRad, Johannesburg, South Africa)

- Plate set up was as follows:

	1	2	3	4	5	6	7	8	9	10	11	12
A	0	4	QC1	C3	V4	G5	D7	DG4	V2	G2	D2	DG2
B	0	4	QC1	C3	V4	G5	D7	DG4	V2	G2	D2	DG2
C	1	5	QC2	C5	V5	G6	D8	DG5	V3	G3	D3	DG3
D	1	5	QC2	C5	V5	G6	D8	DG5	V3	G3	D3	DG3
E	2	6	C1	C6	V6	D5	D9	DG7	V4	G4	D4	DG4
F	2	6	C1	C6	V6	D5	D9	DG7	V4	G4	D4	DG4
G	3	7	C2	C7	G4	D6	DG2	V1	G1	D1	DG1	DG5
H	3	7	C2	C7	G4	D6	DG2	V1	G1	D1	DG1	DG5

Rat Metabolic Hormone Antibody Immobilised Magnetic Beads:

Bead/Analyte Name	Luminex® Magnetic Bead Region	Catalogue Number
Anti-Glucagon Beads	33	HGLU-MAG
Anti-IL-6 Beads	35	RIL6-MAG
Anti-Insulin Beads	37	RMINS-MAG
Anti-TNFα Beads	65	RMTNFA-MAG

APPENDIX E: Standard histological processing protocol

Materials & Reagents:

- Alcohol (70%, 90%, 95%, 100%)
- Xylene (1330-20-7, Sigma-Aldrich, St Louis, USA)
- Paraplast® wax (A6330-4LB, Sigma-Aldrich, St Louis, USA, melting point 56°C)
- Embedding cassettes with lid (Z672122, Sigma-Aldrich, St Louis, USA)

- Leica Modular Tissue Embedding Centre (EG1150, Lecia Biosystems, Biosystems, Wetzlar, Germany)
- Paraffin wax moulds

Method:

1. Fixed tissue in 4% formaldehyde solution (100496, Merck Millipore, Massachusetts, USA) in small labelled containers
2. Followed automated tissue processing protocol

- After 20-hour processing period, the tissues were removed from their cassettes and embedded in paraffin wax

Automated tissue processing protocol:

Step	Solution	Time (hours)
Dehydration	70% alcohol	1.5
	70% alcohol	1.5
	90% alcohol	1.5
	95% alcohol	1.5
	95% alcohol	1.5
	100% alcohol	1.5
	100% alcohol	1.5
	100% alcohol	2
Clearing	Xylene	1.5
	Xylene	2
Impregnation	Paraffin wax	2
	Paraffin wax	2
Total processing time		**20**

APPENDIX F: Haematoxylin & Eosin (H&E) staining protocol

Materials & Reagents:

1. Manual microtome (RM 2125 RT, Leica Biosystems, Wetzlar, Germany)
2. Leica Auto Stainer XL (ST5010, Leica Biosystems, Wetzlar, Germany
3. Microscope slides (GLAS4S22M3000F, Lasec, Cape Town, South Africa)
4. Microscope coverslips (GLAS2C9M2250REC, Lasec, Cape Town, South Africa)
5. DPX mountant (06522, Sigma-Aldrich, St Louis, USA)
6. Xylene (1330-20-7, Sigma-Aldrich, St Louis, USA)
7. Mayer's Haematoxylin solution (SAAR2822001LC, Merck Millipore, Massachusetts, USA)
8. Eosin solution (3801600E, Leica Biosystems, Wetzlar, Germany)

Method:

- Sectioned tissue at 5 µm thickness using a manual microtome and transferred to appropriately labelled slides
- Microscope slides were put into plastic rack and placed into the auto stainer machine following the pre-programmed protocol
- After staining, mounted the coverslips with DPX mountant

Pre-programmed H&E staining protocol:

Step	Solution	Time	Repetitions
1	Xylene	10 minutes	2
2	Ethanol (99%)	5 minutes	2
3	Ethanol (96%)	2 minutes	1
4	Ethanol (70%)	2 minutes	1
5	Distilled water	5 seconds	1
6	Haematoxylin	8 minutes	1

7	Running water	5 minutes	1
8	Ethanol (1% acid alcohol)	30 seconds	1
9	Running water	1 minutes	1
10	Ammonia (0.2%)	45 seconds	1
11	Running water	5 minutes	2
12	Ethanol (96%)	10 dips	1
13	Eosin	45 seconds	1
14	Ethanol (96%)	5 minutes	2
15	Xylene	5 minutes	2

APPENDIX G: Masson Trichrome staining protocol

Control: Skin

Staining Solutions:

- Mayer's Haematoxylin solution (SAAR2822001LC, Merck Millipore, Massachusetts, USA) Acetic Acid Water**:**
    - 2 ml Glacial acetic acid
    - 100 ml Distilled water
- Masson Fuchson Ponceau-Orange G:
    - <u>Stock Solution</u>
        - 2 g Ponceau (2R) de xylidine
        - 1 g Acid fuchsin
        - 2 g Orange G
        - 300 ml 0.2% Acetic acid water

- Working solution
    - 10 ml No.3 (MFPOG)
    - 90 ml 0.2% Acetic acid water

- 0.1% Light Green Solution
    - 0.1 g Light green
    - 100 ml 0.2% Acetic acid water
- Phosphotungstic acid 5%
    - 5 g Phosphotungstic acid
    - 100 ml Distilled water

Materials:

- Positively charged Histobond microscope slides (GLAS2S13M0810401, Lasec, Cape Town, South Africa)
- Microscope coverslips (GLAS2C9M2250REC, Lasec, Cape Town, South Africa)
- DPX mountant (06522, Sigma-Aldrich, St Louis, USA)

Method:

- Sectioned tissue at 5 µm thickness using a manual microtome and transferred to appropriately labelled slides
- Microscope slides were put into plastic rack and a manual deparaffinization process was followed
- After staining, mounted the coverslips with DPX mountant

Manual Deparaffinization:

Step	Solution	Time	Repetitions
1	Xylene	5 mins	2
2	Ethanol (99%)	5 mins	2
3	Ethanol (96%)	5 mins	2
4	Ethanol (70%)	5 mins	2
5	Water	3 mins	1

Staining Procedure:

1. Rinsed slides that have been deparaffinised in distilled water.
2. Stained in haematoxylin for 5 minutes.
3. Placed in tap water for 3 minutes till dark blue and rinse in distilled water.
4. Stained the sections in filtered working solution of fuchsin ponceau-orange G for 5 - 30 minutes.
5. Rinsed in acetic acid water.
6. Mordant in 5% phosphotungtic acid solution for 5 minutes.
7. Rinsed in acetic acid water for 1 minute to eliminate the phosphotungstic acid and differentiate the colour tones.
8. Stained in light green solution for 5 - 20 minutes.
9. Treated with acetic acid water for 5 minutes
10. Dehydrated through alcohols with (70%, 96%, 99% ethanol)
11. Cleared in xylene and mounted the coverslips with DPX mounting medium

Result:

Nuclei - black

Cytoplasm - red

Collagen - green

Mucin - green

Erythrocytes - yellow to orange

APPENDIX H: Immunohistochemistry (IHC) staining protocol

Materials & Reagents:

1. Positively charged Histobond microscope slides (GLAS2S13M0810401, Lasec, Cape Town, South Africa)
2. Microscope coverslips (GLAS2C9M2250REC, Lasec, Cape Town, South Africa)
3. DPX mountant (06522, Sigma-Aldrich, St Louis, USA)
4. Bond™ Polymer Refine Detection Kit (DS9800, Leica Biosystems, Wetzlar, Germany)
5. Bond™ Polymer Refine Red Detection Kit (DS9390, Leica Biosystems, Wetzlar, Germany)
6. Leica Bond-Max™ Immuno-Autostainer (ST5010, Lecia Biosystems, Wetzlar, Germany)
7. BOND™ Software ©2009, Version 4.0 (Lecia Biosystems, Wetzlar, Germany)

Method:

- Sectioned tissue at 5 µm thickness using a manual microtome and transferred to appropriately labelled slides
- Microscope slides were put into plastic rack and placed using the immune-autostainer machine following the pre-programmed protocol
- After staining, mounted the coverslips with DPX mountant

Automated IHC double staining protocol:

Step	**Solution**	**Time**	**Temperature**
1	Bond Wash Solution	0 minutes	72°C
2	Bond Wash Solution	0 minutes	72°C
3	Bond Wash Solution	0 minutes	Ambient
4	Alcohol	0 minutes	Ambient
5	Alcohol	0 minutes	Ambient
6	Alcohol	0 minutes	Ambient
7	Bond Wash Solution	0 minutes	Ambient
8	Bond Wash Solution	0 minutes	Ambient
9	Bond Wash Solution	0 minutes	Ambient
10	Bond ER Wash Solution 1	0 minutes	Ambient
11	Bond ER Wash Solution 1	0 minutes	Ambient
12	Bond ER Wash Solution 1	20 minutes	100°C
13	Bond ER Wash Solution 1	12 minutes	Ambient
14	Bond Wash Solution	0 minutes	35°C
15	Bond Wash Solution	0 minutes	35°C
16	Bond Wash Solution	0 minutes	35°C
17	Bond Wash Solution	3 minutes	Ambient
18	Peroxide Block	5 minutes	Ambient
19	Bond Wash Solution	0 minutes	Ambient
20	Bond Wash Solution	0 minutes	Ambient
21	Bond Wash Solution	0 minutes	Ambient
22	Primary Antibody 1	30 minutes	Ambient
23	Bond Wash Solution	0 minutes	Ambient
24	Bond Wash Solution	0 minutes	Ambient

25	Bond Wash Solution	0 minutes	Ambient
26	Post Primary	8 minutes	Ambient
27	Bond Wash Solution	2 m minutes	Ambient
28	Bond Wash Solution	2 minutes	Ambient
29	Bond Wash Solution	2 minutes	Ambient
30	Polymer	8 minutes	Ambient
31	Bond Wash Solution	2 minutes	Ambient
32	Bond Wash Solution	2 minutes	Ambient
33	Deionised Water	0 minutes	Ambient
34	Mixed DAB Refine	0 minutes	Ambient
35	Mixed DAB Refine	10 minutes	Ambient
36	Deionised Water	0 minutes	Ambient
37	Deionised Water	0 minutes	Ambient
38	Deionised Water	0 minutes	Ambient
39	Haematoxylin	5 minutes	Ambient
40	Deionised Water	0 minutes	Ambient
41	Bond Wash Solution	0 minutes	Ambient
42	Deionised Water	0 minutes	Ambient
43	Primary Antibody 2	15 minutes	Ambient
44	Bond Wash Solution	0 minutes	Ambient
45	Bond Wash Solution	0 minutes	Ambient
46	Bond Wash Solution	0 minutes	Ambient
47	Post Primary AP	20 minutes	Ambient
48	Bond Wash Solution	2 minutes	Ambient
49	Bond Wash Solution	2 minutes	Ambient
50	Bond Wash Solution	2 minutes	Ambient
51	Polymer AP	30 minutes	Ambient
52	Bond Wash Solution	2 minutes	Ambient

53	Bond Wash Solution	2 minutes	Ambient
54	Bond Wash Solution	5 minutes	Ambient
55	Bond Wash Solution	2 minutes	Ambient
56	Bond Wash Solution	0 minutes	Ambient
57	Deionised Water	0 minutes	Ambient
58	Mixed Red Refine	10 minutes	Ambient
59	Mixed Red Refine	5 minutes	Ambient
60	Deionised Water	0 minutes	Ambient
61	Deionised Water	0 minutes	Ambient
62	Deionised Water	0 minutes	Ambient
63	Haematoxylin	5 minutes	Ambient
64	Deionised Water	0 minutes	Ambient
65	Bond Wash Solution	0 minutes	Ambient
66	Deionised Water	0 minutes	Ambient

Manual rehydration protocol:

Step	Solution	Time	Repetitions
1	Ethanol (70%)	5 dips	1
2	Ethanol (96%)	5 dips	1
3	Ethanol (99%)	5 dips	1
4	Xylene	1 min	2

Antibodies used for IHC staining:

Antibody	Company	Antibody Catalogue number	Clonality	Raised in	Dilution
Anti-insulin	Abcam	ab181547	Monoclonal	Mouse	1:1000
Anti-glucagon	Abcam	ab113694	Monoclonal	Rabbit	1:1500

APPENDIX I: Oxidative Stress Assays

Preparation of Reagents:

- 50 mM of phosphate buffer:
    - Dissolved in 50 ml distilled water:
        - 0.7098 g of sodium phosphate monobasic (NaH_2PO_4, S8282, Sigma-Aldrich, St Louis, USA)
        - 0.029 g of Ethylenediaminetetraacetic acid (EDTA, EDS-100G, Sigma-Aldrich, St Louis, USA)
    - Adjusted the pH to 7.5
    - Adjusted final volume to 100 ml
- 1-methyl-2-vinylpyridinium (M2VP)
    - Made up 0.1 M HCl:
        - Added 4.91 ml HCl (SAAR3063040LP, Merck Millipore, Massachusetts, USA) to 500 ml distilled water
    - Added 12.5 ml of 0.1 M HCl to 100 mg M2VP (69701, Sigma-Aldrich, St Louis, USA)
    - Vortexed thoroughly

Preparation of samples:

- Stored the harvested tissues at - 80 °C in labelled centrifuge tubes
- Each pancreas was carefully crushed using a sterile mortar and pestle on ice and separated into chilled centrifuge tubes
- <u>For the ORAC, SOD, GSH, and conjugated dienes assays:</u> approximately 100 mg of tissue was weighed and transferred into new chilled Centrifuge tubes and 50 mM of phosphate buffer was added into each centrifuge tube

  - Phosphate buffer was added in a ratio of 1 000 µl phosphate buffer to 100 mg of sample

- For the GSSG assay: approximately 100 mg of tissue was weighed and transferred into new chilled centrifuge tubes and 50 mM of phosphate buffer and M2VP was added into each centrifuge tube
  - The exact weight of tissue was recorded
  - Phosphate buffer was added in a ratio of 1 000 µl phosphate buffer to 100 mg of sample
- Con10ts of each centrifuge tube were homogenised on ice in an attempt to avoid heating of the con10ts
- The centrifuge tubes were centrifuged at 14 000 rpm (16 000 *x g*) at 4 °C for 10 minutes.
- The supernatant was transferred to new centrifuge tubes and frozen at – 80 °C

APPENDIX J: ORAC (Oxygen Radical Antioxidant Reactive Capacity) assay

Preparation of Reagents:

- Fluorescein (F6377, Sigma-Aldrich, St Louis, USA) Stock:
  - Dissolved 0.0225 g in 50 ml of phosphate buffer
  - Can be stored at 4 °C in a brown bottle and can be reused for 1 year
- Fluorescein Working Solution:
  - Added 10 µl of the stock to 2 ml of phosphate buffer in a falcon tube
  - Took 240 µl of this and diluted it in 15 ml of phosphate buffer in new falcon tube
- 25 mg/ml 2,2'-Azobis(2-methyl-propionamidine) dihydrochloride (AAPH) peroxyl radical (440914, Sigma-Aldrich, St Louis, USA):
  - Weighed 150 mg of AAPH in a falcon tube and added 6 ml of phosphate buffer to the falcon tube

- 250 µM stock Trolox (standard) (238831, Sigma-Aldrich, St Louis, USA):
    - Weighed 0.00312 g in a falcon tube and added 50 ml of phosphate buffer

Method:

- The centrifuge tubes were thawed on ice, and then centrifuged at 14 000 rpm (16 000 *x g*) for 10 minutes at 4 °C
- 100 µl of homogenate was added to new centrifuge tubes, and 100 µl of perchloric acid (PCA) was then added to each centrifuge tube
- Standards were prepared as follows:

Tube	Concentration (µM)	Trolox (µl)	Phosphate Buffer (µl)
(Blank) 1	0	0	750
2	83	125	625
3	167	250	500
4	250	375	375
5	333	500	250
6	417	625	125

- A 96-well black plate was used for the assay. First, second and last columns (1, 2, 12) of plate were not used.
- Set up of plate 1:

	1	2	3	4	5	6	7	8	9	10	11	12
A			1	1	1	2	2	2	3	3	3	
B			4	4	4	5	5	5	6	6	6	
C			C5	C5	C5	C6	C6	C6	C7	C7	C7	
D			V4	V4	V4	V5	V5	V5	V6	V6	V6	
E			G4	G4	G4	G5	G5	G5	G6	G6	G6	

F			D5	D5	D5	D6	D6	D6	D7	D7	D7	
G			D8	D8	D8	D9	D9	D9	DG2	DG2	DG2	
H			DG4	DG4	DG4	DG5	DG5	DG5	DG7	DG7	DG7	

- Set up of plate 2:

	1	**2**	**3**	**4**	**5**	**6**	**7**	**8**	**9**	**10**	**11**	**12**
A			1	1	1	2	2	2	3	3	3	
B			4	4	4	5	5	5	6	6	6	
C			V1	V1	V1	V2	V2	V2	V3	V3	V3	
D			V4	V4	V4	G1	G1	G1	G3	G3	G3	
E			G4	G4	G4	D1	D1	D1	D2	D2	D2	
F			D3	D3	D3	D4	D4	D4	DG1	DG1	DG1	
G			DG2	DG2	DG2	DG3	DG3	DG3	DG4	DG4	DG4	
H			DG5	DG5	DG5							

- Added 12 µl of standards into standard wells
- Added 12 µl of sample into sample wells
- Added 138 µl of fluorescein solution using a multichannel into all wells
- At the plate reader machine, added 50 µl of AAPH using a multichannel into all wells
- Placed plate immediately into Fluoroskan Ascent™ microplate fluometer (5210470, Thermo Fishcher Scientific, Massachusetts, USA)
- Read plate every five minutes for two hours
    - Excitation wavelength for fluorescein = 485 nm
    - Emission wavelength for fluorescein = 538 nm

APPENDIX K: Superoxide Dismutase (SOD) assay

Preparation of Reagents:

- 6-Hydroxydopamine (6-HD) + PCA solution:
    - Added 50 µl PCA (100514, Merck Millipore, Massachusetts, USA) to 10 ml of distilled water
    - Added 10 ml of this solution and to 4 mg 6-HD (162957, Sigma-Aldrich, St Louis, USA)
    - Wrapped falcon tube in foil and stored on ice
- Diethylenetriaminepentaacetic acid (DETAPAC):
    - Added 2 mg of DETAPAC (D6518, Sigma-Aldrich, St Louis, USA) to 50 ml of phosphate solution

Method:

- The centrifuge tubes were thawed on ice and then centrifuged at 12 000 rpm (13 300 *x g*) for 10 minutes at 4 °C
- Set up of plate 1:

	1	2	3	4	5	6	7	8	9	10	11	12
A	Blank	Blank	Blank	C5	C5	C5	C6	C6	C6	C7	C7	C7
B	V4	V4	V4	V5	V5	V5	V6	V6	V6	G4	G4	G4
C	G5	G5	G5	G6	G6	G6	D5	D5	D5	D6	D6	D6
D	D7	D7	D7	D8	D8	D8	D9	D9	D9	DG2	DG2	DG2
E	DG4	DG4	DG4	DG5	DG5	DG5	DG7	DG7	DG7			
F												
G												
H												

- Set up of plate 2:

	1	2	3	4	5	6	7	8	9	10	11	12
A	Blank	Blank	Blank	V1	V1	V1	V2	V2	V2	V3	V3	V3
B	V4	V4	V4	G1	G1	G1	G3	G3	G3	G4	G4	G4
C	D1	D1	D1	D2	D2	D2	D3	D3	D3	D4	D4	D4
D	DG1	DG1	DG1	DG2	DG2	DG2	DG3	DG3	DG3	DG4	DG4	DG4
E	DG5	DG5	DG5									
F												
G												
H												

- Added 12 µl of SOD assay buffer into blank wells
- Added 12 µl of samples in sample wells
- Added 15 µl of 6-HD + PCA solution into all wells
- At the machine, 170 µl DETAPAC was added to all wells and the plate was read immediately at 490 nm

APPENDIX L: Glutathione assays (GSH and GSSG)

Preparation of Reagents:

- Glutathione reductase (GR, G3664, Sigma-Aldrich, St Louis, USA)
    - Add 80 µl of glutathione reductase to 4920 µl of phosphate buffer
- 5 5'-dithiobis-(2-nitrobenzoic acid) (DTNB, D218200, Sigma-Aldrich, St Louis, USA)
    - Added 6 mg to 50 ml of phosphate buffer
- NADPH, reduced disodium salt (N6785, Sigma-Aldrich, St Louis, USA)
    - Added 12 ml of phosphate buffer straight into the NADPH bottle
- Glutathione (GSH) (Standard): 3uM
    - Weighed 0.046 g of GSH stock and added to 50 ml of phosphate buffer in a falcon tube

- Then took 50 µl of this and diluted in 50 ml of phosphate buffer in a new falcon tube

For GSH:

Method:

- The centrifuge tubes were thawed on ice and then centrifuged at 14 000 rpm (16 000 *x g*) for 10 minutes at 4 °C
- GSH standards were prepared as follows:

Tube	GSH (µl)	Buffer A (µl)
(Blank) 1	0	1000
2	167	833
3	334	667
4	500	500
5	667	334
6	833	167

- A 96-well clear plate was used for this assay
- Set up of plate 1:

	1	2	3	4	5	6	7	8	9	10	11	12
A	1	1	1	2	2	2	3	3	3	4	4	4
B	5	5	5	6	6	6	C5	C5	C5	C6	C6	C6
C	C7	C7	C7	V4	V4	V4	V5	V5	V5	V6	V6	V6
D	G4	G4	G4	G5	G5	G5	G6	G6	G6	D5	D5	D5
E	D6	D6	D6	D7	D7	D7	D8	D8	D8	D9	D9	D9
F	DG2	DG2	DG2	DG4	DG4	DG4	DG5	DG5	DG5	DG7	DG7	DG7
G												
H												

- Set up of plate 2:

	1	2	3	4	5	6	7	8	9	10	11	12
A	1	1	1	2	2	2	3	3	3	4	4	4
B	5	5	5	6	6	6	V1	V1	V1	V2	V2	V2
C	V3	V3	V3	V4	V4	V4	G1	G1	G1	G3	G3	G3
D	G4	G4	G4	D1	D1	D1	D2	D2	D2	D3	D3	D3
E	D4	D4	D4	DG1	DG1	DG1	DG2	DG2	DG2	DG3	DG3	DG3
F	DG4	DG4	DG4	DG5	DG5	DG5						
G												
H												

- Added 50 µl of standards into standard wells
- Added 35 µl of sample and 15 µl of phosphate buffer into sample wells (0.5 X dilution)
- Added 50 µl DTNB using a multichannel into all wells
- Added 50 µl GR using a multichannel into all wells
- At the plate reader machine, added 50 µl of NADPH using a multichannel into all wells
- Placed plate immediately into the Multiskan™ Spectrum microplate spectrophotometer (51119200, Thermo Fisher Scientific, Massachusetts, USA).
- Read plate every 30 seconds for 5 minutes at 412 nm using

For GSSG:

Method:

- The centrifuge tubes were thawed on ice and then centrifuged at 14 000 rpm (16 000 *x g*) for 10 minutes at 4 °C
- GSSG standards were prepared as follows:

Tube	GSSG (µl))	Buffer A (µl))
(Blank) 1	0	1000
2	167	833
3	334	667
4	500	500
5	667	334
6	833	167

- Set up of plate 1:

	1	2	3	4	5	6	7	8	9	10	11	12
A	1	1	1	2	2	2	3	3	3	4	4	4
B	5	5	5	6	6	6	C5	C5	C5	C6	C6	C6
C	C7	C7	C7	V4	V4	V4	V5	V5	V5	V6	V6	V6
D	G4	G4	G4	G5	G5	G5	G6	G6	G6	D5	D5	D5
E	D6	D6	D6	D7	D7	D7	D8	D8	D8	D9	D9	D9
F	DG2	DG2	DG2	DG4	DG4	DG4	DG5	DG5	DG5	DG7	DG7	DG7
G												
H												

- Set up of plate 2:

	1	2	3	4	5	6	7	8	9	10	11	12
A	1	1	1	2	2	2	3	3	3	4	4	4
B	5	5	5	6	6	6	V1	V1	V1	V2	V2	V2
C	V3	V3	V3	V4	V4	V4	G1	G1	G1	G3	G3	G3
D	G4	G4	G4	D1	D1	D1	D2	D2	D2	D3	D3	D3
E	D4	D4	D4	DG1	DG1	DG1	DG2	DG2	DG2	DG3	DG3	DG3
F	DG4	DG4	DG4	DG5	DG5	DG5						
G												
H												

- Added 50 µl of standards into standard wells
- Added 50 µl of sample into sample wells
- Added 50 µl of DTNB using a multichannel into all wells
- Added 50 µl of GR using a multichannel into all wells
- At the plate reader machine, added 50 µl of NADPH using a multichannel into all wells
- Placed plate immediately into the Multiskan™ Spectrum microplate spectrophotometer (51119200, Thermo Fisher Scientific, Massachusetts, USA).
- Read plate every 30 seconds for five minutes at 412 nm

APPENDIX M: Conjugated Dienes (CDs) assay

Reagents:

- Chloroform (102444, Merck Millipore, Massachusetts, USA)
- Methanol (106007, Merck Millipore, Massachusetts, USA)
- Cyclohexane (102822, Merck Millipore, Massachusetts, USA)

Method:

- The centrifuge tubes were thawed on ice
- 200 µl of homogenate was transferred into a new centrifuge tube
- 450 µl of chloroform and methanol solution (2:1 ratio) was added to each centrifuge tube
- 150 µl of distilled water was added to each centrifuge tube and vortexed
- Centrifuge tubes were centrifuged at 12 000 rpm (13 300 x *g*) at 4 °C for 10 minutes to separate the phases
- 150 µl of bottom chloroform layer was removed and transferred into a new centrifuge tube

- Centrifuge tubes were left open to dry at 4 °C overnight
- The residue was reconstituted with 750 µl cyclohexane (102822, Merck Millipore, Massachusetts, USA) and vortexed
- Set up of plate 1:

	1	2	3	4	5	6	7	8	9	10	11	12
A	Blank	Blank	Blank	V4	V4	V4	V5	V5	V5	V6	V6	V6
B	G4	G4	G4	G5	G5	G5	G6	G6	G6	D5	D5	D5
C	D6	D6	D6	D7	D7	D7	D8	D8	D8	D9	D9	D9
D	DG2	DG2	DG2	DG4	DG4	DG4	DG5	DG5	DG5	DG7	DG7	DG7
E	V1	V1	V1	V2	V2	V2	V3	V3	V3	V4	V4	V4
F	G1	G1	G1	G3	G3	G3	G4	G4	G4	D2	D2	D2
G	D3	D3	D3	D4	D4	D4	DG1	DG1	DG1	DG2	DG2	DG2
H	DG3	DG3	DG3	DG4	DG4	DG4	DG5	DG5	DG5			

- Added 200 µl of cyclohexane into blank wells
- Added 200 µl of sample into sample wells
- Placed plate into the Multiskan™ Spectrum microplate spectrophotometer (51119200, Thermo Fisher Scientific, Massachusetts, USA)
- Read absorbance at 234 nm

APPENDIX N: Thiobarbituric Acid Reactive Substances (TBARS) Assay

Reagents for TBARS assay:

- 0.1 M Sodium hydroxide (NaOH, S5881, Sigma-Aldrich, St Louis, USA):
    - Added 250 µl of NaOH in 10 ml of distilled water
- 2-Thiobarbituric acid (TBA, T5500, Sigma-Aldrich, St Louis, USA):
    - Weighed 0.125 g and dissolved in 10 ml of NaOH
- Butylated hydroxytroluene (BHT, B1378, Sigma-Aldrich, St Louis, USA):

  - Added 0.008 g of BHT in 10 ml of 96% ethanol (16368, Sigma-Aldrich, St Louis, USA)

- 14.6 M Ortho-phosphoric acid (OPA, 100573, Merck Millipore, Massachusetts, USA)
  - Added 684.93 µl OPA to 50 ml distilled water
- Saturated salt solution
  - A falcon tube was filled to three quarters full and distilled water was added
  - Solution was shaken until the salt was not completely dissolved after approximately two minutes of shaking

Method:

- The centrifuge tubes were thawed on ice and then centrifuged at 14 000 rpm (16 000 *x g*) for 10 minutes at 4 °C
- Centrifuge tubes were labelled, and holes were punctured into the lids
- Added 50 µl of sample to each tube
- Added 6.25 µl of 4 mM BHT solution to each tube
- Added 50 µl of 0.2 M OPA solution to each tube
- Added 6.25 µl of 0.11 M TBA to each tube
- The tubes were placed in a 90 °C waterbath for 45 minutes
- The tubes were cooled immediately in an ice bath
- Added 50 µl of saturated salt solution to each tube
- Added 1000 µl of butanol to each tube
- The tubes were centrifuged at 14 000 rpm (16 000 *x g*) for 20 seconds, during which the solution in the tubes were separated into two layers. The top layer had a slight pink colour. This is known as the butanol phase

- Set up of plate:

	1	2	3	4	5	6	7	8	9	10	11	12
A	Blank	Blank	Blank	C5	C5	C5	C6	C6	C6	C7	C7	C7
B	V4	V4	V4	V5	V5	V5	V6	V6	V6	G4	G4	G4
C	G5	G5	G5	G6	G6	G6	D5	D5	D5	D6	D6	D6
D	D7	D7	D7	D8	D8	D8	D9	D9	D9	DG2	DG2	DG2
E	DG4	DG4	DG4	DG5	DG5	DG5	DG7	DG7	DG7			
F												
G												
H												

- Added 300 µl of butanol into blank wells
- Added 300 µl of butanol phase into sample wells
- Placed plate into the Multiskan^{TM} Spectrum microplate spectrophotometer (51119200, Thermo Fisher Scientific, Massachusetts, USA)
- Read absorbance at 532 nm

APPENDIX O: Western blotting protocol

Preparation of lysates:

- Stored the harvested tissues at - 80 °C in labelled centrifuge tubes
- Each pancreas was carefully crushed using a sterile mortar and pestle on ice and separated into chilled centrifuge tubes
- 300 µl of modified radio-immunoprecipitation (RIPA) buffer was added to each centrifuge tube
- Contents of each centrifuge tube were homogenised on ice, in an attempt to avoid heating of the contents

- After homogenisation, the centrifuge tubes were left on ice for an hour to allow for the froth to settle
- Once the froth had settled, the centrifuge tubes were centrifuged at 14 000 rpm (16 000 *x g*) at 4 °C for an hour
- The supernatant was transferred to new centrifuge tubes and centrifuged again at 14 000 rpm (16 000 *x g*) at 4 °C for 15 minutes
- The supernatant was removed again and transferred to a new centrifuge tube
- Protein content was determined using Direct Detect™ Infrared Spectrometer (DDHW00010-WW, Merck Millipore, Massachusetts, USA, Massachusetts, USA), where RIPA buffer was used as the blank
- The lysates were diluted accordingly with Laemmli's solution and RIPA buffer into centrifuge tubes, in which a hole was punched into each lid. Laemmli's solution was prepared as follows: 850 µl Laemmli's Sample Buffer and 150 µl of 2-mercaptoethanol
- The prepared lysates were boiled at 95 °C for five minutes and stored at - 80 °C until required

Preparation and assembly of gels and loading tank:

- On the day of experiment, the prepared lysates were thawed on ice
- The thawed lysates were boiled at 95 °C for five minutes, and then centrifuged at 9 300 rpm (8000 *x g*) for 10 seconds and placed back on ice
- 1 mm plates (10 wells) (Biorad, Johannesburg, South Africa) were cleaned with 70% ethanol spray
- The plates were assembled into the cassette. Distilled water was used to check for leaks.
- For the 12% gels, used a clean Pasteur pipette to pour the prepared resolving gel between the two plates at one corner to avoid making bubbles. Immediately, the stacking gel was then poured on top of the resolving gel in the same manner with

a clean Pasteur pipette, and the 10 well comb (Biorad, Johannesburg, South Africa) was inserted perpendicular to the plates to avoid forming bubbles. The gel was allowed to set for approximately an hour

- For the 15% gels, the prepared resolving gel was poured between the two plated at one corner to avoid making bubbles using a clean Pasteur pipette. 100% ethanol was then poured on top and the resolving gel was allowed to set at room temperature for approximately an hour. Once the resolving gel had set, the ethanol was poured off and plates were dabbed dry. Another clean Pasteur pipette was used to pour the prepared stacking gel on top of the resolving gel in the same manner as the resolving gel and the 10 well comb (Biorad, Johannesburg, South Africa) was inserted perpendicular to the plates to avoid forming bubbles. The gel was allowed to set for approximately 30 minutes

- Once the gel had set, the plates were removed from the cassette and placed into a U-shaped adaptor ensuring that the short plates face inwards, which was then placed into loading tank

- 10 X running buffer was poured into the tank and filled to the top of the plates

- The comb was removed carefully and perpendicular to the plates

- A syringe was used to flush and clean out each well with 10 X running buffer

Loading the protein samples:

- A flexible loading tip was used and loaded 4 µl of BLUeye Prestained Protein Ladder (PM007-0500, GeneDireX, Inc., Beijing, China) into the first well of the gel

- The samples were loaded into the remaining wells using a new tip for each sample

- Once all the samples were loaded, the lid was placed on the tank ensuring the electrode colours matched up (black on black, and red on red)

- Connected the wires to the electrophoresis machine and ensured that the wires were connected correctly (black in black, and red in red)

For the 12% gels:

- The samples ran at 100V, 400 mA for 10 minutes to allow for the samples to migrate through the stacking gel
- After 10 minutes, the samples ran at 150V, 400 mA until smallest standard of protein marker reached the bottom of the gel (about an hour)

For the 15% gels:

- The samples ran at 100V, 400 mA until smallest standard of protein marker reached the bottom of the gel (about 80 minutes)

Transferring protein from gel to membrane:

- Assembled the Trans-Blot® Turbo™ Mini PVDF Transfer Packs (Biorad, Johannesburg, South Africa)
    - Soaked the blotting paper in transfer buffer
    - Soaked the LF PVDF membrane in methanol (1.06007.2500, Merck Millipore, Massachusetts, USA) for 30 seconds, and then soaked in transfer buffer for two to three minutes
- Placed the “bottom” blotting paper into the cassette using the TransBlot® Turbo™ Transfer System (Biorad, Johannesburg, South Africa) and then the membrane on top of the blotting paper. Rolled out any bubbles with mini roller
- Carefully removed the gel from the plates and activated it using ChemiDoc™ XRS+ System with the Image Lab™ Software (Bio-Rad, Johannesburg, South Africa)
- Once the gel had been activated, it was carefully placed on top of the membrane in the cassette. Rolled out any bubble with mini roller
- Placed the “top” blotting paper on top of the gel in the cassette. Rolled our any bubbles with mini roller
- Closed and locked the cassette, and placed into the transfer machine

For 12% gels:

- Set system to transfer for seven minutes at 15 V

For 15% gels:

- Set system to transfer for 10 minutes at 15 V
- Once the protein transfer was complete, a stain-free blot image of the membrane was taken using the ChemiDoc™ XRS+ System with the Image Lab™ Software (Bio-Rad, Johannesburg, South Africa) to ensure protein had transferred to the membrane
- The membrane was then rinsed in methanol (1.06007.2500, Merck Millipore, Massachusetts, USA), air dried, and then rinsed back in methanol to ensure the protein was fixed to the membrane
- The membrane was washed with 1 X TBS-T (Tris Buffered Saline-Tween Solution) three times for five minutes
- The membrane was blocked in 5% milk solution for an hour on shaker at a gentle speed
- The membranes were washed with 1 X TBS-T three times for five minutes

Preparation of antibodies:

- Made up each primary antibody solution in a clean falcon tube
- Placed the membrane inside the falcon tube by rolling the membrane and ensured the “top” of the membrane was facing inward
- Placed the falcon tubes on rotator in 4 °C fridge overnight
- The membrane was washed with 1 X TBS-T three times for five minutes
- Made up the appropriate secondary antibody solution in a clean falcon tube
- Placed the membrane inside the falcon tube by rolling the membrane and ensuring the “top” of the membrane was facing inward

- The falcon tube was rolled on a roller at room temperature for an hour
- The membrane was washed with 1 X TBS-T three times for five minutes

Exposing with BioRad ChemiDoc™

- Made up Clarity™ Western ECL Substrate (1705061, Bio-Rad, Johannesburg, South Africa) in a falcon tube that was wrapped in tinfoil (light-sensitive)
- Turned off the lights in the room
- Pipetted ECl on area of membrane where protein is expected to be (used protein ladder as a guide)
- Rolled the ECL with mini roller to ensure an even distribution over membrane
- Exposed the membrane using the ChemiDoc™ XRS+ System with the Image Lab™ Software (Bio-Rad, Johannesburg, South Africa) until protein bands appeared. A stain-free blot image was then taken for protein normalisation

Stripping membranes:

- The membrane was washed in Paul's Stripping Buffer (Appendix I) twice for 10 minutes
- The membrane was washed in distilled water twice for five minutes
- The membrane was blocked in 5% milk solution for an hour at a gentle speed

Preparation of both the primary and secondary antibodies with their appropriate dilutions:

Primary Antibody	Company	Dilution	Molecular Weight
Caspase 3	CST (9662)	1:1000	17, 19, 35
SOD1 (Cu/Zn SOD)	CST (71G8)	1:1000	18
SOD2 (Mn SOD)	CST (13141)	1:1000	22
Secondary Antibody			
HRP-Linked	CST (7074)	1:10 000	
HRP-Linked	CST (7076S)	1:10 000	

APPENDIX P: Western Blotting reagents and polyacrylamide gel preparations

RIPA Buffer:

- Prepared 50 mM Tris-HCl:
    - Added 790 mg Tris (648310, Merck Millipore, Massachusetts, USA) to 75 ml distilled water
    - Added 900 mg NaCl and stir solution until all solids are dissolved.
    - Used HCl, adjust pH to 7.4.
    - Poured into 100 ml beaker
- Prepared 10% NP-40:
    - Wrapped small beaker in tinfoil
    - Dissolved 10 ml NP-40 (Nonidet P 40) (74385, Sigma-Aldrich, St Louis, USA) into 90 ml distilled water
    - Placed a stirrer in beaker and placed beaker on heated magnetic stirrer until completely dissolved

- Added 10 mL of prepared 10% NP-40 to prepared 50 mM Tris-HCl
- Added 2.5 ml of 10 % Na-deoxycholate (D6750, Sigma-Aldrich, St Louis, USA) and stir until solution is clear
- Added 1 ml of 100 mM EDTA (Ethylenediaminetetraacetic acid) (EDS, Sigma-Aldrich, St Louis, USA) and adjusted final volume of solution to 100 ml with distilled water

Working RIPA:

- For every 1 ml of RIPA added
    - 1 µg/ml leupeptin
    - 10 µg/ml pepstatin
    - 1 µg/ml aprotonin
    - 10 µl phenylmethylsulfonyl fluoride (PMSF, 93482, Sigma-Aldrich, St Louis, USA)
    - 1 mM activated sodium orthovanadate (Na_3VO_4, S6508, Sigma-Aldrich, St Louis, USA)
    - 1 mM sodium fluoride (NaF) (106449, Merck Millipore, Massachusetts, USA)

Laemmli's Sample Buffer:

Stock solution:

- Prepared 0.5 M Tris-HCl (pH 6.8):
    - Weighed 30.285 g of Tris (648310, Merck Millipore, Massachusetts, USA) in a small glass beaker
    - Added 400 ml of distilled water
    - Adjusted pH to 6.8
    - Adjusted final volume to 500 ml with distilled water

- Prepared 10 % Sodium dodecyle sulfate (SDS)
    - Weighed 5 g of SDS (L3771, Sigma-Aldrich, St Louis, USA) in a small glass beaker
    - Added 50 ml of distilled water and stir to dissolve
- Dissolved in 38 ml distilled water:
    - 10 ml 0.5 M Tris-HCl (pH 6.8)
    - 8 ml glycerol (SAAR2676520, Merck Millipore, Massachusetts, USA)
    - 16 ml 10% sodium SDS (L3771, Sigma-Aldrich, St Louis, USA)
    - 4 ml 0.05% (w/v) Bromophenol blue (SAAR1437500CB, Merck Millipore, Massachusetts, USA)

Working solution of Laemmli's solution

- For every 850 µl of Laemmli's Buffer Stock Solution, added 150 µl of β-mercaptoethanol

10 X TBS:

- Dissolved in 600 ml distilled water:
    - 4.2 g Tris (648310, Merck Millipore, Massachusetts, USA)
    - 80 g NaCl (1.06404, Merck Millipore, Massachusetts, USA)
    - Adjusted pH to 7.6
    - Adjust final volume to 1 L

1 X TBS-T

- Mixed together:
    - 200 ml of 10 X TBS
    - 1800 ml distilled water
    - 2 ml Tween20 (P9416, Sigma-Aldrich, St Louis, USA)

Running Buffer:

- Mixed together:
    - 200 ml of 10 X TGS (Tris/Glycine/SDS Buffer, 161-0772, BioRad, Johannesburg, South Africa)
    - 1800 ml distilled water

Paul's Stripping Buffer:

- Dissolved in 400 ml distilled water:
    - 7.5 g glycine (357002-1KG, Merck Millipore, Massachusetts, USA)
    - 0.5 g SDS (L3771, Sigma-Aldrich, St Louis, USA)
    - 5 ml Tween20 (P9416, Sigma-Aldrich, St Louis, USA)
- Adjusted pH to 2.2
- Adjusted final volume to 500 ml

5% fat-free milk solution:

- Mix together:
    - 5 ml fat-free milk
    - 95 ml 1 X TBS-T

Preparation of stain-free acrylamide gels:

For 12% Gels:

- TGX Stain-Free™ Fastcast™ Acrylamide Solutions (161-0185, Biorad, Johannesburg, South Africa) was used to make up gels. All instructions in the kit were followed when making up gels

For 15% Gels (enough for 2 gels)

15% gel constituent (Resolving Gel)	
Distilled water	5.245 ml
40% Acrylamide solution (100638, Merck Millipore, Massachusetts, USA)	5.62 5ml
1.5M Tris-HCl (pH 8.8)	3.75 ml
10% w/v SDS	150 µl
10% w/v APS	150 µl
TCE (T54801, Sigma-Aldrich, St Louis, USA)	75 µl
TEMED (add last) (1.10732.0100, Merck Millipore, Massachusetts, USA)	6 µl

4% gel constituent (Stacking Gel)	
Distilled water	4.84 ml
40% Acrylamide solution (100638, Merck Millipore, Massachusetts, USA)	1 ml
1.5M Tris-HCl (pH 8.8)	2 ml
10% w/v SDS	80 µl
10% w/v APS	80 µl
TEMED (add last) (1.10732.0100, Merck Millipore, Massachusetts, USA)	8 µl

Membranes of representative images for Western blotting:

Left: Membrane with protein **Right: Total Protein**

SOD1: Ladder,V,V,G,D,DG,V,G,D,DG

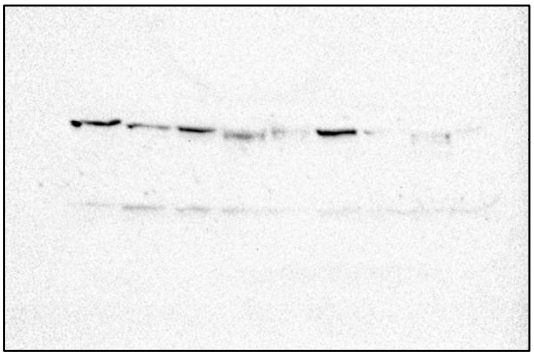

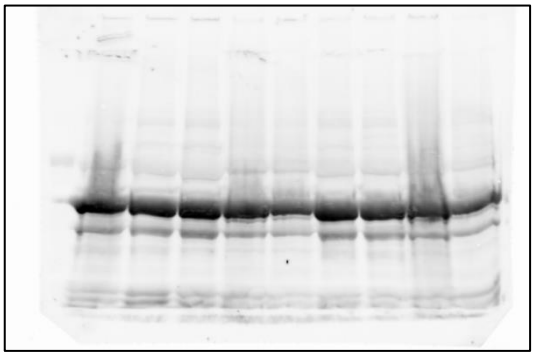

SOD2: Ladder,V,V,G,D,DG,V,D,D,DG

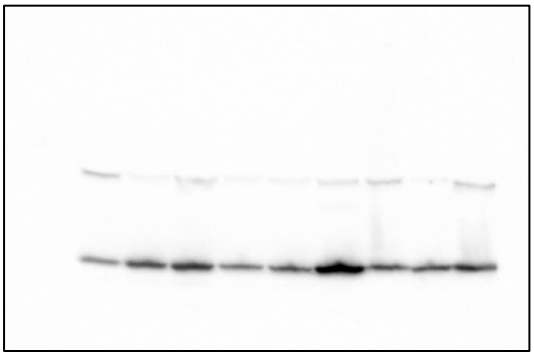

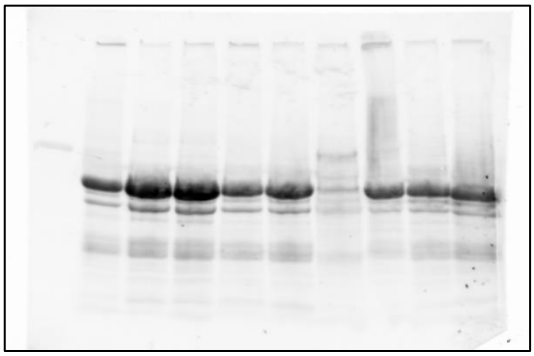

Total & Cleaved caspase-3: Ladder,V,G,D,DG,V,D,D,DG